GSI-2018-2
REPORT
July 2018

News and Reports from

High Energy Density generated by Heavy Ion and Laser Beams

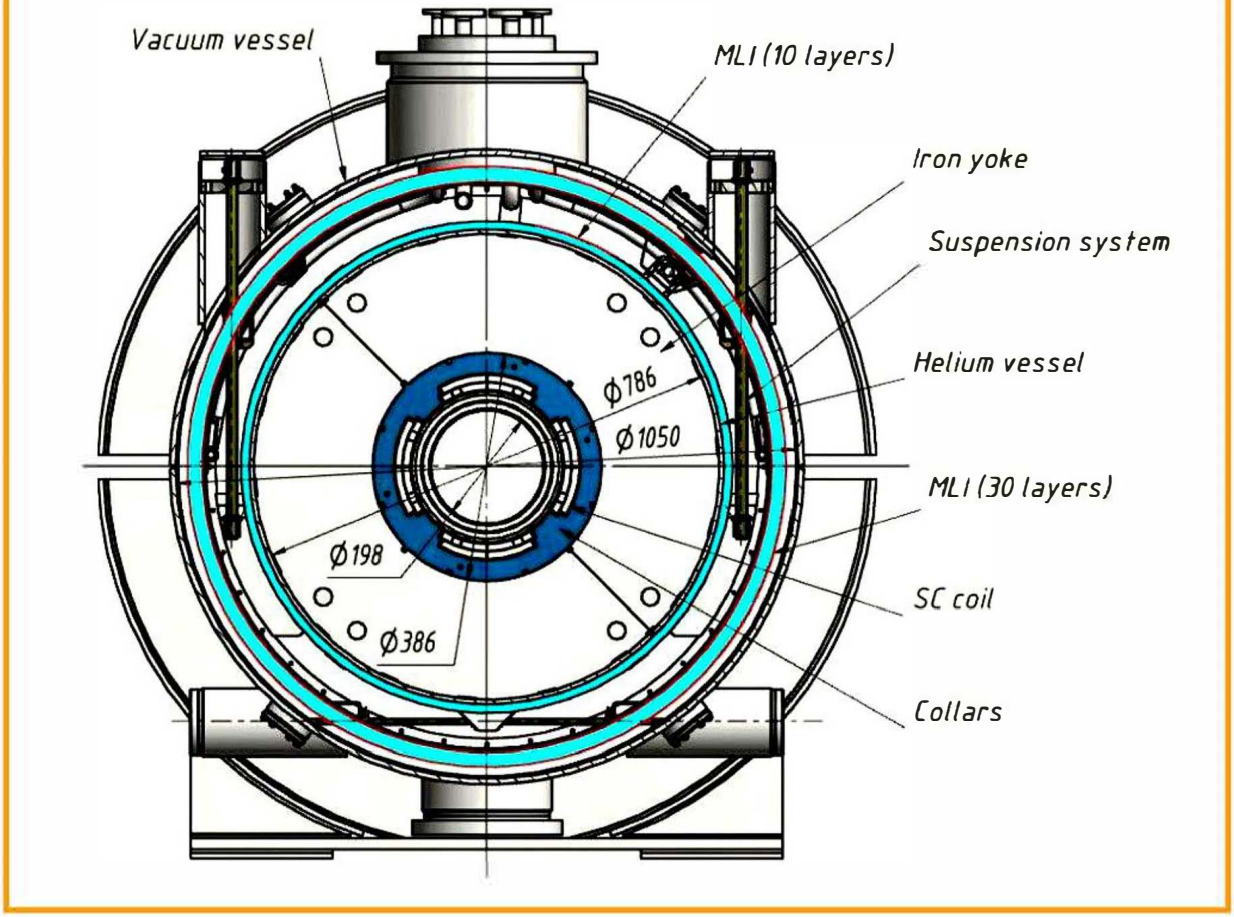

The HED@FAIR Collaboration - Report 2017

The figure on the cover shows a schematic picture of the cross-section of one of the four super-conducting quadrupoles of the plasma physics beamline in the APPA-cave at FAIR. Shown are details like the vacuum and helium vessel, the iron yoke and the sc-coil. The four super-conducting quadrupoles form the final focusing system (FFS), which transports the beam, which is prepared in the beam matching section (BMS) to the necessary conditions for the different experimental scenarios (HIHEX, PRIOR, LAPLAS) into the target chamber to the focal point. The FFS is located in the beamline directly in front of the target chamber. These sc-quadrupoles are an essential part of the beamline. Their function, design and construction are described in the first contribution of chapter 2, page 13.

News and Reports from

High Energy Density generated by Heavy Ion and Laser Beams

2017

July 2018

Editor: K. Weyrich

Co-editor: D.H.H. Hoffmann

Editorial

Dear Colleagues,

right in time for the next meeting of the high energy density physics collaboration at FAIR - now called HED@FAIR- we were again able to complete a report on recent news and developments of our collaboration. Again not only collaboration members contribute but also groups and individual scientist interested in the progress of High Energy Density Physics.

A new idea is that from this issue on the first chapter of the report will be dedicated to a choosen special topic, which is of importance, up-to-dateness or interest in this report period. This time we choose 'Diagnostics' with respect to the main topic of the collaboration meeting in Spain in October, because progress of the research field is strongly interconnected to the development of new diagnostic methods. Among all those excellent contributions in this chapter attention should be paid to the X-ray Thomson scattering experiment performed by a group from Lawrence Berkeley Lab and LLE-Rochester. This contribution is represented by Alison Saunders (Berkeley) as first author, who was awarded the 'Laser and Particle Beam Prize 2018'. Based on this work she will also give an invited talk at the European Conference on 'Laser Interaction with Matter'.

Since the collaboration is responsible and has to launch the preparations for the upcoming experiments at FAIR the second chapter of the report addresses FAIR related issues and related facilities for HED research. The construction of the superconducting quadrupoles for the final focusing system of the PP-beamline at FAIR is an important milestone and therefore the cover picture of this report shows a drawn scheme of one of these devices, while the contribution of IHEP, Protvino in chapter 2 describes details of it and the status of the construction.

The collaboration keeps close contact to the development at the large laser facilities. This is expressed by the contribution of the National Ignition Facility at LLNL and the experiments at the Kumgang Laser Facility in Korea.

The following chapter is about the interaction of ion- and laser beams with matter. In addition to contributions from Germany and Europe, Russia and USA one finds a striking number of contributions from China. At the annual collaboration meeting in Hirschegg, China presented the strongest foreign group.

The chapter 'Radiation- Particle and Plasma Sources' deals also with laser-plasma issues relevant for High Energy Density Physics. The chapter on accelerator and beam physics is rather short, but this indicates that our accelerator physicists are busy with the construction of the FAIR facility.

Theoretical work on all aspects of the topics concludes the chapters with the contributions of research in 2017. Finally we decided to include the report on the EMMI workshop on 'Plasma Physics at FAIR' (June 2017) here, which served as a frame for the collaboration meeting 2017 and included the important topic, that the plasma physics collaborations HEDgeHOB

and WDM were renewed in the collaboration now called HED@FAIR founded during the EMMI workshop, where also Alexander Golubev from ITEP was elected spokesperson of this new collaboration. Also as a conclusion of this workshop the participants decided to further develop FAIR Plasma Physics and during the FAIR phase 0 provide the experimental infrastructure to be prepared with the initial conditions for the 'first day experiments".

With kind regards,

Dieter H.H. Hoffmann and Karin Weyrich

July 2018

Contents

1 New Diagnostic Methods and Diagnostic Tools

2 FAIR related Issues and New Facilities for HED/WDM Research

3 Interaction Experiments with Ion- and Laser Beams

Several of the contributions in this report are also published in the GSI Scientific Report 2017.

1 New Diagnostic Methods and Diagnostic Tools

Modernized diagnostic system for shock processes investigation in matter under the influence of intense laser pulses

A. Mikhaylyuk[1], K. Gubskiy[1], A. Kuznetsov[1], A. Golubev[1,2]

[1]National Research Nuclear University MEPhI (Moscow Engineering Physics Institute), Moscow, Russia

[2] SSC RF Institute forTheoreticaland Experimental Physics of National Research Centre „Kurchatov Institute“, Moscow, Russia

For laser-driven EOS experiments a diagnostic system consisting of VISAR-based vernier velocimeter, target luminescence registration system and target illumination system was developed [1]. The system was modernized to achieve wider field of view. To assess the spatial resolution of the system test measurements were carried out.

The system designed for study of shock-wave processes occurring in the interaction of intense laser light with matter. It based on a line imaging VISAR and allows to measure shock wave velocity in the range of 5—50 km/s. The system shown in figure 1 consists of:

- Laser light source with adjustable power (probe laser at a wavelength of 660nm);
- Light transportation system (40m Ø1mm core fiber, collimators, adjust laser)
- Active channel. Two vernier nonequal arm Mach--Zehnder interferometers for measuring shock wave velocity;
- Passive channel. SOP for measuring temperature by self-luminous;
- Adjustment and control system based on motorized mechanical elements that provide adjustment of the optical scheme. The angular and spatial position of the beam in the measuring system is monitored using digital cameras with a PC output;
- Registration system, based on three streak cameras, that records images, including interferometric, with a temporal resolution 10ps.

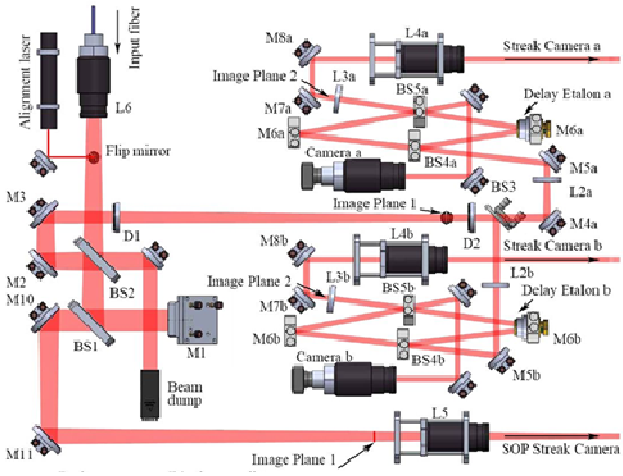

Figure 1: Vernier line-imaging VISAR layout. M – mirrors, BS – beam splitters, L – lenses, D – diaphragms

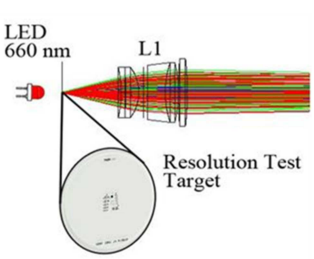

Figure 2: Position of optical elements for resolution tests

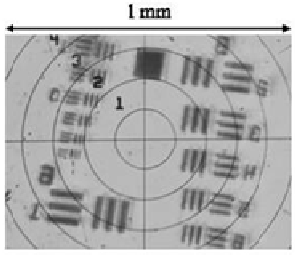

Figure 3: Test target image of 0.6 mm target size configuration

Optical layout was recalculated in ZEMAX, which made it possible to reduce aberration and to obtain diffraction-limited image of 1 mm size target. Maximum field of view of the imaging system is 1.6 mm in the target plane now. The overall magnification of the optical system is 13.6–27.3 for the target sizes of 1.0–0.3 mm. Resolution in the target plane raise from 10 to 3 µm. The depth of field on the cameras is estimated to be ~100 mm, which does not create obstacles to the focus and does not reduce the resolution of the system.

To assess the spatial resolution of the system, test measurements were carried out. Target was replaced by the USAF-51 test target (see figure 2).

Behind the test target was placed a red LED at a wavelength of 660~nm with a power of 1W. Beam configuration completely corresponds to the scattered light obtained during the experiments. The location of the test target is shown in figure 3. The images of test bars of an optical system corresponding of 0.3 to 1.0 mm target sizes were obtained. One of this test images is shown in figure 3. It is clearly seen that allows to resolve the 4th element of the 7th group of strokes, which corresponds to a resolution of 3µm (200 stroke/mm).

All components of the diagnostic system have the potential for modification and can be adapted for various HED setups.

References

[1] A. Mikhaylyuk, D. Koshkin K. Gubskii, A. Kuznetsov, A. Golubev, "Line-imaging velocimeter in Laser-Driven EOS Experiments", HEDgeHOB 2015 GSI Report (2016) p.36

Application of a TLD-based ten channel system for the spectrometry of bremsstrahlung generated by laser-matter interaction*

N. Zahn[1], O. Rosmej[1,2], F. Horst[2], S. Zähter[1], A. Sokolov[2], N. Borisenko[3], L. Borisenko[3], N. Pimenov[4] and J. Jacoby[1]

[1]Goethe University, Frankfurt, Germany; [2]GSI, Darmstadt, Germany; [3]P. N. Lebedev Physical Institute (RAS), Moscow, Russia ; [4]Zelinsky Institute of Organic Chemistry (RAS), Moscow, Russia

The interaction of relativistically intense laser pulses produced by the PHELIX-system with near critical plasmas has been investigated in order to optimize the energy and the total charge of the laser-accelerated electron bunch for FAIR-relevant applications. The enormous increase of total charge and energy of the laser-accelerated electrons was predicted by the theory [1], that is much higher than defined by Wilks law [2]. In described experiments, electrons were accelerated in plasma of near critical density. The electron energy distribution was directly analysed by applying a static magnetic field and indirectly by measuring the bremsstrahlung radiation produced when MeV electrons were passing through the 17 mm-thick steel flange placed 87 cm distant from the target in the laser propagation direction. For measurements of the gamma bremsstrahlung spectra 10 channels TLD detector-based thermoluminescence dosimetry method was applied.

The schematic drawing of the ten channel spectrometer is shown in fig. 1. The TLD-spectrometer has a cylindrical shape with a default incident direction of the radiation. Ten TLD-cards are placed between absorbers of different material and thickness inside a shielding from lower to higher Z materials with a collimator window in the front. The incident x-rays penetrate the TLD's. The absorbers cause a different response of every TLD, which can be used as information about the spectrum of the incident x-rays. The spectrometer is designed for an energy range from 30 keV to 100 MeV [3].

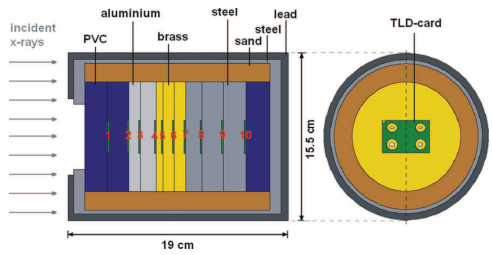

Figure 1: Schematic view of the TLD-spectrometer [3]

The materials of the TLD cards used in these measurements are pieces of doped lithium fluoride in two variations - Harshaw TLD 700 (^{7}LiF: Mg, Ti) and TLD 700H (^{7}LiF: Mg, Cu, P). TLDs absorb radiation and emit photons proportionally to the deposited dose when heated to a few hundred degrees Celsius.

In the experiment (P138, Oktober 2017) electrons were accelerated in the interactions of the PHELIX-laser pulse of $3\cdot10^{19}$ W/cm^2 intensity with different foil-targets (Ti, Cu, Ta) of 5-20 µm thickness and with low density foams. Additionally, foil-targets were combined with the CHO foam layer (2mg/cm^3 Triacetate-Cellulose $C_{12}H_{16}O_8$) with thickness of 300 and 500 µm. The laser energy was 100 J, with pulse duration of 750± 250 fs. Supplementary to the shots with a single laser pulse, a double pulse configuration was used where a 1.5 ns prepulse with a time delay of 0.5-3 ns before the main pulse and energies of 1-3 J was applied in order to drive a super-sonic ionization in the low density CHO-foams and create a homogeneous channel of near critical plasma. Using pre-ionized by the ns-prepulse low-density CHO-plasma with a mean density near to the PHELIX-laser critical density ($n_e=10^{21}\cdot$cm^{-3}) it was possible to increase by 2-3 orders of magnitude the fraction of 20-100 MeV electrons compared to the case of the laser interaction with planar foils and thus to gain 2-3 orders of magnitude increase of the gamma-rays. Preliminary results for the spectrometer response to different laser shots are shown in fig. 2. The experiments have shown the effective generation of electrons with tens of MeV-energy if the relativistic laser pulse interacts with extended plasmas of near critical density.

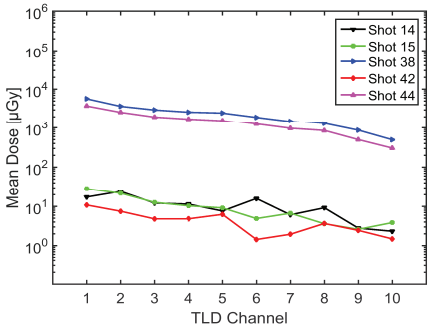

Figure 2: Preliminary results for five different shots. Shots 14, 15 and 42: contrast 10^{-10}, no prepulse, target – 25 µm Cu-foil. Shots 38 and 44: contrast 10^{-10}, prepulse – 1 J, t = 1.5 ns, dt = 5 ns, target – CHO-Foam 500 µm

The main mechanisms leading to extreme high electron energies are the laser beam self-focusing in the preplasma and a betatron mechanism of the electron acceleration. TLD measurements of the radiation dose are consistent with results of the electron spectrometers. Using the Monte Carlo code FLUKA [4] the electron spectra will be evaluated from the photon radiation doses measured by the TLDs.

References

[1] L. P. Pugachev et al., NIM A **829** (2016) 88-93
[2] S. C. Wilks et al., Phys. Rev. Lett. **69** (1992) 1383
[3] F. Horst et al., NIM A **782** (2015) p. 69-76
[4] http://www.fluka.org.

* This report is also submitted to the GSI Scientific Report 2017

Spectroscopy-based femto-clock for the electron kinetics in swift heavy ion tracks

N. Medvedev[1,#], A.E. Volkov[2,3,4]

[1]Institute of Physics and Institute of Plasma Physics, Czech Academy of Sciences, Prague, Czechia; [2]National Research Center 'Kurchatov Institute', Moscow, Russia; [3]Joint Institute for Nuclear Research, Dubna, Russia; [4]Lebedev Physical Institute of the Russian Academy of Sciences, Moscow, Russia.

The details of femtosecond kinetics of the excited electronic system of targets around the trajectories of swift heavy ions (SHI, E>1 MeV/amu) still remain poorly understood. Indeed, by the time of sub-100 fs, an essential part of the electron kinetics is already finished. But contemporary state-of-the-art experimental techniques in ion-beam research have ~0.5 ps resolution [1], insufficient to monitor this femtosecond dynamics. As a result, there is a variety of theoretical models of electronic behavior in SHI tracks that could not have yet been validated by experiments: ranging from the two-temperature model, to Coulomb explosion, to point defects accumulation, and nonthermal melting, see e.g. [2,3].

We proposed an idea for developing a technique for monitoring of transient states of the electronic system in materials irradiated with swift heavy ions [4]. It is based on spectroscopic measurements of photon emission due to radiative decays of holes from different inner shells of ionized target atoms. Since a hole in each shell of each element decays with its own characteristic time, it potentially allows extracting femtosecond time-resolved information about the excited electronic system in the valence and the conduction band of a target.

Using our Monte Carlo code TREKIS [5], we simulated evolution of the state of the electronic system of Al target in tracks of 2187 MeV Au ions. From that, we constructed emitted photon spectra from different shells decaying at different times after the ion impact and thus carrying information about different transient electronic temperatures, Fig. 1 [4].

It is also demonstrated that shifts of the inner-shell ionization potentials in atoms multiply-ionized by a direct SHI impact should allow to distinguish the track core within a few angstroms around the ion trajectory from the track periphery [4]. The angstrom-size track core produces shifted peaks, in comparison to the single-ionized peaks from the periphery. Both calculated spectra are shown in Fig. 1. Thus, we demonstrated that sorting of peaks in the measured spectra can, theoretically, provide an access to a number of time points in the electron kinetics.

Additionally to using natural atomic shells of elements constituting the target, we propose also to apply a prior ion implantation into the target, utilizing selected ions with desirable characteristic times of inner-shell holes decays. Appropriate choice of implanted ions should allow to make a well-defined time grid [4].

The same ideology of extracting time-grid from the energy-resolved spectra can, in principle, be applied for Auger-electron spectra [6]. However, transport of charged particles through matter differs from the photon transport: electrons are sensitive to electro-magnetic fields created by excited electrons and holes after an SHI impact. This effect allows one to address development of the charge neutralization [6]. However, interaction and deceleration of electrons precludes from precise temperature evaluation, for which the use of X-ray photons is more favorable. Thus, these two techniques may be considered as complementary to each other [4].

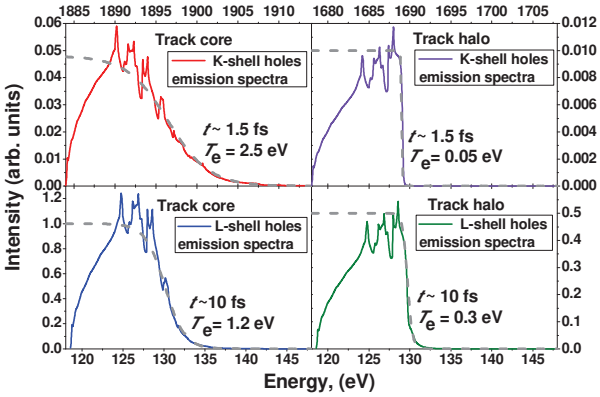

Figure 1: Calculated spectra of photons emitted during decays of K-shell (upper raw) and L-shell holes (bottom raw) filled by electrons from the conduction band in Al irradiated with Au ion (2187 MeV); reproduced from [4].

References

[1] B. Dromey *et al.*,, Nature Comm. **7**, 10642 (2016)
[2] F. F. Komarov, Physics-Uspekhi **60**, 435 (2017)
[3] N. Medvedev, A. E. Volkov, and B. Ziaja, Nucl. Instrum. Meth. B **365**, 437 (2015)
[4] N. Medvedev and A. E. Volkov, Journal of Physics D **50**, 445302 (2017)
[5] N. A. Medvedev, R. A. Rymzhanov, and A. E. Volkov, Journal of Physics D **48**, 355303 (2015)
[6] G. Schiwietz, G. Xiao, E. Luderer, and P. L. Grande, Nucl. Instrum. Meth. B **164**, 353 (2000)

nikita.medvedev@fzu.cz

Fundamental Studies for the Development of Optical Beam Profile Monitors

A. Ulrich[1], R. Hampf[1], A. Himpsl[1], J. Wieser[2]
[1]TU-München, Germany, [2]Excitech GmbH, Schortens, Germany

Optical beam diagnostic is planned for intense ion beams which would destroy conventional beam diagnostic devices. The concept is to measure beam induced light from a gas target space-resolved and to deduce beam profiles from these data. A more detailed description of the concept is given in [1] and references therein.

In 2017 we continued model experiments at the Munich Tandem accelerator using a DC-beam of 87 MeV ^{32}S ions (2.72 MeV/u) exciting various gases over a wide pressure range. Low pressure is relevant for beam transport sections and high pressure at fixed target stations. Both spectroscopic studies and preliminary profile measurements have been made. The spectroscopic studies are used to identify appropriate optical transitions. Based on the results transmission filters were used to take pictures of the beam in various wavelength regions.

Gas purification was improved with respect to data in [1] and differential pumping installed at the beam entrance for pressures below 1mbar. A f = 30 cm vacuum monochromator (McPherson model 218) was used to record beam induced spectra of Ne, Ar, Kr, Xe, and N_2. Overview spectra were recorded at medium gas pressures to identify the emission lines. An example of a short section of such a spectrum is shown in fig. 1. It shows mainly lines of singly ionized gas (ArII). Atomic lines (ArI) are found at longer wavelengths. This is the structure for all rare gases (RG): ionic lines in the ultraviolet - atomic lines in the visible and near infrared.

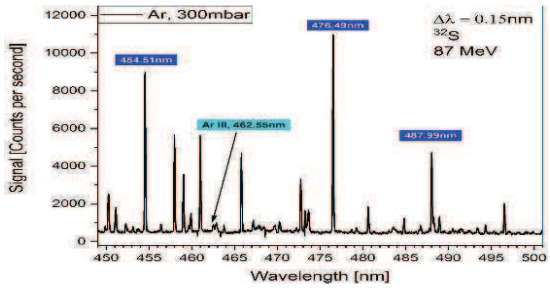

Figure 1: Expanded region of an ion beam induced emission spectrum of argon at 300 mbar. It shows that the lines can be clearly assigned with 0.15 nm resolution. Ion lines are marked in blue.

Spectra around stronger RGI and RGII lines were recorded for a wide pressure range of the rare gases in particular towards low pressures (fig. 2). Two interesting aspects were discovered: Ion lines are more intense at low pressure than atomic lines. Atomic lines increase with a steeper slope, an effect which may be due to recombination processes. The fact that ionic lines are intense at low pressure is helpful for profile measurements at a low beam-line pressure since they represent the beam profile better than the atomic lines (see next section).

Beam profile measurements were performed with a sensitive and cooled CCD camera (ATIK 383L+) combined with a f = 6 cm broadband (315 to 1100 nm) apochromatic lens. Appropriate filters were used to select various RGI and II lines. The RGII lines represent the 1mm diameter beam very well. RGI lines show the expected ([1]) "wings" due to secondary electrons emitted from the ion tracks (fig. 3).

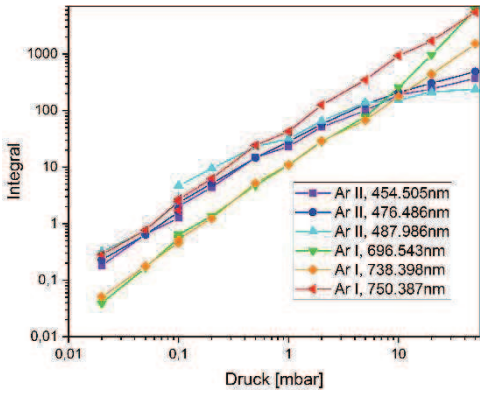

Fig. 2: Intensity of selected beam induced lines versus target gas pressure. ArII lines are more intense at low pressure than ArI lines. Collisional quenching becomes visible at higher pressures for the ArII lines (blue).

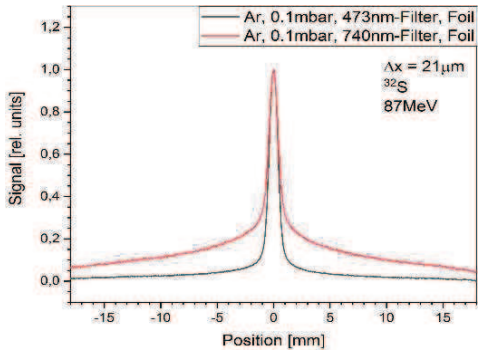

Fig. 3: Beam profiles deduced from ionic and atomic lines, respectively for 0.1 mbar gas pressure. The atomic lines show pronounced wings due to excitation by secondary electrons (red). This effect disappears for both significantly higher and lower pressure because of very short and very long ranges of the electrons, respectively.

References

[1] A. Ulrich et al., High Energy Density generated by Heavy Ions and Laser Beams Report 2016 (GSI-2016-2), page 31

Acknowlegement

This work has been funded by the BMBF project APPA R&D, FKZ 05P15WOFA1, Maier Leibnitz Labor München (MLL) and GSI Vorhaben TUM ULRI1719.

Measurement of fast ion source configuration by means of pinhole imaging in experiments with cluster targets*

S. Makarov[1,2], S. Pikuz[1,3], A. Faenov[1,4], T. Pikuz[1,4,#], Y. Fukuda[5], I. Skobelev[1,3], I. Zhvaniya[6], S.Varzar[2], M. Kando[5], and R. Kodama[4,7]

[1]JIHTRAS, Moscow 125412, Russia, [2]Faculty of Physics of Moscow State University (MSU), Moscow 119991, Russia, [3]MEPhI, Moscow 115409, Russia,[4]Open and Transdisciplinary Research Initiatives Institute, Osaka University, Suita, Osaka 565-0871, Japan, [5]Kansai Photon Science Institute, Kizugawa, Kyoto, Japan,[6]International Laser Center of MSU, Moscow 119991, Russia, [7]ILE, Osaka University, Suita, Osaka 565-0871 Japan

The target consisting of gas clusters become increasingly common in experiments on the interaction of intense ($I > 10^{15}$ W/cm^2) laser radiation with matter due to possibility of efficient generation of x-ray radiation, electrons and ions. In this work, for the first time, the spatial configuration of the ion source in cluster plasma was registered using pinhole imaging method.

The experiment has been carried out at JLITE-X Ti;Sa laser at Kansai Pohoton Science Institute (Japan). Laser pulse with energy of 160 mJ and duration of 36 fs was focused by an off-axis f/13 parabola into supersonic gas jet about 1.5 mm from nozzle outlet (the focal spot size of ~ 50 μm, laser intensity of ~ $4\cdot10^{17}$ W/cm^2, contrast of ~10^5). Nozzle was specially designed to produce big size clusters. The mixture of 90% He and 10 % CO_2 driven at 50 bar pressure contained CO_2 clusters of up 0.22 μm diameter and of $5\cdot10^8$ molecules per cluster [1]. The laser propagation in the cluster jet was monitored by shadowgraphy with the probe laser beam at the same duration.

To measure shape of ion source, two pinholes with diameter 5 and 25 μm were placed symmetrically to the laser beam propagation direction at angles ± 45° and at 50 mm distance from plasma source. Images with magnification 3 were detected using CR-39 polymer detector. The pits formed in CR-39 were established following 9-hours of etching in 6N-KOH solution of 70 C° temperature, and then read out by optical scanner.

Experimental images obtained on CR-39 show decrease of ion production in the centre when laser was focused to the centre of jet despite that laser intensity and cluster density have maximum values (Figure 1).Most likely this local gap in ion yield around the best laser focusing is associated with the destruction of clusters by the impact of laser prepulse of ~10^{12} W/cm^2 intensity (see left shadow images in Figure 2 (c)). Pinhole images obtained in orthogonal directions (Figure 2(a)) are similar confirming wide-angle generation of ions due to Coulomb explosion mechanism. However the ion source is not isotropic. It is expanding for few mm along the laser beam propagation in cluster media. Measured source size is to be of (300 ÷ 400) × (1500 ÷ 2500) μm . Further, the asymmetry in the ion yield before and after best focus, associated with laser self-focussing effect, was observed (Figure 2(b)). Estimation show that ions accelerated to energy of 100 keV and above while the laser intensity exceeds ~$2\cdot10^{16}$ W/cm^2.

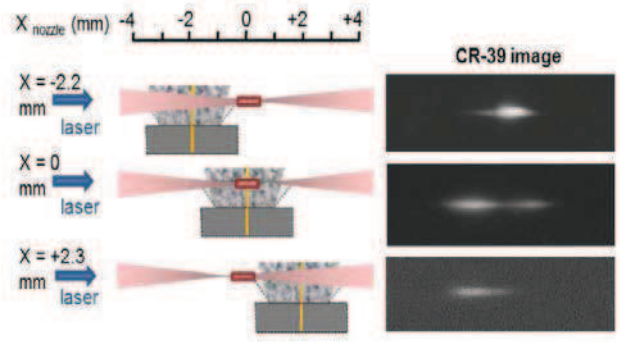

Figure 1. Pinhole images on CR-39 for different focus positions.

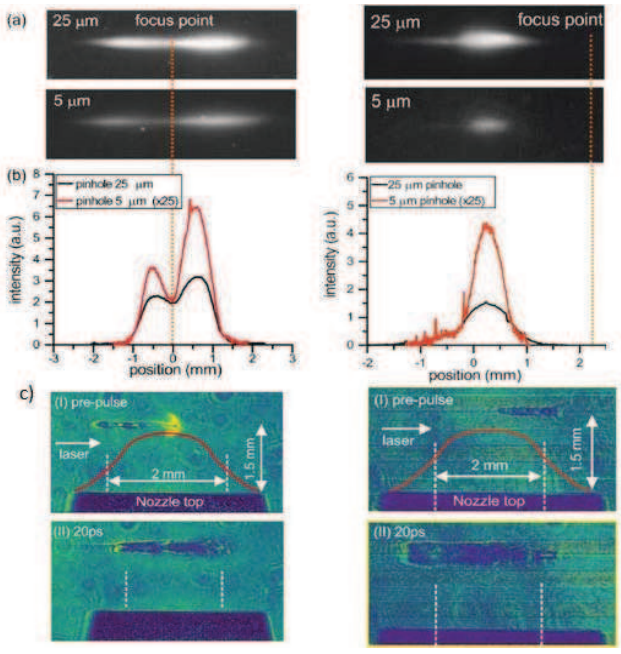

Figure 2. (a) 25 μm and 5 μm pinhole images on CR-39, (b)spatial distribution of ions intensity, (c) optical shadowgraphy image for different time. Laser focused to the centre of jet x=0 (on left), focus at x=2.2 mm (on right)

References

[1] S. Jinno et al. "Characterization of submicron-sized CO_2 clusters formed with a supersonic expansion of a mixed-gas using a three-staged nozzle", Appl. Phys. Lett. 102(16), 164103 (2013)

* Work supported by RSF #14-50-00124, KAKENHI(A)26247100.
#pikuz.tatiana@gmail.com

X-Ray Thomson Scattering from Shock-Compressed Diamond Spheres on the OMEGA Laser

Alison M. Saunders [1*], Michael MacDonald[1], Ryan Nora[2], Amy Lazicki[2], Otto Landen[2], Damian Swift[2], Joe Nilsen[2], Wolfgang Theobald[3], Roger W. Falcone[1], and Tilo Döppner [2]

[1]University of California Berkeley, USA, [2]Lawrence Livermore National Laboratory, USA,

[3]Laboratory for Laser Energetics, USA

X-ray Thomson scattering (XRTS) is an experimental technique that directly probes the complex physics of warm and dense matter. The Compton-shifted profile of inelastically-scattered x-rays reflects the electron velocity distribution and can yield temperature and density measurements [1]. The ratio of elastically versus inelastically scattered x-rays is related to the number of tightly bound versus free electrons, and thus reflects the ionization state of the sample [1]. Recent experiments have highlighted uncertainties in the ionization models often used to describe warm dense matter [2-4]. Therefore, experimental validation of these models using XRTS is valuable.

We performed an experiment on the OMEGA laser in which a combination of XRTS and x-ray radiography were used to measure plasma conditions in a spherical implosion. Fifty-two beams were used to compress a 1 mm diamond sphere with a 1 ns square pulse. Six beams heated a Zn backlighter foil to generate Zn He-α x-rays. A spectrometer collected scattered Zn x-rays at a scattering angle of 135˚. X-rays that propagated through the sphere were collected by an x-ray framing camera. A sequence of time-resolved radiographs will allow us to confirm that the rad-hydro simulations correctly predict shock speed and density. To first order, XRTS provides a mass weighted average of the plasma conditions [5]. The rad hydro simulations predict an average mass density of $\rho = 4.2$ g cm^{-3} and average electron temperature of $T_e = 6$ eV. We generate theoretical scattering spectra and vary the electron density, shown in Figure 1. The spectra show reasonable sensitivity to electron density, which will allow us to benchmark the average ionization state in these warm dense matter conditions.

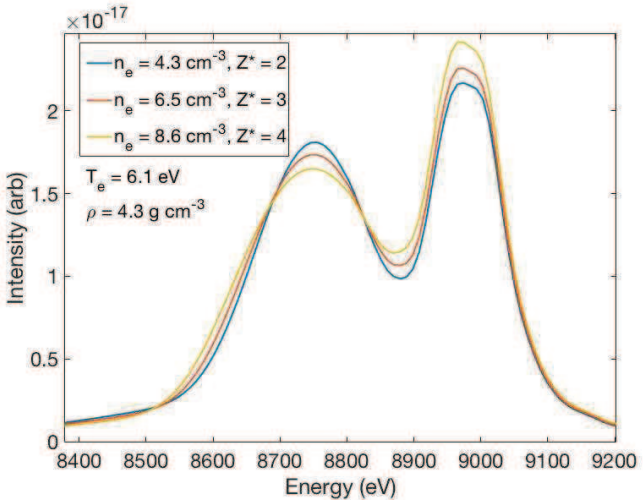

Figure 1: Simulated XRTS spectra from shock-compressed diamond spheres that vary electron density. All simulations assume the mass averaged mass density and electron temperature as predicted by a radiation hydrodynamics code. The spectra show reasonable sensitivity to electron density.

References

[1] S. H. Glenzer and R. Redmer. Rev. Mod. Phys. **81**, 1625 (2009)

[2] D. Kraus et al., Phys. Rev. E. **94**, 011202(R) (2016)

[3] L. B. Fletcher et al., Phys. Rev. Lett. **112**, 145004 (2014)

[4] O. Ciricosta et al., Nat. Comm**. 7**, 11713 (2016)

[5] D. Chapman et al., Phys. Plasmas **21**, 082709 (2014)

* This work was performed under the auspices of the US Department of Energy by Lawrence Livermore National Laboratory under Contract DE-AC52-07NA27344 and supported by Laboratory Directed Research and Development (LDRD) Grant No. 18-ERD-033, and under the Stewardship Science Graduate Fellowship program support, grant number DE- NA0002135.

*E-mail: saunders@berkeley.edu

X-rays diagnostics of the hot electron energy distribution in the intense laser interaction with metal targets*

O. F. Kostenko† [1], *N. E. Andreev*[1], *and O. N. Rosmej*[2]
[1]JIHT RAS, Moscow, Russia; [2]GSI, Darmstadt, Germany

In the experiment, performed at the PHELIX laser facility, the hot electron energy distribution has been inferred from measurements of bremsstrahlung and K_α emissions from a massive silver cylinder irradiated by a subpicosecond *s*-polarized laser pulse with a peak intensity of about 2×10^{19} W/cm^2. The bremsstrahlung emission has been measured by the radiation attenuation and half-shade methods. To deduce parameters of the hot electron spectrum, we have developed semi-analytic models of generation and measurement of the x-rays under given experimental conditions. The models are based on analytical expressions and tabulated data on electron stopping power as well as cross-sections of generation and absorption of the x-rays. The K_α emission from thin silver foils deposited on low-Z substrates has been used to verify developed models and obtained hot electron spectrum.

It is shown that a two-temperature hot electron energy distribution is in better agreement with the bremsstrahlung emission measurements (Figs. 1 and 2) than a single-temperature one. The K_α yield calculated using obtained distribution function is in good agreement with measured K_α yields from silver foils of 10 μm thickness deposited on aluminum or plexiglass substrates (Fig. 3). Obtained temperatures of the colder and hotter electron components are in agreement with the values predicted by kinetic simulations of the cone-guided approach to fast ignition [1]. The temperature of the high-energy component is described by the ponderomotive scaling. The temperature of the low-energy component is well below the ponderomotive scaling and the Beg's law. We have obtained relatively low conversion efficiency of laser energy into the energy of hot electrons propagating through the solid target of about 2%. The assumption about single-temperature hot electron energy distribution with temperature described by the ponderomotive scaling relationship [2], without detailed analysis of the hot electron spectrum [3], strongly overestimates the laser-to-electron energy-conversion efficiency.

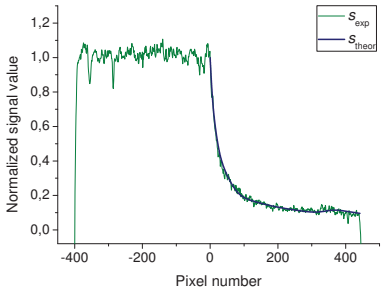

Figure 1: Normalized signals in the measurement by the half-shade method, both experimental (thin line) and theoretical (thick line), calculated using a two-temperature hot electron energy distribution, as functions of the imaging plate pixel number.

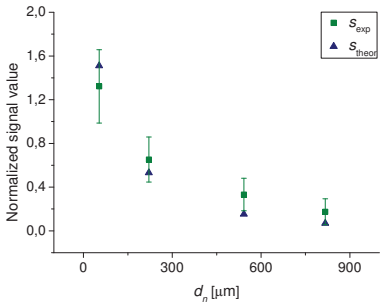

Figure 2: Normalized signals in the measurement by the radiation attenuation method, both experimental (squares) and theoretical (triangles), calculated using a two-temperature hot electron energy distribution, as functions of the lead filter thickness.

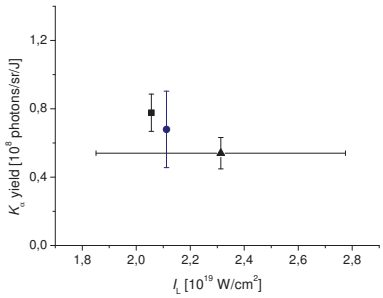

Figure 3: Measured K_α yields from a silver foil of 10 μm thickness deposited on aluminum (triangle) or plexiglass (square) substrates as well as the K_α yield (circle), calculated using obtained hot electron distribution, at close laser pulse intensities.

References

[1] B. Chrisman, Y. Sentoku, A. J. Kemp, Phys. Plasmas 15 (2008) 056309.

[2] O. F. Kostenko, N. E. Andreev, O. N. Rosmej, A. Schönlein, J. Phys.: Conf. Ser. 774 (2016) 012112.

[3] O. F. Kostenko, N. E. Andreev, O. N. Rosmej, Phys. Plasmas 25 (2018) 033105.

* The theoretical part of this work was supported by the Russian Science Foundation (Grant No. 14-50-00124).

† olegkost@ihed.ras.ru

The X-ray radiography of detonation nanodiamonds after heat treatment

V.P. Efremov, E.I. Zakatilova*
JIHT RAS, Moscow, Russia

Introduction

Carbon nanoparticles with a diamond crystal lattice (detonation nanodiamonds) are detected in the products of the explosives detonation. These particles have heterogeneous structure. They consist of diamond core and impurity shell. This shell contains nondiamond carbon, metal impurity and there are radical groups: C-H, C-N, C-O on the surface shell. This structure influences on properties of nanoparticle and powder of detonation nanodiamond (DND). Published properties of DND are ambiguous and contradictory. Then temperature of graphitization beginning is in the wide range from 670˚C [1] to 980˚C [2]. A more detailed study of the behavior of nanodiamond under various heat impacts will expand its applicability.

The purpose of this article is the experimental investigation of the thermal stability of detonation nanodiamonds.

Thermal stability

In our works, the analysis of the behavior of detonation nanodiamond under growth of temperature has carried out. The thermal loading was carried out by synchronous thermal analysis in the range from room temperature to 1500˚C at the rate 2 and 10˚C/min in a dynamic argon atmosphere.

Initial data of powders from nano and micro diamonds obtained at explosion of the mixture TNT/RDX (50/50) in the different environment are given in work [3]. After the thermal treatment, the saved sample is investigated by the x-ray diffraction analysis and by the electron microscope.

The grains of detonation nanodiamond have heterogeneous structure. They consists of the surface shell, when includes the non-diamond carbon, gas and metal admixtures and a surface radicals C-H, C-O, C-N, and the diamond core.

The removal of radical groups with surface was taken place with the rise of temperature. This process in our conditions leads to decreasing of sample mass about 10-20% [4]. The mass loss of the nanodiamond sample is 16% at the heat to 1500˚C at rate 10˚C/min. From the literature data it was established that the graphitization of nanodiamond begins at a temperature of about 600˚C [3]. From the results of the X-ray diffraction analysis of the detonation nanodiamond powder, it follows that the diamond phase in the sample after treatment to 600˚C somewhat decreased only [5]. The formation of phase sp^2 did not occur. Therefore energy released at 600˚C does not correspond to the graphitization process.

The exothermal peak near 600˚C may be connected with the removal of lacton groups from the surface of nano-diamond grains. This process goes with release of a certain amount of heat and production of CO_2 [2].

The X-ray analysis of the stored samples before and after the heat treatment is shown in figure 3. From the ratio of the integral intensities from base plane (111) at 2θ=44° in the x-ray line is seen that the content of diamond phase is decreased with increased the thermal treatment (figure 1, lines 2 - 5).

From figure 3 is seen that the graphite peak in the x-ray line from base plane (002) 2θ = 26° is not increased with the increase of temperature. This could mean that the initial grains of detonation nanodiamond are destroyed. They transit to amorphous phase which the mount is impossible identified by the x-ray method. The crystalline ordered graphite structure with sp^2-bonds is not observed. However, there is halo at the temperature 1500˚C in the x-ray line near the Bragg angles 2θ=20 – 32° which it corresponds graphite-like structure (figure 3, lines 4, 5). This carbon structure consists of sp^2 bonds as and in graphite, but the interplanar distance (0.3707 nm) is larger than in graphite. This structure is stable and at further heating, it will not turn in the ordered graphite. In addition to the x-ray amorphous graphite-like structure, the crystal structure of diamond at the Bragg angle 2θ=44° was found in the treated sample (figure 3, lines 4 and 5).

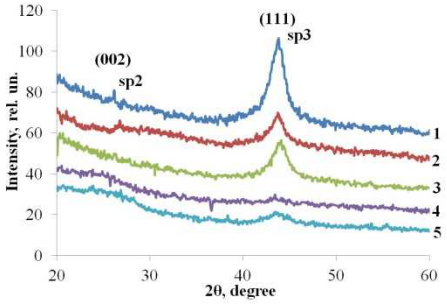

Figure 3. The XRD pattern of the powder detonation nanodiamond before and after the heat treatment: 1 – the initial powder, 2 – after to 600˚C at the rate 10˚C/min, 3 – after to 1000˚C at the rate 10˚C /min, 4 – after to 1500˚C at the rate 10˚C/min, 5 – after to 1500˚C at the rate 2˚C/min.

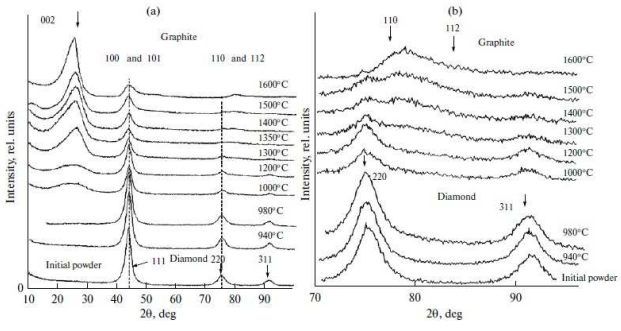

Figure 4. The diffractograms of the initial nanodiamond poweders and anneling products at temperatures of 940 – 1600˚C [2].

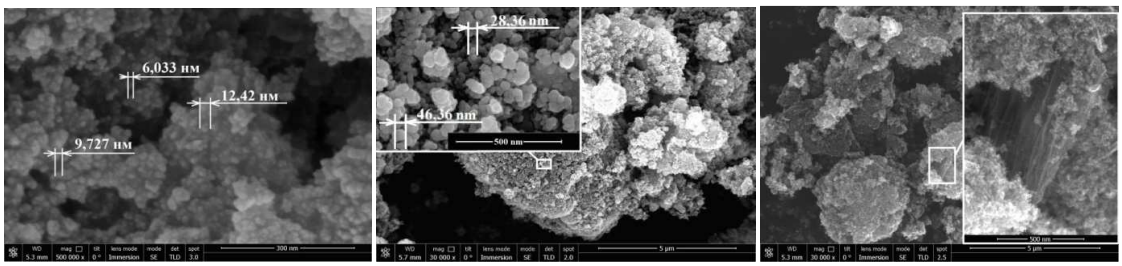

a) b) c)

Figure 5. The microstructure of the nanodiamond powder: a) before the heat treatment, b) after the heat treatment to temperature 1500˚C at heating rate 10◦C/min and c) after the heat treatment to temperature 1500˚C at heating rate 2˚C/min.

From the ratio of the integral intensities from base plane (111) in x-ray line of diamond, it was determined that content of diamond phase was about 10%.

Our data are agreed with results of work [2]. In figure 4, the diffractogram of nanodiamond samples before and after the heating [2] is shown. The decreased of the integral intensity of the x-ray peak from diamond base plane (111) begins with 1000˚C. This indicates on the decrease of diamond phase in the sample. Just like in our experiments, the certain amount of diamond is saved up to 1500˚C. But halo is seen already at the temperature 1000˚C [2] in the near Bragg angels 2θ=20 – 32°. It is indicated on the presence of graphite-like phase in the sample. This phase is only seen at the heat treatment up to 1500˚C in our experiments [6].

Also the investigations of thermal stability of detonation microdiamonds were carried out [6]. Detonation microdiamonds were got by the explosion of mixture TNT/RDX (50/50) in the water environment. The investigation of the heat treatment is shown that microdiamond is stable up to 1500˚C (a mass loss was about 2% at the heat). The x-ray peak from base plane of diamond (111) for the microdiamond samples before and after treatment is practically identical. This means that microdiamond is stable at the heat to 1500˚C. The comparison of the x-ray peak width of nano and microdiamond shown that the width of diamond peak in the x-ray line of the nanodiamond sample is large than width of peak for microdiamond [6]. This difference is connected with the small size and the defect structure of nanograins. With the decrease of their size, the part of the surface atoms increases. This leads to the increase of mean square distance of the atoms and the symmetry violation of the lattice atoms in the space. Thus, the grains of diamond microcrystal have more perfect structure and their properties close to bulk diamond.

The investigation of the microphotographs of the nanodiamond sample before and after the heat treatment was shown the effect of heating rate on the parameters of powder grains. The initial matter of the powder nanodiamond consists of nanograins the size 6 – 8 nm (figure 3a). After the heating of the nanodiamond sample at the rate 10˚C/min to 1500˚C, the grains agglomeration taken on the spherical form the size 30 – 40 nm (figure 3b) [3]. I. e the average size of powder grains is increased with the temperature increase. May be the conglutination nanograins with each other occur (figure 3b). At the heating with the rate 2˚C/min, the size of the spherical grains was less 10 nm and the planar formations are appeared (figure 3c). The nature and origin this planar formation requires the future investigation.

The main process of graphitization of DND occurs at temperatures above 800°C. Thermal stability of detonation nanodiamond is 1500°C and not depends on the heating rate. It was found that the heating rate effects on the shape and size of particles (agglomerates). As a result of the study, it was found that the data obtained for the thermal stability of the nanodiamond grains can be useful for development on their base a new composite materials and the optimization of ion-plasma hardening of steel parts surfaces.

References

[1] Xu N.S., Chen Jian, Deng S.Z. Effect of heat treatment on the properties of nano-diamond under oxygen and argon ambient // Diamond and Related Materials. 2002. V. 11. № 2. Pp. 249–256.

[2] V.A. Popov, A.V. Egorov, S.V. Savilov, V.V. Lunin, A.N. Kirichenko, V.N. Denisov, V.D. Blank, O.M. Vyaselev and T.B. Sagalova // Journal of Surface Investigation. X-ray, Synchrotron and Neutron Techniques. 2013. V. 7. Pp. 1034–43.

[3] V.P. Efremov, E.I. Zakatilova, I.V. Maklashova and N.V. Shevchenko // Konstrukcii iz kompozicionnyh materialov. 2016. Pp. 48 – 53.

[4] A.P. Koshcheev 2008. Rossijskij himicheskij zhurnal (Zh. Ros. him. ob-va im D.I. Mendeleeva) LII 88 – 96.

[5] V.P. Efremov and E.I. Zakatilova // Journal of Physics: Conference Series. 2016. P. 012014.

[6] V.P. Efremov, E.I. Zakatilova, I.V. Maklashova and N.V. Shevchenko Thermal stability of detonation-produced micro and nanodiamonds // Journal of Physics: Conf. Series: Journal of Physics: Conf. Series. 2018. 946. P. 012107.

Study of Shock Wave Compressibility of Epoxy Resin for experiments at PRIOR*

V. Mochalova[1,2,#], A. Utkin[1], M. Endres[3], and D.H.H. Hoffmann[3]
[1]Institute of Problems of Chemical Physics RAS, Chernogolovka, Russia;
[2]FSBI "SSC RF ITEP" of NRC "Kurchatov Institute", Moscow, Russia;
[3]Technical University Darmstadt, Darmstadt, Germany.

The experimental study of the shock wave structure, spall strength and determination of Hugoniot parameters for epoxy resin were conducted. Epoxy resin is a common binder for some anisotropic materials, which were studied by the authors earlier (carbon fiber, fiberglass, textolite) [1], and it largely determines the properties of these materials, in particular, their response on the shock wave action. The density of the samples from epoxy resin is $\rho_0 = 1.2$ g/cm^3, the measured sound speed is C = 2.63 km/s. The shock wave profiles were recorded by laser interferometer VISAR with a nanosecond time resolution. The shock-wave compressibility of epoxy resin was studied in the experiments with high explosive generators. Pressure of shock compression varied by change in the thickness and the velocity of flyer plates from 700 m/s to 2500 m/s. The goal of this study is development of targets for experiments at a novel diagnostic system proton microscope (PRIOR). Shock waves will be produced by a two stage light gas gun, which is developing at the TU Darmstadt.

In the experiments on investigation of the shock waves structure of epoxy resin, after the shock jump the particle velocity is almost constant until the arrival of a rarefaction wave from the flyer plate. As a result of the processing of the experimental data the Hugoniot of epoxy resin was plotted in the coordinates of the shock wave velocity D - particle velocity u (see fig.1). The filled circles represent experimental data, the solid line is their linear approximation: $D = 2.6 + 1.18*u$, km/s. And the first coefficient of this dependence is in the good agreement with the sound speed measured at atmospheric pressure.

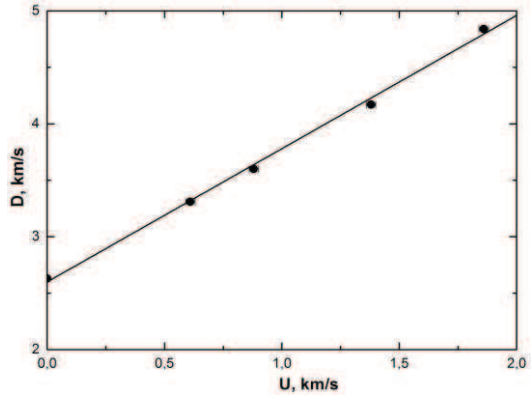

Figure 1: Hugoniot parameters of epoxy resin.

Also a study of spall strength for epoxy resin was conducted. The measured particle velocity profiles of free surface of epoxy resin are shown in fig.2. In the experiments 1 and 3, the aluminum flyer plate impacted directly the sample, and in experiment 2 the shock wave was initiated by a plane wave explosive generator, which was separated from the sample by a steel plate.

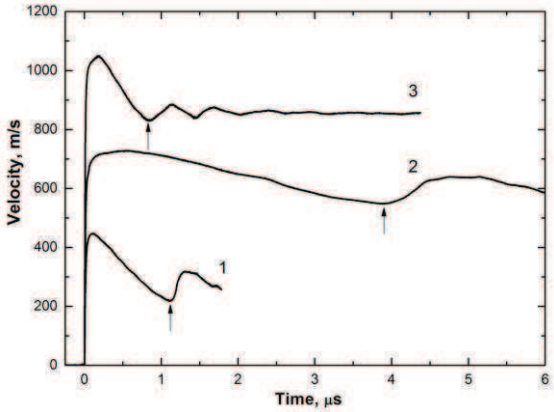

Figure 2: Spall strength of epoxy resin.

The exit of the shock wave on the free surface causes a sharp increase in the velocity of the surface up to the maximum value W_0. A centered rarefaction wave propagates inside the sample, which, interacting with the incident unloading wave, results in an internal fracture - a spall. In the process of failure, the tensile stress reaches zero, forming a compression wave that exits on the free surface as a spall pulse. The noted features are observed on the velocity profiles shown in Fig.2. The spall strength σ, which characterizes the maximum tensile stress in the sample, was determined by the equation: $\sigma=0.5\ \rho_0 C_0\ \Delta W$, where ΔW - the velocity difference between its maximum (W_0) and value at the moment of arrival of spall pulse , C_0 – the sound speed at zero pressure, ρ_0 – the initial density of the sample.

It was found that the spall strength values for epoxy resin varied from 286 MPa (profile 2, fig.2) to 360 MPa (profile 1, fig.2). The most distinctive feature is the significant decrease in spall strength on the profile 2. This result agrees with the general idea of the dependence of σ on the strain rate of the sample under tension - the value of strain rate in the experiment 2 is approximately 5 times less than that in the experiments 1 and 3, which is responsible for the decrease in spall strength.

References

[1] V. Mochalova, A. Utkin, "Investigation of shock wave compressibility of fiberglass for experiments at PRIOR", News and reports from High energy density generated by heavy ion and laser beams - 2016, June 2017, p.37.

* The work is carried out with the financial support of FAIR-Russia Research Center.
#roxete20000@hotmail.com

Investigation of the current distribution and compression of Magnetized-Plasma

D. Mikitchuk[1], *M. Cvejić*[1], *R. Doron*[1], *E. Kroupp*[1], *Y. Maron*[1], *C. Stollberg*[1], *A. L. Velikovich*[2], *J. L. Giuliani*[2], *E. P. Yu*[3], *and A. Fruchtman*[4]

[1]Weizmann Institute of Science, Rehovot 76100, Israel; [2]Plasma Physics Division, Naval Research Laboratory, Washington, D.C. 20375, USA; [3]Sandia National Laboratories, P.O. Box 5800, Albuquerque, NM 87185-1186, USA; [4]Holon Institute of Technology, P.O. Box 305, Holon 58102, Israel

We investigate fundamental phenomena occurring when magnetic-field flux and magnetized-plasma are compressed by applied azimuthal magnetic fields. This subject is relevant to numerous studies in laboratory and space plasmas. Recently, it has gained particular interest due to the advances in producing plasmas of high temperature and density in experiments based on the approach of magnetized plasma compression [1,2] for achieving controlled nuclear fusion. To advance this approach, it is essential to study experimentally the governing physical mechanisms that take place during the compression.

In our experiment (see Fig. 1), we employ a cylindrical (z-pinch) configuration, in which a current (300 kA, rise time 1.6 μs) driven through a cylindrical plasma (19 mm initial radius) that is preembedded in an axial magnetic field, B_{z0} (up to 0.4 T).

Here, for the first time in the research of magnetized plasma compression, Zeeman effect is used to measure the evolution and spatial distribution of the axial (B_z) and azimuthal magnetic fields (B_θ) during the implosion and stagnation stages. The two fields are measured simultaneously, which is important due to the irreproducibility that characterizes such experiments of high-current pulses. The B-fields measurements were performed using spectroscopic techniques based on the polarization properties of Zeeman effect, combined with a laser generated doping technique that provided a mm-scale spatial resolution (see Fig. 1). The B_z determination is based on the line-width comparison of the π and σ Zeeman components emitted from an aluminum dopant transition (see upper part of Fig. 1). The B_θ determination is based on the relative shift between the σ^+ and σ^- Zeeman components of light emitted from the imploding argon plasma shell (see lower part of Fig. 1).

Systematic measurements are performed for different initial conditions of B_{z0} and gas loads. The simultaneously measured B_z and B_θ, together with the plasma parameters, plasma radius, and the discharge current, are used to study the effects of B_z on the current distribution in the plasma, the pressure and energy balance during the implosion and stagnation, the effects of the electrodes on B_z compression, and the diffusion mechanism of B_z. For example, we measure at stagnation $B_z \sim 15 \times B_{z0}$. This compression factor, together with the observed plasma radius allows for the estimation of B_z confinement efficiency, which is found to be $\sim 50\%$. Another phenomenon observed is an axial gradient of B_z in which its magnitude increases by a factor of 2 from the anode (low B_z) to the middle of the plasma column ($z \sim 5$ mm, high B_z). This measurement demonstrates the existence of a transition region from the uncompressed $B_z = B_{z0}$ inside the electrodes to the compressed B_z farther away from the electrode surface.

In addition, 2D images of the plasma self-emission and interferometric images are used to study the dependence of instabilities on different initial conditions. The measurements show clearly the mitigation effect of B_z on the magneto-Rayleigh-Taylor instabilities [3].

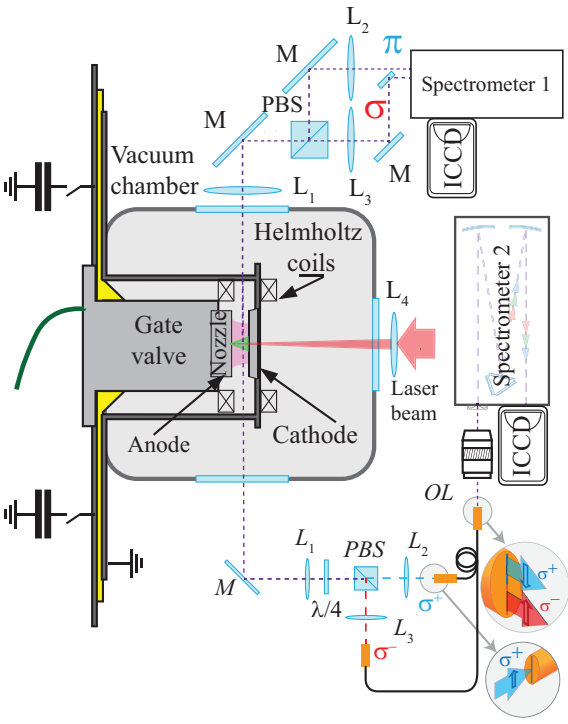

Figure 1: Experimental and diagnostics setups. L - lens, M - mirror, PBS - polarizing beam splitter, $\lambda/4$ - quarter wave-plate, OL - objective lens

References

[1] M. R. Gomez *et al.*, Phys. Rev. Lett., 113:155003, (2014).

[2] S. A. Slutz *et al.*, Physics of Plasmas, 17(5):056303, (2010).

[3] D. Mikitchuk *et al.*, Transactions on Plasma Science, 42(10):2524-2525, (2014).

Explosive Generators of Warm Dense Matter for Proton Radiography at PRIOR

N.S. Shilkin[1#], V.B. Mintsev[1], V.Ya. Ternovoi[1], D.N. Nikolaev[1], D.S. Yuriev[1], V.V. Yakushev[1], A.V. Utkin[1], A.V. Skobliakov[2], A.V. Bogdanov[2], A.V. Kantsyrev[2], A.A. Golubev[2], D.V. Varentsov[3], D.H.H. Hoffmann[4]

[1]Institute of Problems of Chemical Physics of the Russian Academy of Sciences, Chernogolovka; Russia; [2]Institute for Theoretical and Experimental Physics named by A.I. Alikhanov of National Research Center «Kurchatov Institute», Moscow, Russia; [3]GSI Helmholtzzentrum fur Schwerionenforschung, Darmstadt, Germany; [4]Xi'An Jiaotong University, School of Science, Xianning, China.

Physical properties of Warm Dense Matter (WDM) are of great interest in various branches of physics and numerous practical applications. Comprehensive description of such states is far from completion due to difficulties of both a theoretical and an experimental character. WDM is often generated by shock or isentropic compression with help of powerful drivers on a short period of time. The density of matter in these experiments is usually defined by x-ray pulse radiography or derived from conservation laws through a discontinuity surface by the measured kinematic parameters of gas-dynamic flow. High-energy proton radiography with special magnetic optics provided much better accuracy of density measurements in a dynamic experiment. This method was developed recently [1] and now it is available at PRIOR microscope [2] at GSI Darmstadt facility.

Existing proton radiography facilities at LANL (USA) and IHEP (Russia) are equipped with chambers where explosive related phenomena are investigated. An explosive chamber for charges with mass up to 150 grams was transferred to GSI from IPCP (Russia) earlier and it has been already used for joint investigations of stopping power of ions in shock-compressed non-ideal plasma. This chamber could be employed with proton microscope, than PRIOR will be the third functional high-energy proton radiography setup in the world suitable for investigation of explosive driven states of matter. The expected accuracy of areal density measurements in high explosive experiments at PRIOR is about percent and it exceeds accuracy of other techniques about an order of magnitude.

The field of view of the PRIOR microscope is about 15 mm therefore the external diameter of an explosive generator should be restricted by 25 mm to ensure registering at least half of cross-section of the symmetric explosive setup. The proton microscope PUMA [3] at ITEP had approximately the same field of view and it was equipped with similar explosive chamber for small charges. So compact explosive generators earlier developed for the PUMA microscope could be used or adapted for the PRIOR [4]. Short description of several types of proposed experiments with compact explosive generators is presented below.

Equation of state of non-ideal plasma

Linear explosive generators are one of standard tools for producing non-ideal gas plasma, i.e. energy of interparticle interaction greater than kinetic energy. Plasma is formed by compression of a gas behind the shock wave front arising at the expansion of products of detonation in it. Different theoretical approaches are used for description of equation of state of plasma with strong interparticle interaction. Direct measurements of density could strongly support the theory. Earlier developed linear explosive generators for PUMA contained 20–40 grams of high explosive to produce single compressed plasma of xenon or argon with pressures of several kbars, temperatures of 2–3 eV and Coulomb parameter of non-ideality up to 3.

Phase transitions in compressed planetary liquids

There is a number of theoretical predictions of phase transitions in liquid molecular gases at pressures about 50–200 GPa and low temperatures. Such states will be generated by multiple shock compression of liquids in front-collision generators (FCG). A prototype of the compact FCG for the research of shock-compressed liquids at cryogenic temperatures has been developed and tested at the PUMA facility. It consisted of two explosive devices symmetrically placed relative to cryogenic capsule with the studied liquid. Each device contained 30 g of high explosive and accelerated the steel plate of 2–3 mm thick to the speeds of 1.0–1.6 km/s. Proton radiography could be used for confirmation of new phases in planetary liquids compressed in FCG.

Plane shock-wave generator

Compact plane shock-wave generator for accelerating aluminium impactors was developed for experiments at the PUMA [5]. It was designed according to the classical scheme: a conical explosive lens formed a flat detonation wave that was transferred to an active charge of a high explosive. An impactor was pressed in a steel ring. An air gap between the charge and the impactor was used for adjustment of velocity of the impactor. The total mass of explosives in the generator was within 20 g, and it accelerated Al plates of 20 mm in diameter and of 2 mm thickness to a velocity about 3 km/s.

Conclusion

Explosive generators of high pressures could be used at PRIOR for experiments in the following branches of physics: warm dense matter, non-ideal plasmas, phase transitions in condensed matter, extreme states of matter, chemical physics, shock wave synthesis of high pressure phases, physics of detonation, dynamic strength of materials and others.

References

[1] N. S. P. King et al., Nucl. Instrum. Methods Phys. Res. A 1999, 424, 84.
[2] D. Varentsov et al., Rev. Sci. Instrum. 2016, 87, 023303.
[3] A.V. Kantsyrev et al., Instrum. Exp. Tech. 2014, 57, 1.
[4] V.B. Mintsev et al., Contrib. Plasma Phys. 2018, doi:10.1002/ctpp.201700141.
[5] V.V. Yakushev, A.V. Utkin, S.A. Koldunov, M.I. Kulish, Instrum. Exp. Tech. 2011, 54, 430.

shilkinns@mail.ru

2 FAIR related Issues and New Facilities for HED/WDM Research

Development of the Superconducting Quadrupole for Final Focusing System of the HED@FAIR Beamline

E. Kashtanov, S. Kozub, L. Tkachenko
IHEP, Protvino, Moscow region, Russia, 142281

Introduction

Novel experiments to study fundamental properties of high-energy-density states in matter generated by intense heavy ion beams will be carried out by the HED@FAIR [1], [2] at FAIR [3]. For strong transverse focusing, a special final focus system (FFS) has to be installed at the end of the HED@FAIR beam line. In order to provide a focal spot of the order of 1 mm, a large focal angle is needed and consequently, large-aperture high-gradient quadrupole magnets have to be used in a FFS. The proposed focusing system will have a length of 40 m. "Specification for the Design, Construction and Testing of a Superconducting Wide-Aperture Quadrupole Magnets for Plasma Experiments within the FAIR Project" [4] examines the main characteristics of four large-aperture high-gradient quadrupole magnets to be used in the HED@FAIR FFS. On the basis of the Specification requirements, calculations of the design of the quadrupole magnets have been performed, the results of which are presented in this report.

Requirements to Quadrupole

The main requirements to the quadrupole are: DC operating mode; the coil inner diameter is 260 mm; the minimal distance between quadrupole centres of two nearby magnets is 2.5 m; the integral of field gradient is 66 T.

For geometry optimization the following criteria have been chosen: the radius of the good field quality is 110 mm; the field multipole $|b_6|$, are less than 2×10^{-4}; the integral multipole $|b_n^{int}|$ n = 6, 10, 14 is less than 2×10^{-4}; the temperature margin is about 1 K. , The integral multipoles are suppressed by changing the central field multipoles. Note that in a real magnet the radius of a good field will be 95 mm and a spread of the above multipoles will be allowed no more 2×10^{-3}. Design studies have shown the maximum length of the magnet coil should not exceed 1.89 m.

Quadrupole Magnet Design

The cross section of the quadrupole magnet with its main parts is shown in fig. 1. The two-layer coil is wound from a Rutherford type superconducting cable with 28 strands. The strands were made from NbTi alloy composite superconducting wire consisting 8910 filaments of 6 μm diameter with 2.4 kA/mm^2 the critical current density at 5 T, 4.2 K [5]. The insulation of the cable is composed of a dry polyimide tape and an epoxidized glass fiber tape to bond adjacent coil turns together. During the operation of the magnet the coils are subjected to significant forces. These forces are compensated by installing the plate collars around the windings. The iron yoke has a layer structure and consists of plates made of soft magnetic steel. The grade of 2081 steel properties (saturation magnetization is 2.19 T) were used for the calculation of the iron yoke dimensions [6]. Nitronic 40 as well as 316LN stainless steels are quite suitable for collars production [7].

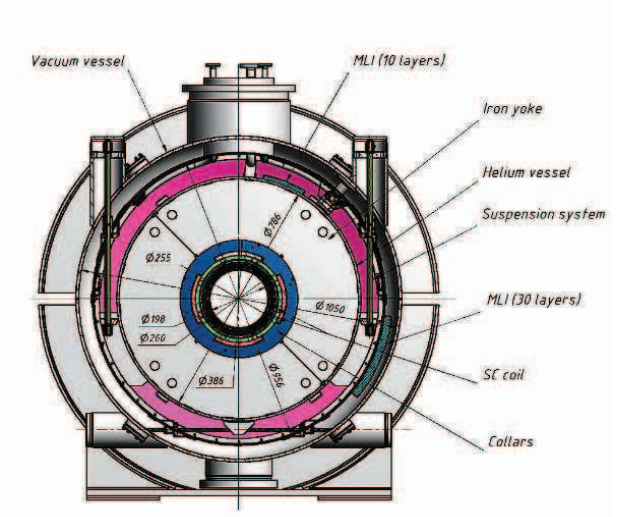

Fig. 1: General view of the quadrupole cross section

The yoke together with the coil block are placed into the helium vessel. The thermal shield is placed between the helium vessel and the vacuum vessel. Thermal shield is cooled with 50 K helium stream flows. The cold mass and the thermal shield are fixed to the vacuum vessel using the suspension system. The coils are powered through current leads.

Manufacture of Cable Samples for FFS SC Quadrupole

Modernization of equipment for the production and insulation of superconducting cable samples was carried out for development of the production technology of the cable for FFS SC Quadrupole. The conducted studies of mechanical characteristics of cable samples with the equilateral and rectangular trapezium cross-section showed the identity of these characteristics (fig. 2).

For technological reasons, the cable with the equilateral trapezium cross-section is more preferable. Dimensions of the cable without insulation is equal to: on the middle line of the trapeze 1.54 mm, height 12.35 mm and dimensions of the cable with insulation is equal to: on the middle line of the trapeze 1.71 mm, height 12.70 mm at 100 MPa pressure.

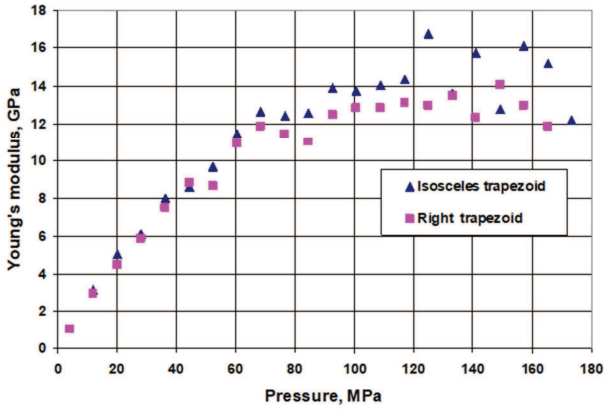

Fig. 2: Dependence of Young's modulus of cable samples on the applied pressure

The study of the electrical strength of the cable insulation showed that the sample does not have turn-to-turn fault at the voltage up to 5 kV at the pressure of 100 MPa in air at room temperature. On the basis of these results, additional calculations are made for final optimization of the quadrupole geometry.

Optimised Geometry

A geometry optimization was done, using the computer codes HARM-3D [8] and MULTIC [9].

The involute of the end parts of the optimized geometry is shown in fig. 3.

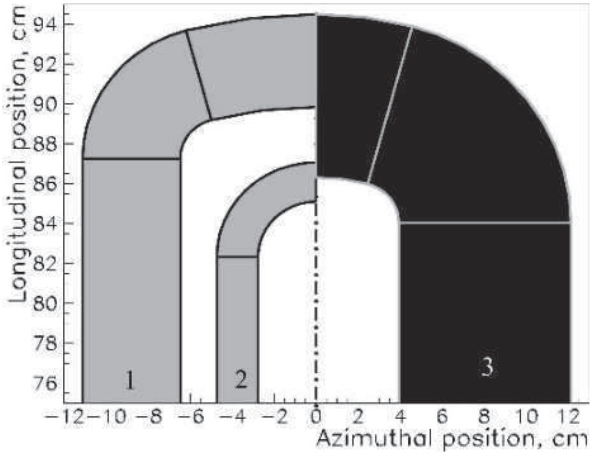

Fig. 3: Involute of end parts of the optimized geometry; left - the inner layer, right – the outer layer.

The main geometric parameters of the cross section for the geometry are presented in table I, where φ and α are the angles of the coil block, r_{in} and a are the inner radius and the width of the layer with an insulation. The basic magnetic parameters such as the lower multipoles b_n, stored energy E and magnetic forces F are shown in table II. The index 0 in the forces corresponds to the central cross section, the index e presents the forces in the end parts. The rest notations in the Table are: S - the spacer thickness of in the end parts B_{max0} and B_{maxe} – maximal field in the central cross section and in the end parts; G_0 – the central gradient; L_{ef} – the effective length of the magnet; I_{op} – the operating current; T_C – the critical temperature of the quadrupole; ΔL_{Fe} – shortening of the iron yoke.

3D model and engineering drawings of the FFS SC quadrupole were developed on basis of the optimised geometry and mechanical analysis.

Table I: Main geometric parameters of the cross section

N	φ, grad.	α, grad.	r_{in}, mm	a, mm	Turn
1	0.1890	18.8829	130.00	12.79	26
2	25.8220	33.7237	130.00	12.79	11
3	0.2488	30.9983	143.29	12.79	47

Table II: Basic magnetic parameters of the optimized geometry

Parameter	Value
S, mm	27.628
ΔL_{Fe}, mm	170
B_{max0}, T	5.910
B_{maxe}, T	5.902
G_0, T/m	37.482
L_{ef}, m	1.761
I_{op}, kA	5.760
T_C, K	5.913
b_6, 10^{-4}	0
b_{10}, 10^{-4}	8.85
b_{14}, 10^{-4}	7.92
b_6^{int}, 10^{-4}	0
b_{10}^{int}, 10^{-4}	0
b_{14}^{int}, 10^{-4}	0
E, kJ/m	592
F_{x0}, kN/m/octant	991
F_{y0}, kN/m/octant	-989
F_{r0}, kN/m/octant	642
$F_{\Theta 0}$, kN/m/octant	-1211
$\|F_0\|$, kN/m/octant	1400
F_{xe}, kN/octant	30.63
F_{ye}, kN/octant	-48.01
F_{ze}, kN/octant	59.89
$\|F_e\|$, kN/octant	82.68

Conclusion

Superconducting quadrupole for the special beam strong final focusing system of the HED@FAIR beam line in the FAIR project has been developed. The quadrupole has 37.5 T/m central gradient, 260 mm superconducting coil inner diameter and 1.89 m geometric length with the effective length of 1.76 m, so the integral gradient is 66 T. The temperature margin of the magnets is equal to 1 K at 4.85 K outlet temperature of liquid helium in the quadrupoles chain. The radius of a good field of the quadrupoles is 95 mm and spreads of the required both lower central field and integral field multipoles are less than 1.2×10^{-3}. Superconducting cable samples were manufactured for development of the production technology of the cable for the magnet. 3D model and working drawings of the FFS SC quadrupole were developed.

References

[1] H. Stocker and C. Sturm. The FAIR start. Nucl. Phys. A855 (2011)

[2] "FAIR Baseline Technical Report", 2006; http://www.gsi.de/fair/reports/btr.html,http://www.fair-center.eu/fair-users/experiments.html; http://hedgehob.physik.tu-darmstadt.de

[3] "An International Accelerator Facility for Beams of Ions and Antiprotons", CDR conceptual design report, GSI (2001)

[4] "HEDgeHOB SC Quads Detailed Specifications", GSI (2016)

[5] V.Ya. Filakin et al. The Properties of Industrial Superconducting Composite Wire for the UNK Magnets. Advances in Cryogenic Engineering, volume 36, part A, p.317; 1990

[6] I.V. Bogdanov and P.A. Shcherbakov. "AC Losses in the Iron Yoke of Superconducting Magnets of UNK," Proceedings of XVI All-Russian PAC, IHEP, Protvino, 1998, V.2, p.45, (in Russian)

[7] C. Lanza and D. Perini, "Characteristics of the Austenitic Steels Used in the LHC Main Dipoles," IEEE Transactions on Applied Superconductivity, Volume 12, Issue 1, pp. 1252-1255, Mar 2002

[8] S.V. Purtov and L.M. Tkachenko. "HARM-3D - a Code to Calculate Magnetic Characteristics of SC Magnets". MT-15, Beijing, China, 1997, Beijing, China, Vol. 1, p.p. 1335-1338

[9] L.M Tkachenko. Code Package MULTIC for Calculation of Magnetic Field with an Arbitrary Configuration. IHEP preprint 92-28, 1992, 48 pp. (in Russian)

Construction, characterization and optimization of a plasma window for FAIR, status update*

B. F. Bohlender[1#], A. Michel[1], M. Dehmer[1], M. Iberler[1], J. Jacoby[1]
[1]IAP, Goethe University, Frankfurt, Germany;

Introduction

The Plasma window is a membrane free beam transition between a region of higher pressure (e.g. Target chamber, gas stripper) and the vacuum of an accelerator. For details on the working principle, the reader is referred to [1], [2], [3].

Constructional remarks

As described within the last report [1], the thermal stress on all parts of the window, especially the stress on the cathode, proved to be a real challenge. Nearly all parts showed thermal caused damage, the cathode being nearly completely devastated after 15 min of operation.

New constructed Cooling plate design and the usage of WIG-welding needles as cathode tips allow to increase the lifetime of the window to at least 5 h.

Experimental results

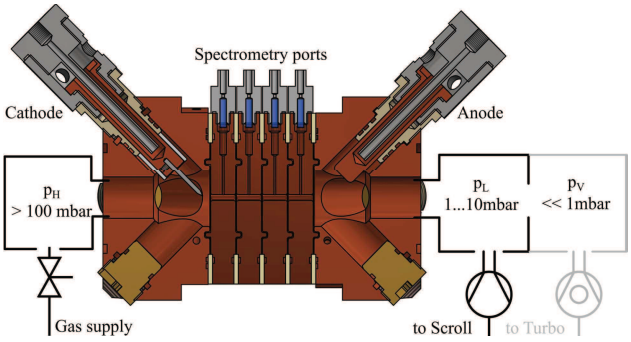

Figure 1: Schematic setup of the pumping stage, the light turbo-stage has not yet been set up but is due this year

The data presented herein has been collected with a residual gas composed of Ar with 2% H_2. Currents between 40 A and 60 A have been used, while the pressure on the high pressure side ranges from 280 mbar to 450 mbar, on the low pressure side from 4 mbar to 7 mbar. The aperture of the discharge channel is 3.3 mm.

Figure 1 shows a schematic view of the setup including a cross-section of the current window. High pressure side is to the left, as is the cathode.

Plasma parameters

First tests of a radial spectrometry setup along the discharge axis enabled the simultaneous determination of (radial integrated) plasma parameters. In comparison to last year's data, the electron temperature increased significantly from around 0.5 eV to 1.2 eV, this is mainly due to the improved cathode construction where now less energy is being deposited into the melting of the material.

In addition, first measurements of the electron density were carried out, showing a strong dependence on the current, pressure and the position inside the discharge channel. Values of n_e vary from $0.2*10^{16}$ cm^{-3} up to $4*10^{16}$ cm^{-3}.

Pressure parameters

The pressure measurements were carried out while holding the pressure on the low pressure side (i.e. pumping side) constant, thus keeping a constant volume flow through the experiment.

The measurements show that the pressure quotient, that is the pressure on the high side divided by the pressure on the low side, is clearly dependent on the discharge current, and seems to depend on the volume flow. This quotient ranges from almost 60 to over 70, see Fig. 2.

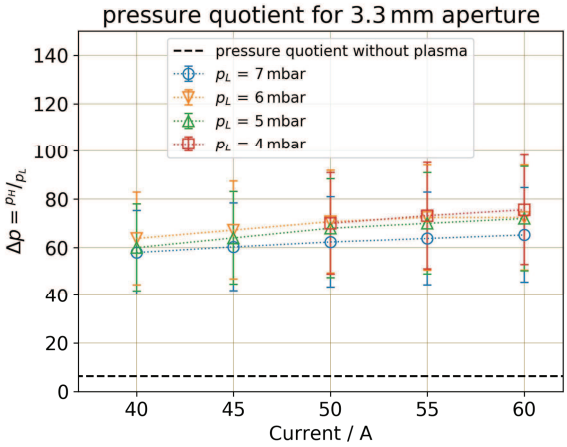

Figure 2: Pressure quotient for different p_L and currents. Quotient without plasma is around 6-7

Compared to the quotient measured when no plasma is burning, it's plain to see that the plasma increases the quotient by a factor around 10, resulting in the same possible reduction in length over a differential pumping system.

Conclusion and outlook

The plasma window is operational for well over 5 h now and realizing an improvement in the pressure quotient by a factor of 10 when compared to a differential pumping system.

In the near future, the complete differential pumping system, including the turbo-stage, will be build and tested. Additional tests with a larger aperture will be performed.

References

[1] B. F. Bohlender et al GSI HED report 2016
[2] B. F. Bohlender et al GSI HED report 2015
[3] A. Hershcovitch, J. Appl. Phys, 1995

* Work supported by BMBF, Ref.no: 05P15 RFRBA
This report is also submitted to the GSI Scientific Report 2017.

Optimisation of laser based sources of electrons and gammas for backlighting of high areal density targets at FAIR*#

Ş. Zähter[1], O. Rosmej[2], N. Andreev[3], L. Borisenko[4], N. Borisenko[4], B. Borm[1,2], P. Christ[1], F. Horst[2,5], P. Neumayer[2], D. Khaghani[2,6], V.Pimenov[7], L. Pugachev[3], K. Schmal[1], C. Wagner[1], N. Zahn[1], K. Zerbe[1], J. Jacoby[1], APPA-HED@FAIR, Plasmaphysics/PHELIX

[1]Institute for Applied Physics (IAP), Goethe University, Fankfurt am Main, Germany; [2]GSI, Darmstadt, Germany; [3]Joint Institute for High Temperatures (JIHT), Russian Academy of Sciences (RAS), Moscow, Russia; [4]Lebedev Physical Institute (LPI), RAS, Moscow, Russia; [5]Justus-Liebig-University, Giessen, Germany; [6]Friedrich Schiller University, Jena, Germany; [7]Zelinsky Institute of Organic Chemistry (ZIOC), RAS, Moscow, Russia

The development of laser based intense and well directed beams of MeV electrons and Gamma-rays for backlighting states of matter with high areal density is of great importance for the planned experiments at FAIR. If the laser parameters cannot be changed, one will be able to optimise the properties of the secondary laser sources using custom made structured targets of near critical density. A significant increase of the electron number at tens of MeV energy makes such type of laser-based electron source very prospective for the diagnostic of high areal density high energy density states. Simulations demonstrate that the interaction of relativistic laser pulses ($2-4\cdot10^{19}\,\mathrm{W/cm^2}$) with a near critical plasma layer ($10^{21}\,\mathrm{cm^{-3}}$) leads to an effective generation of highly energetic electrons (>10-20 MeV), carrying a charge that at least 2 orders of magnitude exceeds prediction by ponderomotive scaling for the incident laser amplitude [1]. Electrons accelerated from the by a ns-prepulse preionised low density foam target (triacetatecellulose, $C_{12}H_{16}O_8$) with a thickness of 500 µm and 2 $\mathrm{mg/cm^3}$ density have the highest energies and the highest charge (ca. 25 nC for electrons with energies higher than 30 MeV). In this work we present first pilot experiments on the characterization of MeV electron beams generated by the interaction of the PHELIX-laser pulse with low density CHO-foams (P138, October 2017).

Electron spectra up to 100 MeV were measured by the application of dipole magnets as dispersive elements. The electrons follow a certain path in the spectrometer according to their kinetic energy and the radius of gyration. That leads to a calculated dispersion. FUJI Film BAS-TR imaging plates were used as detectors. The response function of the imaging plates is known for photons, electrons and several types of heavier particles [2]. The schematic of this electron spectrometer is shown in figure 1.

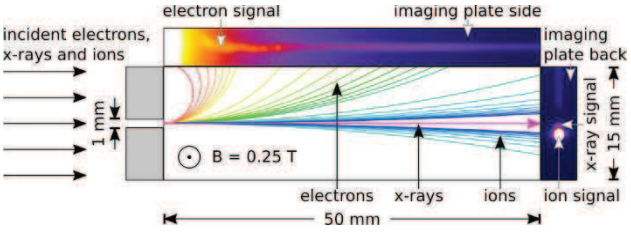

Figure 1: Schematic view of the electron spectrometer. Data shown in false colour images. Image by Ş. Zähter.

The interaction of the high power laser pulse of relativistic intensities with different target materials allow for the generation of MeV electrons. The Ponderomotive law predicts an electron temperature of 2.1 MeV for the used laser intensity. In the mentioned experiments with near critical plasmas the production of intense MeV electron beams is demonstrated. Figure 2 shows the cummulative number of electrons above an energy threshold up to 100 MeV. The usual way for laser-based particle acceleration is to shoot onto Cu-foils (shot 30, black and red solid lines). In comparison the interaction of relativistic laser pulses with preionized low density plasmas of near critical density leads to a strong increase of the number of electrons with energies above 10 MeV (green solid line, shot 44).

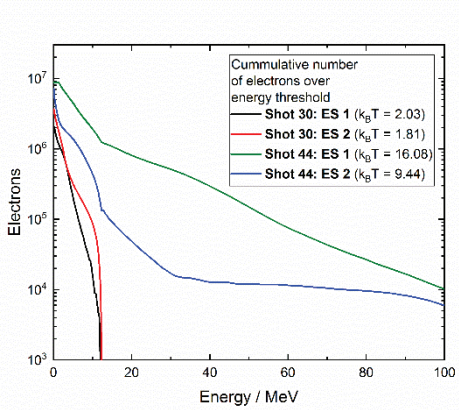

Figure 2: Cummulative number of electrons above energy threshold. Image by Ş. Zähter.

Electrons are mostly accelerated in laser direction reaching a mean energy/temperature of 16 MeV. Hot MeV electrons interacted with a 17 mm thick Fe-flange and created hard bremsstrahlung radiation measured by means of a 10 channel TLD-spectrometer [3]. The radiation dose on the TLD-cards showed the same result as the electron spectrometers: 2-3 orders of magnitude increase in the bremsstrahlung dose for the direction of laser propagation. The experiments have demonstrated the stability of the effect.

References

[1] L.P. Pugachev et al., "Acceleration of electrons under the action of petawatt-class laser pulses onto foam targets", NIM A 829 (2016), pp. 88-93.

[2] T. Bonnet et al., "Response functions of imaging plates to photons, electrons and 4He particles", RSI 84 (2013), pp. 103510-1-103510-7.

[3] F. Horst et al., "A TLD-based ten channel system for the spectrometry of bremsstrahlung generated by laser-matter interaction", NIM A (2015), p. 1.

* Work supported by BMBF-Project: 05P15RGFAA, HGS-Hire.
#This report is also submitted to the "GSI Scientific Report 2017"

Investigation of Proton induced Demagnetisation Effects in Permanent Magnet Quadrupoles*

M. Endres[2] *and M. Schanz*[1,2]
[1]GSI, Darmstadt, Germany; [2]TU Darmstadt

The PRIOR-I (Proton Microscope for FAIR) proton microscope at the GSI experimental area HHT employs a system of permanent magnet quadrupoles (PMQs) for imaging using protons from the SIS-18 accelerator [1]. After the first tests with this particular prototype, the demagnetisation of these PMQs due to primary and secondary radiation was investigated. Therefore, a spare module consisting of several magnetic wedges forming a Halbach Array-type Quadrupole [2] was deliberately irradiated.

Measuring the magnetization direction

In order to measure the hysteresis loops of the irradiated material, samples were cut out of the single wedges. The measurement itself was carried out with a pulsed field magnetometer (Metis HyMPulse)[1] where the magnetization direction of the outer applied field of the magnetometer has to be parallel to the internal field of the sample. This means the surface of the cut sample and the direction of the magnetization have to be parallel. A misalignment could lead to a steep inclination in the flat top region of the loop. The first measurements showed exactly this behaviour. To improve the results, a method for the determination of was developed. A measurement was set up to determine the inclination of the magnetic field at the surface of the wedges. The wedges were scanned with a 1D Hall sensor by the magnet department of GSI. On a path of 30 mm first the Bx component was measured then the sensor was turned by 90 to measure the By component. This was done on the upper and the lower side of the Wedge.

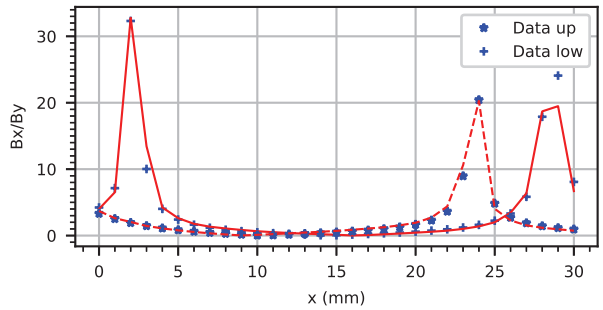

Figure 1: The inclination of the magnetic flux on the lower (full) and upper (dashed) surface of wedge 10 with the best fitting simulation.

This data was compared to simulations [3] of the field of the wedges for different directions of the magnetisation. A fitting routine selected the best fitting pattern of inclinations. With this procedure the magnetisation direction could be determined. For example the magnetization angle of wedge 10 (see figure 1) was found to be 82.5. According to the specification it should be 75. The measured direction differed approximately 7.5 degrees from the specified angles.

Degradation of the HD5 value

Using the known deviations of the magnetization directions the hysteresis loops of different irradiated wedges were measured again. The HD5 value was chosen as a benchmark for the amount of demagnetization. It is given by the intersection of the hysteresis loop itself with 90% of a straight line fitted to the flat top part of the loop. A degradation of the material due to radiation leads to a decreased stability towards a demagnetizing field. This in turn leads to a larger bending of the left section of the loop which also results in a lower HD5 value.

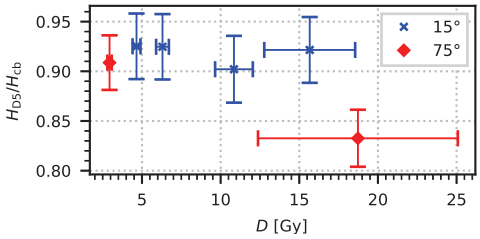

Figure 2: The HD5 values versus the applied dose recorded with Gafchromic films for different segments [4]

The analysis of the hysteresis loops for different wedges revealed that wedges containing a higher internal demagnetization field (type 75) showed a significantly larger degradation of the HD5 value than the wedges from regions with a lower internal demagnetization field (type 15), shown in figure 2. These results and further investigations on the origin of the observed damage were already published [4].

References

[1] D. Varentsov et al, Rev. Sci. Instrum. 87, 023303 (2016)
[2] K. Halbach, Nucl. Instru. Methods 169,1 (1980)
[3] Finite Elements Methods Magnetics (FEMM), Version 4.2, www.femm.info (October 2010)
[4] M. Schanz et al, Rv. Sci. instrum. 88, 125103 (2017)

* Work supported by BMBF (05K13RDB). This report is also submitted to "GSI Scientific Report 2017".
[1]Measurements by K. Löwe (Group Functional Materials, TU Darmstadt)

Progress on the development of an actively cooled glass amplifier at PHELIX

M. Patrizio[1], V. Bagnoud[2,3], B. Zielbauer[2], and M. Roth[1,4]
[1]TU Darmstadt, Darmstadt, Germany; [2]GSI, Darmstadt, Germany;
[3]Helmholtz-Institute Jena, Jena, Germany; [4]FAIR, Darmstadt, Germany

As contribution to FAIR, PHELIX, in cooperation with the Technical University of Darmstadt and funded by the Bundesministerium für Bildung und Forschung (BMBF), is developing an actively cooled glass amplifier for a PHELIX-like laser system planned as a diagnostic tool at the APPA Cave at FAIR. This new amplifier design seeks to improve on the repetition rate of glass disc laser systems to enable more elaborate experimental campaigns [1].

Simulated wave front deformation

Building on the simulations discussed in [2], the temperature distribution in the glass discs can be exported. Considering the temperature induced change in refractive index and expansion of the glass, these temperatures can be converted into a 2D map of the optical path length. From this map the deformation of a plane wave transmitted through the amplifier glass can be calculated (Fig. 1). The simulation results show very low phase deformations after 300 s of cooling. This further encourages development of the concept.

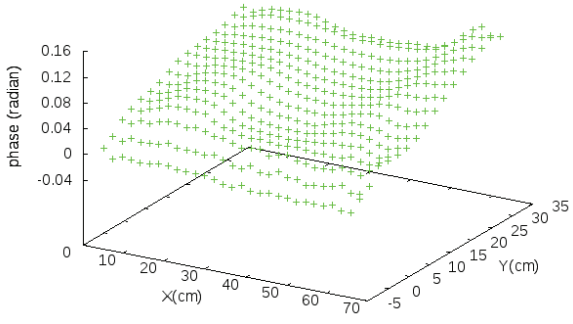

Figure 1: Simulated wave front behind the amplifier after a cooling time of 300 seconds.

Cooling liquids

Extensive research was conducted to find a suitable cooling liquid for our amplifier. During this research the refractive index, absorption coefficient viscosity and chemical compatibility were identified as key parameters of the potential coolant. The heat capacity is negligible due to the low thermal conductivity of the glass. Since data on absorption coefficients is scarce for many liquids, help was acquired from the department of Surface chemistry and spectroscopy at the Technical University of Darmstadt. Their Photo-Spectrometer was used to measure the absorption coefficients for several potential cooling liquids. This was done to assess the viability a perfluorinated hydrocarbons (F2 PP-series). The results are shown in Fig. 2.

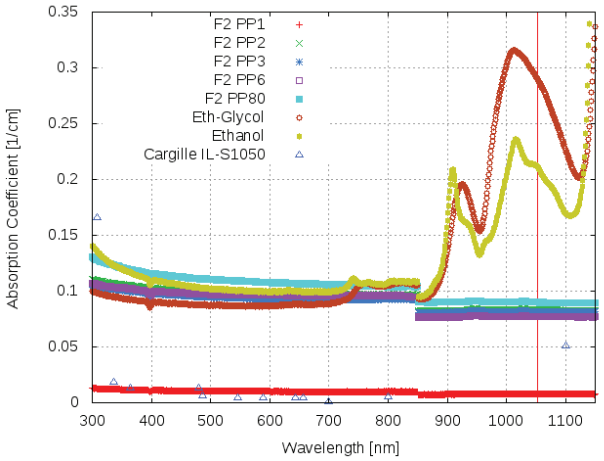

Figure 2: Absorption coefficients of several potential cooling liquids. Measurements conducted at TU Darmstadt, Workgroup Prof. Dr. Hess. Data for Cargille IL-S1050 extracted from data sheet for reference.

Concept Design

The concept calls for a modular design for various prototype configurations, compatibility with the PHELIX infrastructure for potential Phase-0 use, no contact between glass and metal parts to avoid damaging the glass and no bending forces on the glass especially in the direction of the laser beam to avoid additional distortions of the wave front.

References

[1] V. Bagnoud *et al.*, Laser-based pump-probe equipment for the APPA Cave at FAIR, Revision 2.2 (2014) (TDR for the HEDgeHOB/WDM collaborations at FAIR)
[2] M. Patrizio *et al.*, Development of an actively cooled glass amplifier at PHELIX, GSI Scientific Report 2016 (DOI:10.15120/GR-2017-1)

*The content of this report was also submitted to “GSI scientific report 2017"

Indirect Drive ICF Studies on the National Ignition Facility*

The ICF Program Collaboration[1-11]

[1] *Lawrence Livermore National Laboratory, Livermore, CA, USA*
[2] *Laboratory of Laser Energetics, University of Rochester, Rochester, NY, USA*
[3] *General Atomics Corporation, La Jolla, CA, USA*
[4] *Los Alamos National Laboratory, Los Alamos, NM, USA*
[5] *Sandia National Laboratories, Albuquerque, NM, USA*
[6] *Massachusetts Institute of Technology, Cambridge, Massachusetts, USA*
[7] *Atomic Weapons Establishment, Aldermaston, Reading, Berkshire, UK*
[8] *Commissariat à l'énergie atomique et aux énergies alternatives (CEA), France*
[9] *National Security Technologies, LLC (NSTec), Livermore, CA, USA*
[10] *University of California, Berkeley, Berkeley, CA, USA*
[11] *Duke University, Durham, NC, USA*

Current Inertial Confinement Fusion (ICF) implosions of high neutron yield using cryogenically layered deuterium-tritium (DT) filled capsules, are focused on low hohlraum He fill (0.3 mg/cc) targets employing mainly carbon based (high density C – HDC or "diamond", plastic - CH) ablators. These provide low energy losses by laser-plasma instabilities (backscattering) and symmetric implosions that are required to maximize the conversion of implosion kinetic energy into pdV work on the DT fuel and hot-spot, recover 1D implosion scalings, and minimizing the capsule absorbed energy needed to ignite.

During 2017, HDC DT implosions in uranium hohlraums have employed 1 mm radius capsules (8% increase over 2016 experiments) and an extended laser pulse to reduce coasting time (duration between the end of the laser pulse and capsule stagnation time) from 1.4 to ~ 0.6 ns. At similar peak implosion velocities, reduced coasting time up to ~ 0.5 ns results in increased ablation pressure and thus hot spot pressure, for similar hot spot volume and temperature. In these improved implosions we continued assessing the effects of capsule fill tube size, required to insert the DT fuel. Experiments have shown 70% neutron yield increase for 5 µm diameter tubes over 10 µm, hence all high yield implosions going forward on the National Ignition Facility (NIF) employ 5 µm tubes.

These improvements have resulted in new records of fusion neutron yield ($2x10^{16}$ neutrons), fusion energy (56 kJ) and stagnation hot spot pressures (360 GBar), reached simultaneously in ICF implosions on the NIF using up to 1.7 MJ laser energy. Figure 1 shows a summary plot of measured hot spot Brysk temperature (DD ion temperature, same as hot spot electron temperature) vs inferred areal density from data, for all NIF ICF implosions between 2010 and 2017. As shown here, 2017 improved capsule implosions with reduced coasting and smaller 5 µm capsule fill tubes are only ~15% below the modeled 1D static condition required for ignition, that results from balancing the energy gains and losses in the hot spot. The modeled ignition condition has some uncertainty due to hot spot conditions during stagnation that include symmetry and fuel areal density perforations.

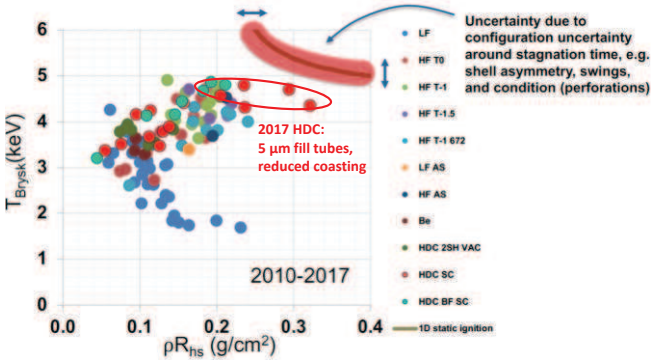

Figure 1: Summary hot spot temperature vs areal density for all ICF DT implosions on the NIF, including 1D ignition static condition. Recent implosions using HDC ablators (bright red and green) and 5 µm capsule fill tubes are very close to the modeled 1D static ignition condition.

Future implosions, based on current designs will strive to continue to improve performance by increasing target size to take full advantage of 2.1 MJ NIF maximum energy, while keeping implosion symmetry under control. Effects of further fill tube size reduction and lowering adiabat (increasing implosion compressibility) on implosions will be also studied.

*This work was performed under the auspices of the U.S. Department of Energy by LLNL under Contract DE-AC52-07NA27344.

Contact E-mail: dewald3@llnl.gov

Future perspectives on Beam Plasma Interaction at Xi'An Jiaotong University

Yongtao Zhao, Jieru Ren Dieter H.H. Hoffmann and Fuli Li
Xi'An Jiaotong University, School of Science, Dept. Laser and particle Beams, Xi'An 710049, Shaanxi, P.R. China

In March 2017 ground-braking for a new science city took place. Within this project Xi'An Jiaotong university (XJTU) will have a new research campus. In November 2017 the bare brickwork was completed. Figure 1 shows the project during construction, when 20000 workers were busy day and night, rain or shine to keep the project on schedule.

The Science and Technology Centre, is a national project by Ministry of Education and Shaanxi Government. It is a new and important platform established by Shaanxi Government and Xi'an Jiaotong University (abbr. XJTU).

Fig. 1: Construction site of the New Xi'An Jiaotong Research Campus

Fig. 2: Layout of the science city. Highlighted (purple) is the research campus and to the right of it the education area.

Moreover it is part of the central government's endorsement to build up greater Xi'An into an "international metropolis. Just some numbers to compare to other science projects worldwide. The science city covers an area of about 3km^2. The total budget cost are roughly 2 billion Euro (15 billion RMB). Completion of the project is scheduled for October 2018 and at the moment everything is on time and budget. The school of science of XJTU will have research facilities at this new campus (see fig, 2) and we plan to set up the low energy beam transport that is planned for the High Intensity Accelerator facility (HIAF), which is a new accelerator complex similar to the FAIR project at GSI. Similar to the FAIR project HIAF will make high beam intensity available for experiments and High Energy Density Physics is one of the key research topics [1, 2].

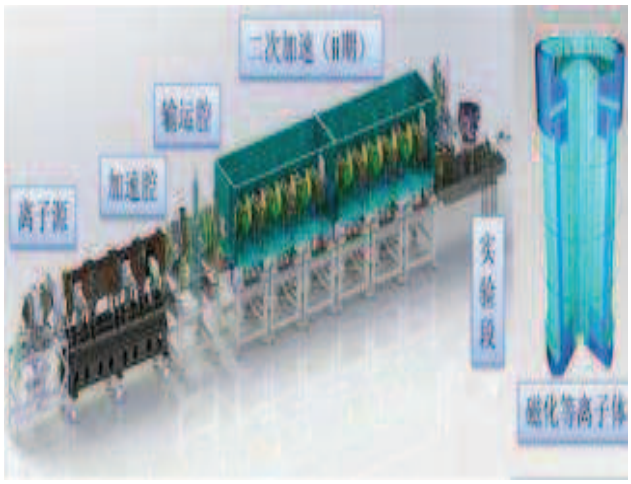

Fig. 3: planned setup u of the low energy beam transport beamline at XJTU. Design by IMP Lanzhou accelerator department

At XJTU we plan to have an intense low energy ion beam with an experimental area for beam plasma interaction experiments and atomic physics issues. The design of the low energy beamline as it is shown in fig. 3 was done by the colleagues from the accelerator department of the Institute of Modern Physics, CAS at Lanzhou. We will equip this with a MEVVA ion source and accelerate heavy ions up to approximately 1 MeV/u. The target station will have a high power laser for beam plasma interaction experiments.

References

[1] Y. Zhao, et al, High energy density physics research at IMP, Lanzhou, China. High Power Laser Science and Engineering, 2, 2014 e39 doi:10.1017/hpl.2014.44

[2] Y. Zhao, XIAO Guo-Qing and LI Fu-Li, The physics of inertial confinement fusion based on modern accelerators: status and perspectives, Physics, 2016, 45(2):8-107

Simulation of phase transition of solid target bombarded by heavy ion beams

Y. Chen[1], R. Cheng [1*], Y.Zhao[2], J.Ren[2], Y. Wang[1], X. Zhou[1], Y. Lei[1], X. Ma[1] and G. Xiao[1]
[1]IMP, Lanzhou, China; [2]XJTU, Xi'an, China

So far, most of the simulation programs related to warm dense matter are hydrodynamics, such as the three-dimensional HYDR primarily for ICF and the one-dimensional DPC [1]. We are currently using one of the one-dimensional hydrodynamic programs named as MEDUSA, which could be used in the research of heavy ion beams driven warm dense matter [2]. In this program, the electrons and the ions are separated into different subsystems and the parameters of pressure, temperature, initial energy, and specific heat rate are considered. The two systems transmit energy through electron-ion or electron-atom collisions. Through the calculation of the deposited energy in the solid target when intense heavy-ion beams impact, the evolutions of temperature, pressure, and other parameters in phase transition are obtained. Meantime, the initial power is calculated by sum of the ions energy losses in the target.

The figure 1 shows an example of the calculated evolution of temperature and pressure respectively of the lead target, when Xe^{20+} ion beams bombard with energy about 0.5 MeV/u, intensity about 2 mA and beam size about 0.6 mm @ LEAF facility at IMP. The result is clear that the heavy ion beams can produce the solid target phase transition. When we increase the intensity, energy and focus the beam size to a critical value, the solid even can be heated to very hot to be a plasma state. If the beam pulse is shorter than the target expansion time, a high-pressure, high-temperature, solid-density, which so-called warm dense matter state may be generated in lab. This is the theoretical basis for ion beam driven high energy density physics at future HIAF project.

The potential energy carried by highly charged ions will be deposited along with the kinetic energy. This additional energy could be huge with beam intensity increase. We take the potential energy deposition into account and the phase transition of lead target is shown in figure 2.

Even it seems that the potential energy could induce a more obvious increase of temperature and pressure than the kinetic energy case. However, the potential energy is thought to be only deposited into the subsurface area and just around the ion tracks through the strong electric interaction. Thus the volume related to potential energy is quite small and it may be hard to be identified in experiment.

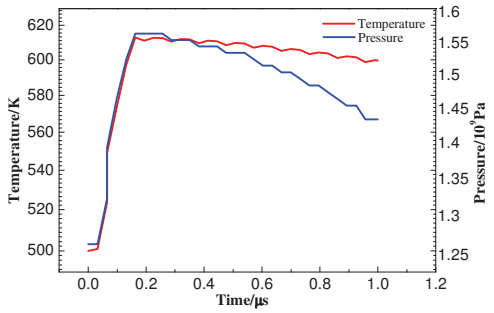

Figure 1: Temperature and pressure change over time when Xe ion beams bombard on lead target

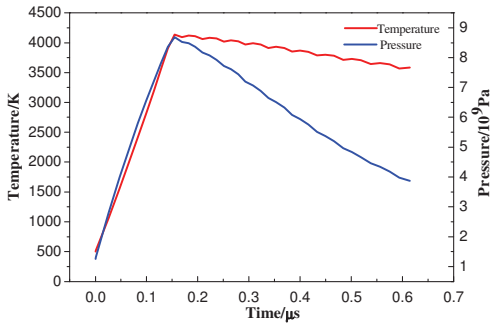

Figure 2: Temperature and pressure change over time when the potential energy deposition is considered of Xe^{20+} ions impact on lead

The theoretical study, as one of the important aspects of high energy density physics research, will be developed to the 2D and 3D simulation programs in next step. The energy loss process of ion beams in matter, as well as potential energy deposition process, will be considered in detail to simulate the whole ion beam driven high energy density matter process in future HIAF project.

References

[1] S. Zhang, et al., High Energy Density Phys., 21, 2016
[2] R. Cheng, et.al., Laser and Particle Beams, doi：10.1017/S02630346180

Supported by the National Key R&D Program of China under Grant No. 2017YFA0402300; National Natural Science Foundation of China (Grant No.U1532263, 11505248, 11775042, 11775278)
*Corresponding person: Rui Cheng, chengrui@impcas.ac.cn

Recent status of the development of the SBS-PCM for high power coherent beam combination laser*

H. J. Kong# and Seongwoo Cha

Department of Physics, KAIST, Daejeon, Korea

Introduction

The highly energetic laser operating at high repetition rate can be applied in various applications, such as laser inertial fusion driver [1] and so on.

However, it is difficult to achieve both a high repetition rate and high output energy in a solid state laser system, because of the thermal effects and the parasitic oscillation in the laser gain medium. One of the most promising techniques to construct a high energetic laser operating at high repetition rate is coherent beam combining (CBC) using stimulated Brillouin scattering phase conjugate mirror [1]. This method combines the available low power laser beams coherently and it becomes possible to achieve the desired output power with CBC. Kong et al. demonstrated coherent 4 beam combination using SBS-PCMs at the W class low average power laser operating at 10 Hz [2].

However, at the high average power of kW class with the high repetition rate over 1 kHz, the thermal load of the SBS liquid medium becomes a serious problem [3]. With high input power and a high repetition rate, the absorbed laser beam changes the refractive index of the SBS medium and defocuses the laser beam at its focal point [4]. This ef-fect reduces the focal spot intensity of the input laser beam and degrades the SBS reflectivity. We report here the re-cent progress of SPC-SBS-PCM for high average power laser using purified HT-110 as an SBS medium.

And also we have demonstrated a pre-pulse technique to preserve the SBS waveform that is distorted by the SBS process.

Experimental Results

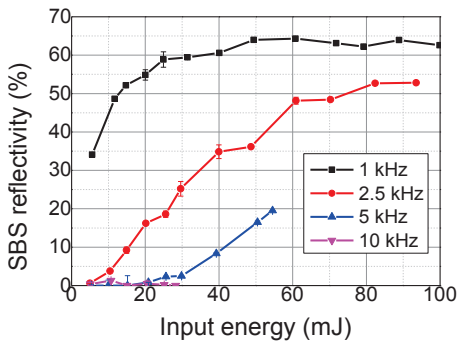

Figure 1: SBS .input energy vs. SBS reflectivity for repetition rates of 1 kHz, 2.5 kHz, 5 kHz, and 10 kHz.

* Work supported by Air Force Office of Scientific Research under award number FA2386-16-1-4133..

#hjkong@kaist.ac.kr

To develop SPC-SBS-PCM, purified HT-110 was used as an SBS medium. Kumgang laser [5] was used to measure the SBS reflectivity and the temporal pulse shape of the SBS reflected beam. Figure 1 shows the experimental results, and the maximum SBS reflectivity was 64% at the input power of 90 W (90 mJ @ 1 kHz.

For the input energy of 10 mJ, the reflectivity at the 1 kHz, 2.5 kHz, 5 kHz, and 10 kHz repetition rate were 49%, 4%, 1%, and 0 %, respectively as shown in the Figure 2.

A pre-pulse technique is applied to preserve the temporal pulse shape for protection of the following optical components. Figure 2 shows the temporal waveforms of the input pulse and the reflected pulses without pre-pulse and with pre-pulse.

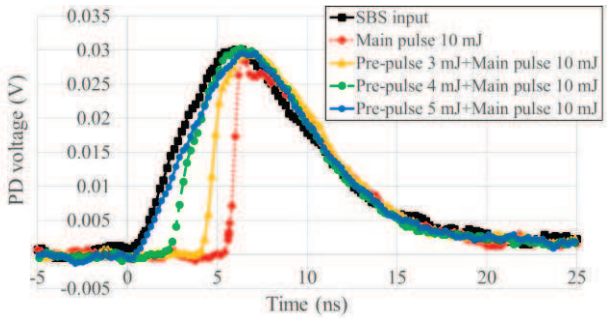

Figure 2: Temporal waveforms of the SBS input and the SBS reflected pulse without and with pre-pulse.

As shown in the figure 2, the pre-pulse relaxes the pulse shortening. When the pre-pulse energy is 5 mJ, the temporal pulse waveform is very similar to the SBS input pulse. However, there remains a jiggling effect in the SBS reflected beam pattern. The jiggling effect in the SBS reflected beam becomes an obstacle for the coherent beam combining. If the jiggling problem is resolved, the dream laser will be realized. Now we are trying to remove the jiggling effect of the SBS reflected wave.

References

[1] H. J. Kong, S. Park, S. ha, and M. Kalal, Opt. Mater. (Amst). 35, (2013) 807.

[2] J. S. Shin, S. Park, H. J. Kong, and J. W. Yoon, Appl. Phys. Lett. 96 (2010)131116.

[3] N. Andreev, E. Khazanov, and G. Pasmanik, IEEE J. Quantum Electron. 28, (1992) 330–341.

[4] H. Yoshida, A. Ohkubo, H. Fujita, and M. Nakatsuka, Rev. Laser Eng. 29(2001) 109.

[5] H. J. Kong, S. Park, S. Cha, H. Ahn, H. Lee, J. Oh, B. J. Lee, S. Choi, and J. S. Kim, Opt. Mater. Express 4 (2014) 2551–2558.

3 Interaction Experiments with Ion- and Laser Beams

Destruction of nanodiamonds under irradiation

V.P. Efremov, E.I. Zakatilova*
JIHT RAS, Moscow, Russia

Introduction

The nanodiamonds formation is existing at extreme actions on the carbon-containing targets. The nanodiamonds distribution on the sizes is function of these actions. In nature the conditions for the formation of diamonds are on the planets giants. At depth about 10000 km from the surface of ice giants (Uranus and Neptune), nanodiamond grains are formed with the diameter about 4 nm [1]. Development of new intense irradiation resources let use new possibilities for obtaining nanodiamonds. So under laser-drive two-stage compression of polystyrene, the pressure is arising up to 150 GPa and the temperature up to 6000 K [1]. In this case, nanodiamonds were found in the sample. In the laboratory conditions at the explosion of TNT/RDX mixture, the nanodiamond grains with the size about 10 nm are detected in the detonation products [2]. These nanodiamonds have unique properties: the high hardness, the high strength, the high thermal conductivity, the high thermal capacity and so on. This substance can be the good filler for composite materials. But, today, there are no valid thermodynamic data for this matter.

The purpose of this article is the data analysis of the radiation damages of the diamond structure.

Radiation stability

Irradiation of single-crystal diamond shows that the formation of graphite phase can form in the ion track [3]. The irradiation by Si^+ ions with energy 1 MeV, at a dose $1*10^{15}$ $Si^+/см^2$, at the room temperature, the point defects are observed in the of diamond. Under irradiation of diamond by Si^+ ions with energy 1 MeV, at a dose $7*10^{15}$ $Si^+/см^2$ the amorphous carbon is formed in the ion track. At the annealing of irradiation sample up to 1350˚C during 24 hours, the transition of amorphous phase to graphite has occurred.

The irradiation of nanodiamond grains by heavy ions creates the amorphous track less density than grains initial density. The calculated densities of irradiation sample demonstrate the radial damages in the range 1 – 4 nm, [4]. In this range the change of density (figure 1a) and of hybridisation of carbon atoms (figure 1b) are observed. The appearance of amorphous phase sp^2 changes electrical conductivity of nanograin and this will allow create grain with unique properties. It was also shown [5] that the character of the damages depends on the grain size.

Sp^3 diamond phase contains essential energy. However, it is very difficult to release it under the normal heating condition. Since diamond is unstable phase, then under external thermal action it passes into graphite with a small amount of energy released. The samples of diamond were irradiated with an integral neutron flux of $3.04*10^{12}$ n/cm^{-2} s^{-1}. About 42.4% of the flux was composed of thermal neutrons with E≤ 0.55 eV, 34.2% epithermal neutrons with 0.55 eV< E≤100 keV and 23.4% fast neutrons with E>100 keV. The accumulation of the point defects occurs [5]. After annealing of the irradiatiated sample in the range of temperatures 230 – 400˚C, significant amount of heat is released. Nanodiamonds exposed by neutrons during 1 hour released 358 J/g , after 2 hours - 387 J/g and finely, the nanodiamond sample exposed during 3 hour - 402 J/g (figure 2) [5].

Thus the analysis of literature data on the irradiation of the diamond phase showed that nanodiamond matter can be a good detector in the targets for identification of processes occurring in the samples under irradiated.

The conditions of structural-phase conversion depend on the types of the action on the substance. Experimentally established, that irradiation can significantly change the conditions of phase conversion (induce a new phase). It affects on the operational characteristics and application of nanodiamonds. The change of the substance structure is one of the important consequences of the irradiation. The irradiation changes the volume characteristics influencing on the phase equilibrium and phase transitions. Before experimental investigation of radiation stability of detonation nanodiamond, the investigations of thermal stability of this matter have carried out.

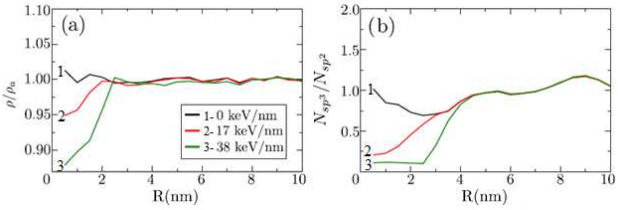

Figure 1: Analysis of the last MD simulation frame for d=7 nm. Top: relative density. Bottom: sp^3/sp^2 fraction. ρ and ρ_a are the local and average densities, respectively [4].

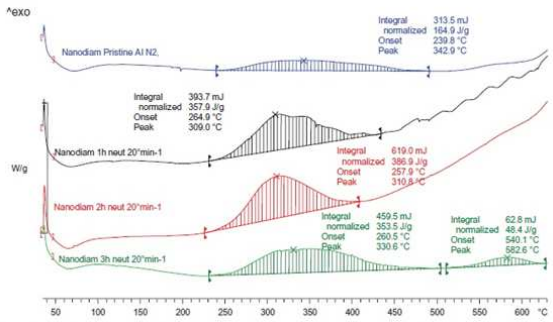

Figure 2: DSC traces of pristine nanodiamond (top, blue, lines), neutron bombarded nanodiamond 1 hour (second trace from top, black lines), 2 hours (third trace from top, red lines), 3 hours (third trace from top, green lines) [5].

*ei.zakatilova@mail.ru

Conclusion

Solid-state transition sp^3 to sp^2 and corresponding changes in the diffraction pattern is perspective for experimental diagnostics. The combination of diamond structure and nanosize with porosity makes it easier for the radiation to exit from the diagnosed area [6]. Such targets with the known thermophysical transition conditions can be used for diagnostic WDM (Warm Dense Matter). The authors thank Dr. Paul Neumayer for the fruitful discussion.

References

[1] D. Kraus, J. Vorberger, A. Pak, N. J. at al Formation of diamonds in laser-compressed hydrocarbons at planetary interior conditions // Nature Astronomy V. 606. 2017. Pp. 606–611.

[2] N.V. SHevchenko, V.A. Gorbachev Perspektivy promyshlennogo polucheniya detonacionnogo nanouglero-da. // Mezhdunarodnaya NP konferenciya «Promyshlen-naya utilizaciya vooruzheniya, special'noj tekhniki i boepripasov». Moskva. «ITER-POLITEKH-2012». S. 335-343.

[3] D.P. Hickey, K.S. Jones, R.G. Elliman // Diamond & Related Materials. 2009. Vol. 18. Pp. 1353–1359.

[4] Felipe Valencia, Jose´ D. Mella, Rafael I. Gonza´ lez and other // Carbon. 2015. Vol. 93. Pp. 458 – 464.

[5] F. Cataldo, G. Angelini, Z. Révay and other // Fullerenes, Nanotubes, and Carbon Nanostructures. 2014. Vol. 22. Pp. 861–865.

[6] O. N. Rosmej, A. Blazevic, S. Korostiy, R. Bock, D. H. H. Hoffmann, S. A. Pikuz, Jr., V. P. Efremov, V. E. Fortov, A. Fertman, T. Mutin, T. A. Pikuz, and A. Ya. Faenov Charge state and stopping dynamics of fast heavy ions in dense matter // Phys. Rev. A. 2005. 72. P. 052901.

Energy penetration of relativistic laser energy into aligned nanowire arrays

C. Bargsten[1], *R. Hollinger*[1], *M. G. Capeluto*[2], *V. Kaymak*[3], *A. Pukhov*[3], *S. Wang*[1], *A. Rockwood*[4], *Y. Wang*[1], *D. Keiss*[4], *R. Tommasini*[5], *R. London*[5], *J. Park*[5], *M. Busquet*[6], *M. Klapisch*[6], *V. N. Shlyaptsev*[1], *and J. J. Rocca*[1,4]

[1]Department of Electrical Computer Engineering, Colorado State University, Fort Collins, Colorado 80523, USA; [2]Departemento de Fisica, Universidad de Buenos Aires, Buenos Aires, Argentina; [3]Institut für Theoretische Physik, Heinrich-Heine-Universität Düsseldorf, 40225 Düsseldorf, Germany; [4]Department of Physics, Colorado State University, Fort Collins, Colorado 80513, USA; [5]Lawrence Livermore National Laboratory, Livermore, CA 94551, USA; [6]ARTEP Inc., Ellicott City, MD 21042, USA

The creation of ultra-high energy density (UHED, $> 1 \times 10^8$ J/cm^3) plasmas in compact laboratory setups enables studies of matter under extreme conditions and can be used for the efficient generation of intense x-ray and neutron pulses. An accessible way to achieve the UHED regime is the irradiation of vertically aligned high-aspect-ratio nanowire arrays with relativistic femtosecond laser pulses. These targets have shown to facilitate near total absorption of laser light several micrometers deep into near-solid-density material. We investigate the depth of the volumetric heating [1].

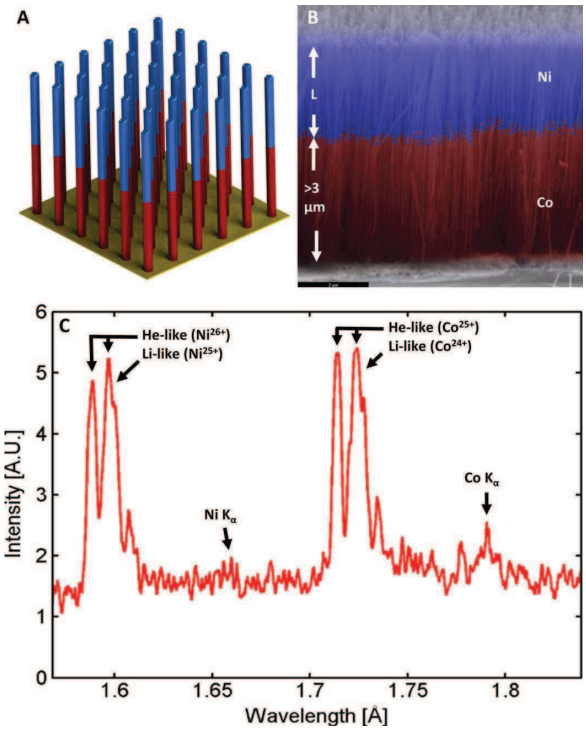

Figure 1: A. Sketch, B. scanning electron microscopy image and C. emission spectrum of a dual composition nanowire array made of nickel and cobalt [1].

Using composite nanowires made of nickel at the tip and cobalt at the bottom, one can monitor the emission of He- and Li-like lines in both these segments in the spectrum (Fig. 1). The length of the cobalt base is 3 μm, and the length of the tip was kept variable. As long as the tip is short enough to let the laser energy heat flow down to the cobalt segment, there will be a He-like signal from both parts. Lengthening the nickel tip, a decrease of the cobalt signal is expected. The heat depth can be found at the transition at which the signal of the tracer material Co vanishes. The experimental results (Fig. 2) show that this happens at a nickel tip length between 4 μm and 5 μm, revealing that the heat penetration depth is at least 4 μm.

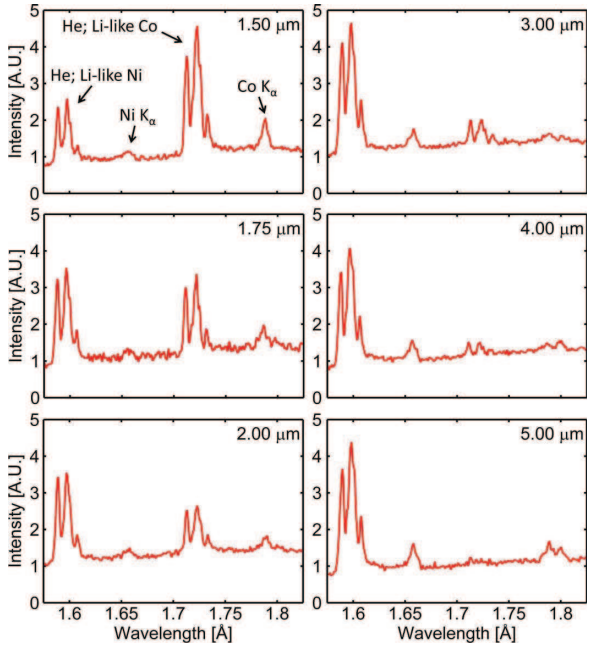

Figure 2: Experimental emission spectra of the dual composition Ni-Co nanowire array for different lengths of the nickel tip (indicated in the upper right corner) [1].

Synthetical emission spectra generated by using PIC simulations are in a good agreement with the experimental spectra [1].

References

[1] C. Bargsten et al., Sci. Adv. 2017; **3**:e1601558

Acceleration of plasma-propelled flyer plates*

S. Sander[1], J.H. Hanten[1], M.M. Basko[2], An. Tauschwitz[3], G. Schaumann[1], D. Schumacher[4], A. Blazevic[4] and M. Roth[1]

[1]Technische Universität Darmstadt, Institut für Kernphysik, Darmstadt, Germany; [2]Keldysh Institute of Applied Mathematics RAS, Moscow, Russia; [3]Goethe Universität, Frankfurt, Germany; [4]GSI Helmholtzzentrum für Schwerionenforschung GmbH, Darmstadt, Germany

Introduction

Man-made space debris is exponentially increasing in the low earth orbit, posting a big threat on current and future space missions [1]. To remove this space debris, high velocity impacts (v > 10 km/s) of tungsten balls with a presumed momentum transfer factor of ~10-15 are proposed to slow down space debris [2]. Thereby, it will decrease in orbit und burn up in the atmosphere sooner.

Experiment

For preliminary experiments in this area of high velocity impacts, a special target design has been developed as seen in figure 1. The objective is the acceleration of a high velocity, solid state tungsten flyer plate for future impact experiments.

Previous experiments, using different target designs, failed to show an acceleration of the flyer but suggested an evaporation of the tungsten disk. Therefore, a target design which allows for a completely free flyer is developed. The target consists of three layers. The bottom layer is a 270 µm thick polyethylene (PE) sample. A steel spacer of 200 µm thickness and with a 500 µm diameter hole is glued on top of the PE. The hole is covered with a tungsten disk with a diameter of 600 µm and 25 µm thickness. In this setup, the to be accelerated disc is completely free and not glued to any structure.

The experiments are performed at the target area Z6 at GSI, where the nhelix laser system is used to drive a shock wave into the PE. After the shock breakout, the material expands through the hole and hits the disk. This is supposed to accelerate the tungsten to high velocities, while retaining its solid stat. As the target is driven from below, a completely new beam path is put in place. The beam is guided through the bottom flange and focused with a lens and random phase plate onto the PE. A laser energy of 2 J is used to ensure the integrity of the accelerated disk.

The targets rear side is observed with two DICAM Pro in a side view configuration with a relative angle of 90° between them. In figure 2, the recorded images can be seen. A background is subtracted to enhance the visibility of the disk for one of the cameras (figure 2a). The disk is observed in flight in both images. The disk clearly rotates, which is thought to originate from a non-uniform plasma expansion inside of the steel spacer. From the two different images and the time delay a velocity of about 110 ± 4 m/s is deduced. With a streak camera the disk movement is observed over a time window of 1000 ns around the expected time of acceleration. The movement speed was determined by linear approximation to 100 ± 30 m/s.

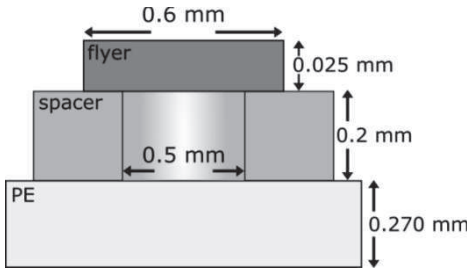

Figure 1: Schematic of the layered target design. A steel spacer is glued on top of a polyethylene foil (PE). The flyer is made of tungsten and placed without fixation. The target is driven from below, accelerating the plasma and flyer upwards.

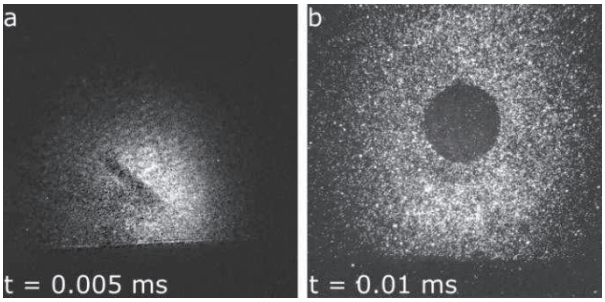

Figure 2: Recorded images of the two DICAM Pro. Abackground image is subtracted from image (a) to increase visibility. The flyer is clearly seen in both images, rotating rather than flying straight up.

Simulation

Simultaneously, hydrodynamic fluid simulations in two dimensions are performed with the RALEF code [3,4], to fur-ther study the target. These simulations with a laser energy of 2 J are in good agreement with the measured velocities, calculating the flyer velocity to 101 m/s. In addition, the simulations suggest a fluid pressure of 19 kbar inside the tungsten. This value closely corresponds to the tensile strength of tungsten, explaining previous failures of the tar-gets driven with higher intensities.

References

[1] D. McKnight, D. Kessler, IEEE Spectrum, Retrieved (2012)

[2] G. Ganguli et al., Aerospace Conference, 2012 IEEE (2012)

[3] M. M. Basko, J. Maruhn, A. Tauschwitz, J. Comp. Physics, 228, (2009)

[4] M. M. Basko, J. Maruhn, A. Tauschwitz, GSI-Report 2010-1, PLASMA-PHYSICS-25 (2010)

* This report is also submitted to “GSI scientific report 2017”

Strong Terahertz radiation generated in intense laser-foil interactions

Yutong Li[1,2#], Guoqian Liao[1,3], Weimin Wang[1], Zhengming Sheng[3,4] and Jie Zhang[3]
[1]Beijing National Laboratory for Condensed Matter Physics, Institute of Physics, Chinese Academy of Sciences, Beijing 100190, China
[2]School of Physical Sciences, University of Chinese Academy of Sciences, Beijing 100190, China
[3]Key Laboratory for Laser Plasmas (MoE) and Department of Physics and Astronomy, Shanghai Jiao Tong University, Shanghai 200240, China
[4]SUPA, Department of Physics, University of Strathclyde, Glasgow G4 0NG, United Kingdom

Over the last decades relativistic electron beams from conventional accelerators have been applied to generate strong THz radiation through transition radiation [1], free electron lasers, synchrotron radiation and the Smith Purcel effect. Relativistic electron beams can also be generated in the interactions of intense laser pulses with low-density gas or high-density solid targets. With the energetic electron beam accelerated by wakefields in gas target, Leemans *et al.* have observed a ~0.3 μJ THz pulse through transition radiation [2].Compared with the gas targets, electron beams from solid targets have much higher charge, up to nC-μC. For a foil target, fast electrons transport forward through the target and will induce transition radiation when crossing the rear surface-vacuum boundary. Usually the bunch length of the fast electrons driven by a laser pulse in tens of femtosecond duration is of the order of ~10 μm, which is smaller than the wavelength of THz radiation. This will lead to the coherent transition radiation (CTR) [3]. One can expect that the THz radiation energy will be high due to the high charge and short bunch duration of the fast electron beam as well as the steep foil-vacuum boundary.

To verify this idea, we have carried out laser-foil experiments using a multi-TW femtosecond laser system at Shanghai Jiao-Tong University and the Vulcan PW laser system at the Rutherford Appleton Laboratory. For fs experiment, a *p*-polarized laser pulse in 30 fs and 2 J was incident onto solid targets at an incidence angle of 54° with a peak intensity of ~1.5×10^{19} W/cm^2. The laser prepulse contrast in the ns range is ~10^{-5}. Different types of targets were used in the experiment, including mass-limited metal targets with different sizes, polyethylene (PE)-metal double-layered targets and single PE targets.

In our experiment we demonstrated intense THz transition radiation of the laser-accelerated relativistic electron beams crossing the solid rear surface (see fig. 1). The total THz energy from the rear of metal foils is estimated to be ~400 μJ/pulse for the fs experiment, comparable to the energy level of the conventional accelerator based THz sources [4]. The corresponding energy conversion efficiency from the laser pulse energy on targets to THz radiation is ~2×10^{-4}. It can be well explained by the model of CTR considering the effects of diffraction radiation and formation zones [5].

In the experiments with the Vulcan ps laser system, we have much enhanced the THz pulse energy. According to the experimental measurements and calculated spatial distribution of THz radiation, the total energy of THz pulses emitted from the target rear, at a pump laser energy of ~60 J, is determined to be ~55 mJ within 3 THz. This corresponds to a peak power of ~36 GW and a laser-THz energy conversion efficiency of ~0.1%. To our knowledge, this is the highest THz pulse energy and peak power reported so far.

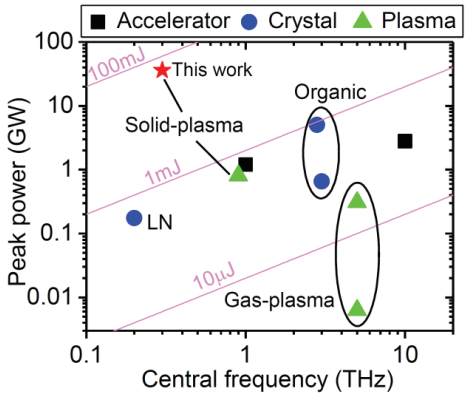

Fig.1 Comparison of currently available high-peak-power THz sources. The data are from previously reported typical results based on conventional accelerators (black square), optical rectification from crystals (blue circle) like lithium niobate (LN) and organic crystals, and gas/solid-density plasmas (green triangle). The red star represents the data presented in this paper.

The laser-plasma-based THz transition radiation presented could be a promising compact strong-field THz source. Moreover, it may provide us a new tool to diagnose forward fast electrons in laser-plasma interactions.

References

[1] U. Happek, A. J. Sievers, and E. B. Blum, Phys. Rev. Lett. 67, 2962 (1991)
[2]W. P. Leemans et al., Phys. Rev. Lett. 91, 074802 (2003); C. B. Schroeder, E. Esarey, J. van Tilborg, and W. P. Leemans, Phys. Rev. E 69, 016501 (2004)
[3]W. J. Ding, Z. M. Sheng and W. S. Koh, Appl. Phys. Lett. 103, 204107 (2013)
[4]Z. Wu *et al.,* Rev. Sci. Instrum. 84, 022701 (2013)
[5]Q. Q. Liao *et al.*, Phys. Rev. Lett. 116 205003 (2016)

#ytli@iphy.ac.cn

Heavy ion acceleration using short pulse lasers*

G. M. Petrov and T. A. Mehlhorn
Naval Research Laboratory, Washington, DC, USA

Heavy ion beams are of interest for many applications such as nuclear reactions, production of super-heavy elements, exotic isomers and isotopes for biomedical use, fast ignition fusion, radiation effects in materials, medical applications and studies of exotic phenomena such as systems relevant to the interior of stars. Traditionally, heavy ion beams are produced by particle accelerators, which are enormous in size and expensive ($billions). In recent years, short pulse lasers emerged as an alternative to conventional accelerators, being more compact and significantly less expensive ($million), affordable for Universities and small organizations. It is based on the fact that short pulse lasers (fs-ps) at relativistic intensities (>10^{18} W/cm^2) become particle accelerators. We present a theoretical study of heavy ion acceleration from ultrathin (20-500 nm) gold foils irradiated by high-intensity sub-picosecond lasers. Two-dimensional particle-in-cell simulations are used to model the interaction between laser pulse and target response in a self-consistent way. We explored different ion acceleration mechanisms ranging from the conventional Target Normal Sheath Acceleration (TNSA) to the more advanced acceleration schemes such as radiation pressure acceleration (RPA) and relativistic induced transparency (RIT) to unravel the fundamental physics of heavy ion acceleration and quantify the properties of the ion beam [1,2]. Sample results are shown in Figures 1 and 2 for peak laser intensity 3×10^{21} W/cm^2, pulse duration 32 fs and laser energy 27 J. The target is a 20 nm Au foil.

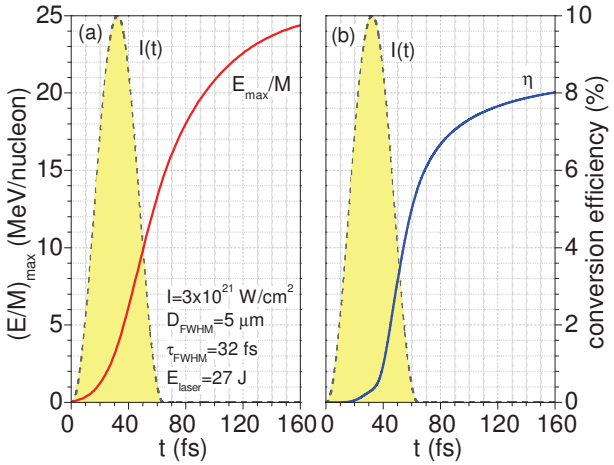

Figure 1: Maximum energy (a) and conversion efficiency into gold ions (b) vs. time. The yellow shaded area is the laser pulse profile.

We focus on the most important ion beam characteristics, specifically maximum ion energy, conversion efficiency, ion charge distribution and flux in the forward direction.

*Work supported by the AFOSR

The conversion efficiency into Au ions is 8 % (Figure 1). The charge distribution of Au ions, shown in Figure 2, indicates highly charge ions with "q" of up to ~70. This is because the pulse can both ionize the material to these high charges due to optical field ionization and accelerate the ions simultaneously. The maximum and average charge-to-mass ratios for Au ions are 0.3 and 0.25, respectively. The Au ion spectrum is shown in Figure 2, right. Ions with energy of up to 5 GeV are generated, which corresponds to reduced energy of E/M=25 MeV/nucleon.

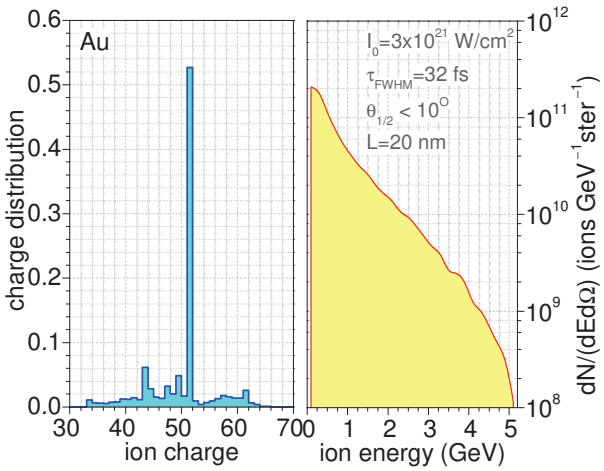

Figure 2: Charge distribution of >100 MeV gold ions (left) and ion flux in the forward direction (right) for ions within 10 degrees from target normal.

In conclusion, short pulse lasers can indeed be used for generation of energetic and directed heavy ion beams from high-Z materials such as Au and Ag. By systematically studying the physics of laser-target interactions at various laser and target parameters, we established that but there are also some limitations specific to heavy ion acceleration. By far the most important one is the available laser energy: for successful outcome the laser energy on target must be at least 20 J.

References

[1] G. M. Petrov, C. McGuffey, A. G. R. Thomas, K. Krushelnick, and F. N. Beg, Phys. Plasmas **23**, 063108 (2016)

[2] G. M. Petrov, C. McGuffey, A. G. R. Thomas, K. Krushelnick and F. N. Beg, Plasma Phys. Control. Fusion **59**, 075003 (2017)

Short, Intense Ion Pulses using NDCX-II and BELLA-i*

P.A. Seidl[1], J. Bin[1], J.J. Barnard[2], E. Bielejec[3], S.S. Bulanov[1], E. Esarey[1], A. Friedman[2], D. Grote[2], W.P. Leemans[1], K. Nakamura, Q. Ji[1], J. Park[1], A. Persaud[1], D.W. Raftrey[1], C. Schroeder[1], A.D. Stepanov[4], S. Steinke[1], F. Treffert[5], B. Vaandrager[3], W.L. Waldron[1], and T. Schenkel[1]

[1] LBNL, Berkeley, California, USA [2] LLNL, Livermore, California, USA
[3] SNL, Albuquerque, NM, USA [4] U. Washington, Seattle, WA, USA
[5] TU Darmstadt, Darmstadt, Germany

Reproducible high intensity ion pulses enable the exploration of radiation effects on materials under high dose rate [1], and also the creation of novel material properties [2]. Helium ions in the Neutralized Drift Compression Experiment (NDCX-II) are accelerated and compressed in an induction accelerator [3], making high perveance and low emittance ion beams, attractive for exploring basic beam physics of general interest, and relevant to the high-current, high-intensity ion beams needed for heavy-ion-driven inertial fusion energy. By choosing the ion mass and kinetic energy to be near the Bragg peak, dE/dx is maximized and a thin target may be heated with high uniformity and specific energy deposition. The NDCX-II peak ion current delivered to the target is up to 2 Amperes of 1.1 MeV He^+ with $7x10^{10}$ He^+ ions/pulse, and a peak fluence of $2x10^{20}$ ions/cm^2/s.

In the past year we have used intense ion pulses to provide neutron equivalent damage rates and fluences that may significantly benefit the characterization of transient radiation effects in electronics, of importance in applications such as space electronics and high-intensity particle accelerator electronics [4]. We have characterized the late time gain degradation of bipolar junction transistors where over tens of shots (or in some cases a single shot) the transistor gain is systematically reduced from $G > 100$ to $G \approx 1$. New comparisons to lower intensity studies show dose-rate effects for equivalent total doses. In related experiments, we have irradiated PIN diodes with varying doses and dose rates to probe the effect on leakage current and charge collection efficiency.

More recently we have demonstrated the ability to generate intense pulses of protons up to 1.1 MeV, enabled by the flexible timing of the induction acceleration pulsed power system. As a first application of this capability, the optical density of radiochromic film (RCF) has been calibrated for high doses beyond the range of published calibrations. The experiments covered doses from 100 Gy to 10^5 Gy. The proton beams will soon be applied to radiation effect studies of semiconductor devices and radiation biology experiments.

In order to measure ion energy loss in materials, including while driving phase-transitions during the ion pulse, we have augmented the target diagnostics with a Thomson parabola [5], see fig. 1 for a Titanium target.

A new capability at Berkeley Lab, BELLA-i generates high intensity short ion pulses through laser-plasma acceleration [6], and experiments have shown $>10^{11}$ ions with kinetic energy Above 2 MeV and up to 7-8 MeV [7]. Various ion species may be chosen based on the target. As an example of first experiments, results on radiation effects on transistors are being analyzed. The BELLA petawatt laser [8] repetition rate is 1 Hz. By employing the capacity to rapidly change the target samples, measurement campaigns with many thousands of shots are possible, making BELLA-i a versatile platform to study a wide range of topics with precision, including novel laser-plasma ion acceleration mechanisms [9], plasma science, materials science, radiation biology, and high energy density physics.

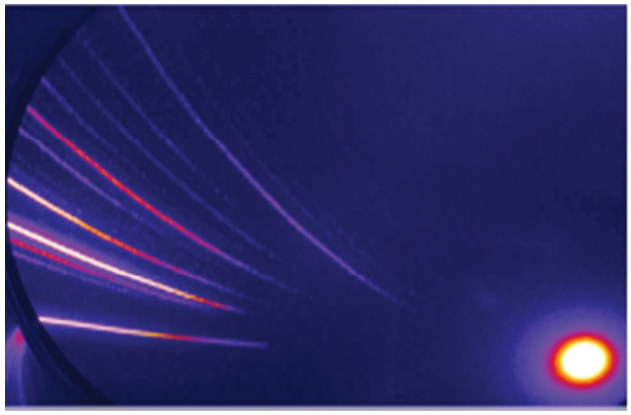

Figure 1: Thomson parabola measurement of the particle energy distribution of a Bella-i ion beam pulse from a Titanium target. Charge states up to Ti^{11+}, C^{5+}, O^{6+} have been measured.

References

[1] A. Persaud, et al., *Phys. Procedia* **66** (2015) 604
[2] A. Bienfait, et al., *Nature Nano.* doi:10.1038/nnano.2015 (2015)
[3] P.A. Seidl, et al., Laser & Particle Beams, doi:10.1017/S0263034617000295 (2017)
[4] B.A. Ludewigt, et al., J. Radiation Effects, Research and Engineering **36** (1) (2018)
[5] F. Treffert, et al., arXiv:1804.03318 (2018)
[6] C. Toth, et al., AIP Conf. Proc. **1812**, 110005 (2017); doi: 10.1063/1.4975918
[7] S. Steinke, et al., manuscript in preparation.
[8] K. Nakamura et al., IEEE J. Quantum Electron. 53 (2017) 1200121.
[9] S.S. Bulanov, et al., Proc., IPAC2016, WEOAB01, http://accelconf.web.cern.ch/AccelConf/ipac2016/papers/weoab01.pdf

* This work was supported by the Office of Science of the US Department of Energy under contract DE-AC0205CH11231 (LBNL), and DE-AC52- 07NA27344 (LLNL).

Study on a dense and high ionized plasma for ion beam stripping*†

P. Christ[1], *K. Cistakov*[1], *T. Ackermann*[1], *A. Blazevic*[2], *A. Fedjuschenko*[1], *R. Gavrilin*[3], *M. Iberler*[1], *T. Manegold*[1], *L. Manganelli*[1], *O. Rosmej*[2], *S. Savin*[3], *K. Weyrich*[2], *G. Xu*[1], *and J. Jacoby*[1]

[1]Goethe University, Frankfurt, Germany; [2]GSI, Darmstadt, Germany; [3]ITEP, Moscow, Russia

After a positive "proof of concept" with the screw-pinch and the spherical theta-pinch at a beam time at GSI in 2014 [1, 2], a revised version of the theta-pinch has been developed and built for future research [3].

Figure 1 shows a first spectroscopic diagnostic on this revised design illustrating a time-averaged peak electron density of about $1.8 \cdot 10^{16}$ cm^{-3} at 60 Pa and 20 kV, from which a maximum momentary electron density of $1 \cdot 10^{17}$ cm^{-3} is inferable. To gain an even higher electron density, the

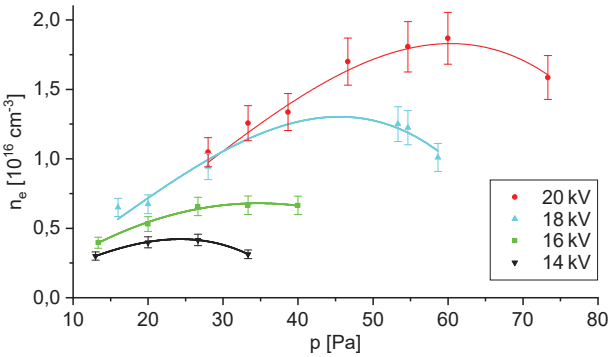

Figure 1: Time-averaged electron density at different pressures and load voltages. Image by L. Manganelli.

load voltage will be increased up to 35 kV. According to a linear behaviour of the maximum electron density and the discharge energy [4], a maximum momentary electron density of approximately $5 \cdot 10^{17}$ cm^{-3} and an advance of the electron temperature from 1 eV up to 4 eV is expected from the increased discharge energy.

Furthermore, the spiral shape of the new coil enhances the ion beam transmission due to a more symmetrical magnetic field and the axial plasma exhalation displaces undesired residual gas extending the plasma ion beam interaction zone. The new design has been tested for its serviceability at GSI in 2016 and will be applied at a beam time at GSI in 2018. Besides researchers form Goethe University, Frankfurt, this beam time will be conducted by scientists from ITEP, Moscow, IMP, Lanzhou and IUAC, New Delhi, who are studying on the same topic.

For a better understanding of the plasma processes, multiple time-resolved spectroscopic diagnostics as well as a laser interferometry are intended. The interferometric diagnostic will be based on previous investigations stated in [5]. Since a high electron density of the order 10^{17} cm^{-3} is expected and to limit the influence of beam refraction, short wavelengths in the visible range are favoured.

During interferometric test measurements on a small-scale z-pinch, a suspected disturbing influence of electromagnetic noise has occurred. Consequently, a sufficient metallic shielding of the interferometer and its vulnerable electric components in a separate set-up as well as an improvement of the signal-to-noise ratio are designated. To carry the laser beam, a fibre connection will be investigated. Figure 2 shows a first draft of the interferometer for future time-resolved measurements of the electron density. A novel combination of an acousto-optic heterodyne

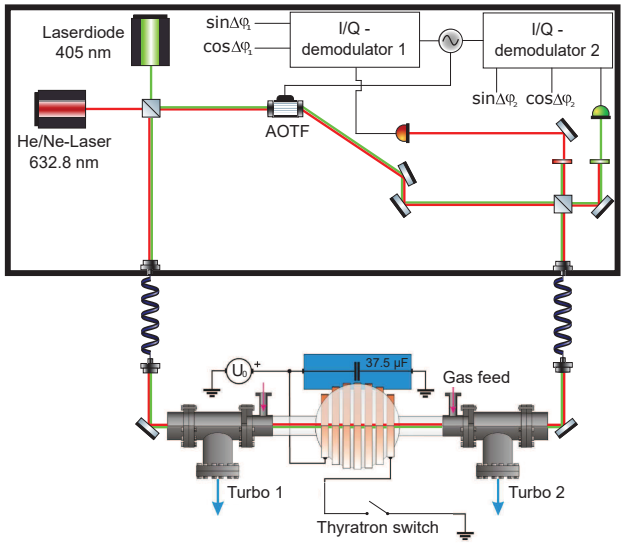

Figure 2: First draft of the future interferometer set-up. Image by P. Christ.

technique and a two-colour vibration compensation with wide separated wavelengths is illustrated. An acousto-optic tuneable filter (AOTF) is intended for maintaining the required collinearity of the wavelengths. In case of a negligible vibrational contribution compared to the plasma contribution, the second wavelength could be utilized to estimate the ionization degree, offering the opportunity for a high precision electron temperature measurement.

References

[1] G. Xu et al., Phys. Rev. Lett. **119**, 204801 (2017).

[2] G. Xu et al., GSI SCIENTIFIC REPORT 2014, APPA-MML-PP-16.

[3] K. Cistakov et al., GSI SCIENTIFIC REPORT 2016, RESEARCH-APPA-PP-22.

[4] C. Teske et al., Physics of Plasmas **19**, 033505 (2012).

[5] P. Christ, Master thesis, 2017.

* This report is also submitted to the GSI Scientific Report 2017.

† Work supported by BMBF, HIC4FAIR, HGS-HIRe.

Low energy ion beams modification by plasma wake field

R. Cheng[1]*, F. Gao[2], Y.Zhao[1,3], Z.Hu[2], X.Zhou[1], Y.Chen[1], Y.Lei[1] Y. Wang[1], J. Ren[3], X.Ma[1] and G.Xiao[1]

[1] IMP, Lanzhou, China; [2]DUT, Dalian, China; [3]XJTU, Xi'an, China

Ion beam is an import tool to understand some properties of plasma itself. Ion-plasma interaction as a very import topic in atomic physics, astrophysics and initial confinement fusion related sciences has been investigating for decades. An enhanced energy loss and the higher charge state distribution of ions in plasma than in cold matter have been reported [1-2]

Our collaborators from DUT have simulated the wake filed generation by the ion beam passing through a plasma and figured out the circular beam could be modified to a hollow beam, as well as the continue beam to the pulsed structure.

Figure 1 shows the 2D PIC simulated results of the longitudinal distribution of plasma electrons and the corresponding distribution of beam ions, where the effect of two-stream instability between ions and plasma electrons are taken into account [3].

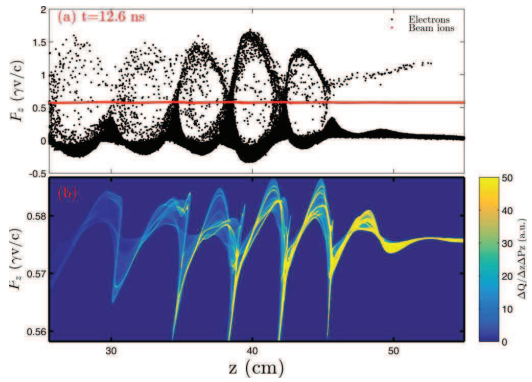

Figure 1: Longitudinal distribution of plasma electrons and the corresponding beam ions

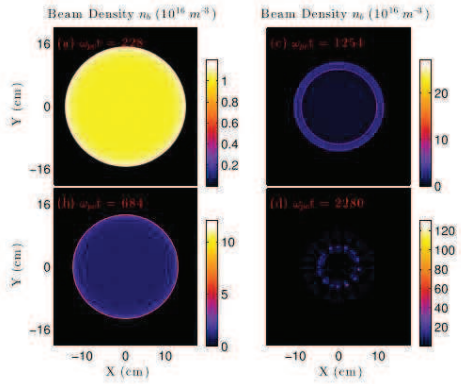

Figure 2: The temporal density evolution of a proton beam which has the radius of $r_b = 12c/\omega_{pe}$ in a plasma

Moreover, the ring structure can be formed due to the transverse focusing magnetic field induced by the unneutralized beam current in the beam edge region. Even a second ring structure appears in the case of ion beams with a radius much larger than the plasma skin depth, due to the polarity change in the transverse magnetic field in the central regions compared with the outer, focusing field [4], see figure 2.

In order to experimentally investigate the modification effect of plasma wake field on ion beam, the ion-plasma interaction platform at IMP is upgraded. A 2.2 m long RF plasma device is installed, which can produce the plasma of temperature about 4-6 eV and free electron density about $10^{13}cm^{-3}$ (see fig. 3). A 4x4 mm^2 SC dia-mond detector is placed at the end of beam line and the time resolution for ion is about1.2- 1.8 ns. A large position-sensitive detector is developed to measure the beam spot and a 1.2 Tm bending magnet is employed to analyze the energy loss and charge state of ion beams.

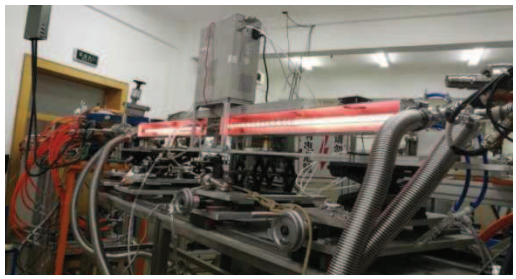

Figure 3: The 2.2 m long RF plasma device, a SC dia-mond detector, a large position-sensitive detector, and a new bending magnet are installed at ion-plasma interaction platform at IMP

The new Theta-pinch plasma and ps-laser induced plasma are developing too and soon the interaction process between the low- and middle energy heavy ion beams and the different kinds of plasmas can be experimentally investigated.

References

[1] R. Cheng, et.al., Laser and Particle Beams, doi: 10.1017/S0263034618000010

[2] G.Xu, et.al., PRL 119, 204801 (2017)

[3] Z.Hu et.al., Phys. Plasmas 23, 083118 (2016)

[4] Z.Hu et.al., Phys. Plasmas 24, 123103 (2017)

Supported by the National Key R&D Program of China under Grant No. 2017YFA0402300; National Natural Science Foundation of China (Grant No.U1532263, 11505248, 11775042, 11775278)

*Corresponding person: Rui Cheng, chengrui@impcas.ac.cn

Ion stopping in hydrogen plasma experiment at linear accelerator at ITEP

R.O Gavrilin*, S.A. Visotskiy, A.O. Khyrchiev, D.S. Kolesnikov, R.P. Kuibeda, P.A. Fedin, A.L. Sitnikov, A.V. Kantsyrev, I.V. Roudskoy, S.M. Savin, A.A. Golubev, A.P. Kuznetsov
NRC «Kurchatov Institute» - ITEP, Moscow, Russia

Introduction

Investigation of ion stopping in an ionized matter is important for obtaining new knowledge in high energy density in matter and plasma physics. Especially interesting is the investigation of the interaction of heavy ions with low energy range from 40 to 500 keV/u with strongly ionized low-temperature hydrogen plasma [1,2]. The experimental setup was developed at ITEP on heavy ion RFQ linac (HIP-1), an ion energy is 101 keV/u [3].

Plasma target

Plasma target (PT) was developed at ITEP [4], plasma in PT ignited by electrical discharge in two coaxial quartz tubes. The capacitor bank with charging voltage range from 2 to 5 kV produces the discharge of hydrogen with maximal current up to 3 kA. The initial pressure of hydrogen is from 1 to 10 mbar.

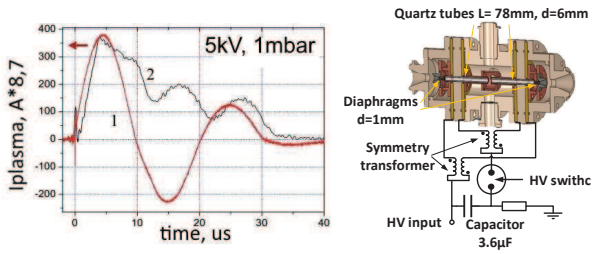

(a) (b)

Fig.1: (a) Example of PT current form (1) and plasma luminosity (2), (b) PT principal scheme

As laser interferometry measurement [5] showed the linear free electron density of plasma is in the range from $3{,}3*10^{17}$ to $1{,}3*10^{18}$ cm^{-2}. For the plasma temperature measurement will be applied spectrometry method. PT diagnostic planned in the near future.

Experimental setup

PT was installed at HIP-1 beamline (fig.2). As projectile ions were used Fe^{+2}, value of beam current after RFQ section was up to 4 mA, with pulse duration 450 μs. Beam microstructure (microbunch) presented on fig.3b is caused by 27,7 MHz frequency. Hydrogen pressure in PT was from 0,5 to 4,5 mbar, depends on differential pumping system parameters. Beam current was from 4 to 30 μA. For current measurement was used Faraday cup. Time of flight method (TOF) was applied for energy loss measurement. Detector system consists of a fast Al_2O_3 based scintillator and Photomultiplier Hamamatsu R760. The time resolution of registration system 0,8 ns.

Experimental data processing and analysis

The Fourier analysis [6] and filtering was used to obtained of useful signal (fig.3a,b). The processing

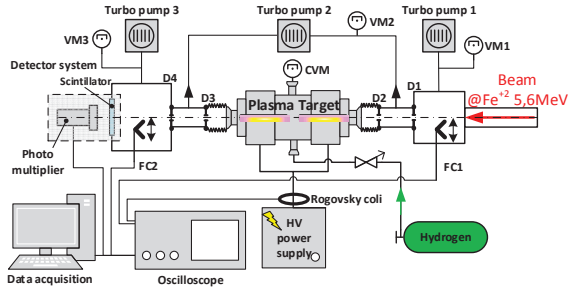

Fig.2 Experiment scheme. FC1,2 - Faraday cups, D1-4 diaphragms of differential pumping system d = 1-3mm, CVM - gas independent vacuum-meter

procedure provides calculates of ions time delaying dT (temporal shift of peak of microbunches in relation to accelerator radiofrequency signal (RF). The data processing also includes correction of microbunches peak value positions in local regions of signal with insufficient signal-to-noise ratio and curve fitting of dT distribution in plasma discharge area. Example of data processing results is represented at fig.3c.

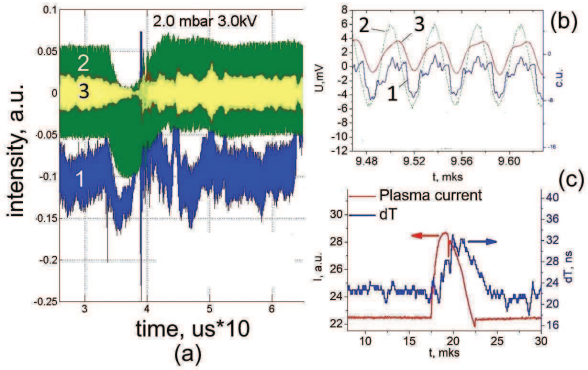

Fig.3 (a,b) 1 - raw photomultiplier signal, 2 – accelerator RF signal, 3 - Fourier correction of row signal. (c) – plasma current(left) and microbunch shift dT(right) compared in time

At the present time, the experimental data are being processed and analyzed.

References

[1] C. Deutsch, G. Maynard, M. Chabot et al., The Open Plasma Physics Journal 3, 88-115 , (2010);
[2]R.O. Gavrilin et al., GSI Report 2016-2, p.18
[3] V. Kulevoy et.al, in Proceedings of International Topical Meeting on Nuclear Research Applications and Utilization of Accelerators, Vienna, 4–8 May 2009
[4] A. Golubev, V. Turtikov, A. Fertman et.al, Nucl. Instr. An d Meth. A, V. 464, (2001), p. 247
[5] A. P. Kuznetsov et al., Plasma Physics Reports, 2013, Vol. 39, No. 3, pp. 248–254
[6] *Müller Meinard.* The Fourier Transform in a Nutshell. — Springer, 2015. — ISBN 978-3-319-21944-8.

*Email: roman_gavrilin@mail.ru
Supported by RFBR grand №18-02-00967

Stopping of laser-accelerated ion beam in a foam-plasma

Y. Zhao[1,2,#], J. Ren[1], W. Liu[1], X. Wang[1], R. Cheng[2], X. Zhou[2], Z. Deng[3], S. Wang[3], Q. Fan[3], W. Qi[3], Y, Zhang[4], Z. Zhang[4], W. Zhou[3], L. Cao[3], Y. Gu[3], Y. Li[4]

[1]Xi'an Jiaotong University, Xi'an China; [2]Institute of Modern Physics, CAS, Lanzhou, China; [3]Laser Fusion Research Center, CAEP, Mianyang, China; [4]Institute of Physics, CAS, Beijing, China

Introduction

The accurate understanding of heavy ion stopping process in wide range plasma is essential in field of DT-alpha transportation, heavy ion inertial confinement fusion, and ion-driven fast ignition. In last decades, amount of experiments about the ion stopping has been done in high energy region, and the experimental data agrees quite well with theories. However, in low energy region especially when the ion velocity is comparable to the average thermal electron velocity of plasma, namely near Bragg peak, the experimental studies are very limited [1-3], and different theories shows great deviation, which are in high demand to be benchmarked. In this report, we presented our preliminary experimental results about the energy deposition of MeV ions in dense plasma.

Results

Experimental Setup: The experiment was carried out at Laser Fusion Research Center, Mianyang. The experimental setup was shown in figure 1. Here, ps laser with energy of 119 J was used to generate heavy ions such as protons and carbon ions. The ns laser with energy of 127.3 J was used to drive hohlraum radiation to uniformly heat CH foam, forming foam plasma. The detailed structure about the hohlraum and the foam could be found in [4]. The density of CH foam is 2 mg/cm^3, which is supposed to be nearly constant in 10ns after the ns laser shot [4]. The thickness of the foam is 1 mm, The hohlraum has a diameter of 1 mm. The height of the hohlraum is 1.8mm, and the diameter of the hole on the hohlraum wall for the laser shot is 0.7 mm. The energies of laser-accelerated ions passing through foam plasma were measured with Thomson Parabola. The energies of ions passing through vacuum were measured simutaneouly for energy loss analysis. Transmission grating spectrometer and flat-field grating spectrometer were used respectively for the hohlraum and foam plasma temperature diagnostic. X-ray diodes with and without filter were used to moniter the hard and soft X-ray flux. The XRD signal indicates that the effective heating time for the foam target is 6 ns after the ns laser beam shot. Therefore, in the experiment, the delay time for the ps and ns laser is set as 5ns. The radiation

Experimental Results: The hohlraum radiation showed perfect Planckian distribution. The wavelength at maximum intensity (λ_m ~ 12.91 nm) corresponded to the temperature of 19 eV according to Wien displacement law. Besides, the transitional lines of $C^{4+,5+,6+}$ from foam plasma were observed with the flat-field spectrometer. This would give hints for the foam temperature, which is just under analysing.

The laser-accelerated ions were deflected by electric and magnetic field in the Thomson Parabola. The deflection image was shown in the left of figure 2. Through analysing the electric deflection, the energy distribution of the laser-accelerated ion passing through vacuum and foam plasma was shown in the right of figure 2. It can be seen that the energy loss was surprisingly large, which is far above the Bethe-Bloch predictions. The influence of electric and magnetic field in plasma will be considered for the disagreement.

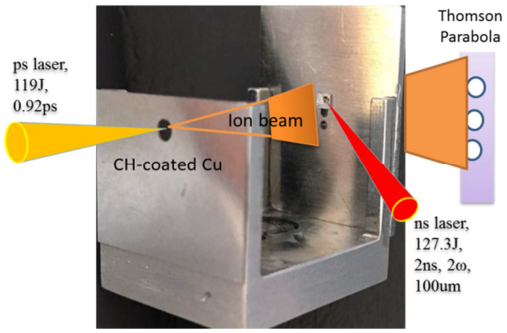

Figure 1: Experimental Setup

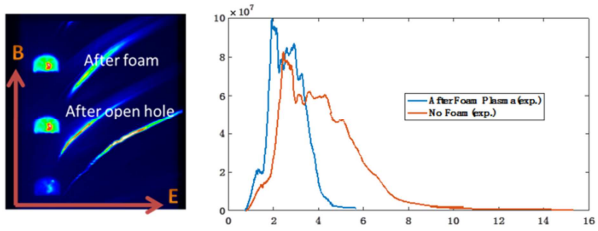

Figure 2: Energy distribution of laser-accelerated ion passing through vacuum and foam plasma

References

[1] C. Witold et al., "Experimental discrimination of ion stopping models near the Bragg peak in highly ionized matter", Nat Commun. 8(2017), 15693.

[2] J. A. Frenje et al., "Measurements of Ion Stopping Around the Bragg Peak in High-Energy-Density Plasmas", Phys. Rev. Lett. 115 (2015), 205001.

[3] A. B. Zylstra et al., "Measurement of Charged-Particle Stopping in Warm Dense Plasma", Phys. Rev. Lett. 114 (2015), 215002.

[4] O. Rosmej et al., "The hydrodynamic and radiative properties of low-density foams heated by x-rays", Plasma Phys. Control. Fusion 57 (2015) 094001.

* Work supported by Science Challenge Project No. TZ2016005

#zhaoyongtao@xjtu.edu.cn

Multiple ionization induced by low energy proton

X. Zhou[1], R. Cheng[1]*, Y. Wang[1], Y. Lei[1] , Y. Chen[1], Y. Zhao[1,2], X. Ma[1] and G. Xiao[1]

[1]IMP, Lanzhou, China; [2]XJTU, Xi'an, China

X-ray emission, an important consequential result from such collisions, involves several inner-shell processes, from primary ionization by the incoming ions, up to the subsequent vacancy decay, including intra-shell transition. Thus, the detailed knowledge of x-ray emission provides important information to understand the complex ionization mechanism and test relevant theories. Furthermore, accurate values of x-ray production cross section are needed for the applications of Particle Induced x-ray Emission (PIXE) technique in the trace element analysis.

Multiple ionization may occur during ion-atom collisions by concurrent or subsequent effect, accompanying with the single ionization of inner-shell electrons. That can reduces the screening of nuclear charge and affects the radiative transition rate due to the presence of some outer-shell vacancies. As a result, it will causes energy shift of the corresponding x ray and change of the relative intensity of sub-shell x rays. Several authors have investigated this effect when heavier projectiles are used, and the similar phenomenon has been discussed in our previous work. However, the case of proton is still largely unexplored. In fact, it is possible as observed in the present work and the studies of Cipolla et al and Miranda, et al and so on.

Here, special attention will be devoted to Nd L-subshell x-ray emission by the measurements at the 320 kV high voltage experimental platform at Institute of Modern Physics, Chinese Academy of Sciences (IMP, CAS) in Lanzhou. Emission of the neodymium $L\gamma_2$ x ray is discussed by the multiple ionization effect. L-subshell x-ray production cross sections of Nd are measured and compared with various theoretical calculations along with different atomic parameter databases.

In fig.1 the typical x-ray emission spectrum of Nd produced by 200 keV proton impact is presented and well fitted using a Gaussian fitting program, and compared with that induced by photon. Although the spectrum for different kind of incident particle is similar, there is an obvious enhancement of the $L\gamma_2$ x-ray emission induced by proton, compared to that for photon radiation.

Such abnormal emission of $L\gamma_2$ can be interpreted by the multiple ionization. When it occurs, since the transition probability of the Auger transition and CK transition are affected due to the absence of some outer-shell electrons, the fluorescence yield could be altered. Consequently, the relative intensity ratio of sub-shell x ray will be changed.

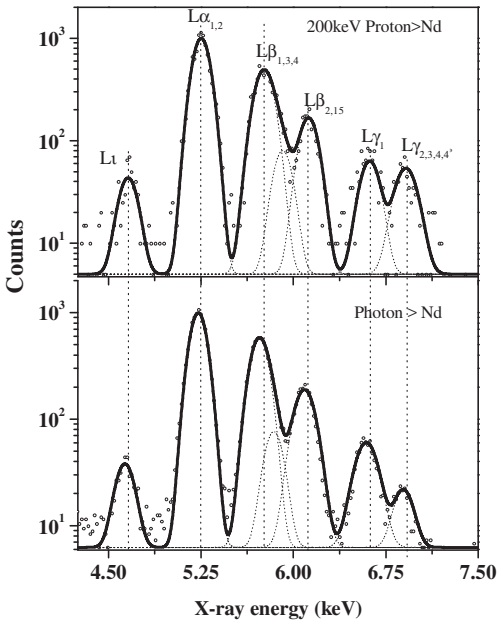

Fig. 1: Characteristic L x-ray spectra of neodymium for proton and photon impacting

In addition to relative intensity change of subshell x rays, line shift of the characteristic x ray is another possible result of multiple ionization. When it occurs, the screening of the nuclear is reduced as the absence of outer-shell electrons. Binding energy of the remaining orbital electrons is increased. This leads to the measured x ray shifting toward the high energy side. It is found that energy of the Six L-subshell x ray for Nd induced by proton are all larger than the values of the singly ionized atom and the experimental data of photon which is nearly the same as theoretical calculation apart from $L\gamma_1$. That provides an authentic evidence for the multiple ionization of Nd by proton and supports the explanation for abnormal emission of Lg_2 x ray.

Supported by the National Key R&D Program of China under Grant No. 2017YFA0402300; National Natural Science Foundation of China (Grant No.U1532263, 11505248, 11775042, 11775278)

*Corresponding person: Rui Cheng, chengrui@impcas.ac.cn

Tomographic reconstruction target at a proton radiography experiments

V. Panyushkin[1#], A. Kantsyrev[1], A. Golubev[1], A. Skobliakov[1], A. Bogdanov[1], D. Kolesnikov[1]
[1]NRC «Kurchatov Institute» - ITEP, Moscow, Russia

Algebraic tomography methods [1] allow reconstructing of internal structure of an object from proton-radiographic images made at several angles of rotation of an object relative to a beam axis. Tomographic reconstruction methods can be applied at radiobiological proton-radiographic experiment (PaNTERA experiment) at PRIOR facility [2].

Algebraic reconstruction technique (ART) [1] was chosen for reconstructing target structure. As a test object for ART was chosen Shepp-Logan phantom Fig.1 (large dynamic range of variation of the density and the presence of areas with large and small differences of density).

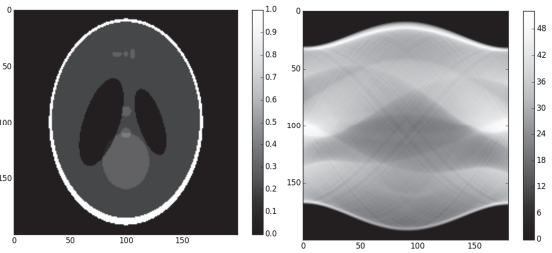

Fig.1: Shepp-Logan phantom (left), sinogram (right)
The reconstruction error depends on the number of projections (for test object with 60 projections – 4.2%, for 90 – 3%, for 180 – 1%)

In this work tomographic reconstruction was used for processing of Monte-Carlo numerical simulation results obtained with proton radiography setup with 247 MeV beam at Geant4 code [3]. Total number of protons at modelling is $5 \cdot 10^8$ per projection. A cylindrical (20 mm diameter) PMMA (ρ=1,19 g/cm^3) target [4] (Fig.2) with three large (5 mm diameter) holes filled by test substances and one small size (1 mm diameter) hole filled by high-density material as marker was chosen for numerical simulation. Depending on the configuration of the target, large holes were filled with one of the materials: aluminium (ρ=2,7 g/cm^3), bone tissue (ρ=1,45 g/cm^3), muscle tissue (ρ=1,11 g/cm^3), water (ρ=1,0 g/cm^3). The marker can be filled with copper (ρ=8,96 g/cm^3).

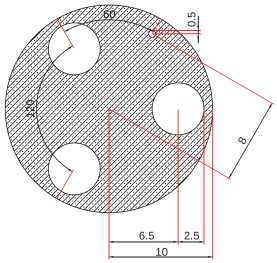

Fig. 2. Drawing of the target

Monte Carlo calculations were performed for three target configurations:

1. bone tissue (1), muscle tissue (2), water (3); copper (4);
2. bone tissue (1), muscle tissue (2), water (3); 4-th is not filled;
3. aluminum (1,2,3); 4-th is not filled;

As a result of the calculations, 180 projections was obtained with an angular step 1°, the axis of rotation coincides with the axis of symmetry of the target; examples of single proton-radiographic images are shown in Fig. 3.

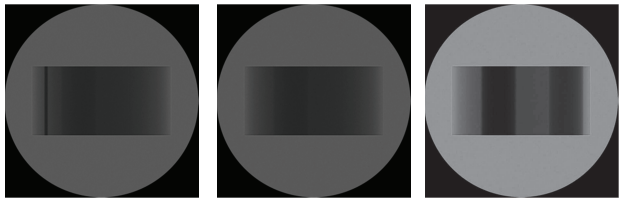

1) 2) 3)

Fig.3:Examples of single proton-radiographic images for three target configurations

The reconstructed images of the transverse sections in Fig. 4. These result shows that for a given energy (247 MeV), the contrast is sufficient to discriminate objects when difference in areal density is about 5%.

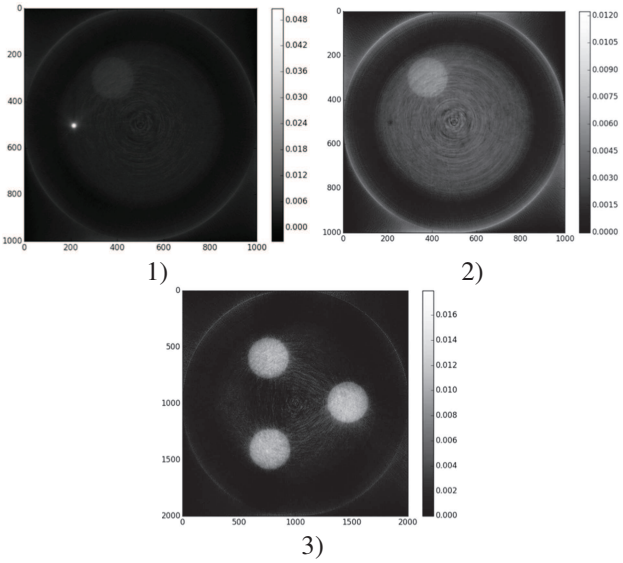

1) 2)

3)

Fig. 4: Result of tomographic reconstruction of target

References

[1] R. Gordon et al., Journal of Theoretical Biology. 29(3), 471–81. doi:10.1016/0022-5193(70)90109-8.
[2] D. Varentsov et al., PRIOR - Proton Microscope for FAIR, Technical Design Report, October 2016.
[3] A.V. Kantsyrev et al., J. Phys.: Conf. Ser. 2018, 946, 012019.
[4] M. Schanz et al., GSI Report 2017-2, p.34.

*Work supported by grant of FAIR-Russia Research Center and RFBR grant 18-38-00708
Vsevolod.Panyushkin@itep.ru

4 Radiation-, Particle- and Plasma Sources

Characterization of hard X-ray sources for radiographic purposes at the PHELIX laser*

B. Borm[1], J. Hornung[2], D. Khaghani[2,3], P. Neumayer[4]

[1]Goethe-Universität Frankfurt, Germany; [2]Helmholtz-Institut Jena, Germany; [3]Friedrich-Schiller-Universität Jena, Germany; [4]GSI, Darmstadt, Germany

High-energy high-intensity lasers – like the Petawatt Laser for Heavy Ion Experiments (PHELIX) at GSI – are a formidable tool to create hard X-ray sources with extraordinary properties. These are mainly the short emission duration, which is in the same order of magnitude as the laser pulse duration, the small source size, which is defined by both the target geometry and the laser focus size, and the spectral distribution which extends into the several 100 keV range [1,2]. All of these properties make laser-based hard X-ray sources very suitable for radio-graphy of hydrodynamically evolving high-Z high-density plasmas, like they will be produced in the future plasma physics experiments at FAIR (e.g. LAPLAS). Since the emitted X-ray spectrum depends on a variety of experi-mental parameters, particularly the laser intensity and the target geometry, a full characterization of the source prop-erties is an appropriate step to reliably predict radio-graphic imaging performance.

We have performed an experiment at the PHELIX laser with the goal to determine the emission characteristics of bremsstrahlung X-ray sources regarding spectral and angular distribution, depending on the laser intensity and contrast and on the target geometry. Furthermore, the source sizes were measured. The laser intensity was varied between 4.1×10^{16} and 1.1×10^{20} W/cm², the contrast between the "low" of 10^{-6} and the high of $<10^{-10}$. Two target types were used: gold foils of 5 µm thickness and tungsten wires of 5 µm diameter. Bremsstrahlung was detected by a set of 12 hard x-ray spectrometers, placed in the horizontal and vertical around the target (white tubes in Fig. 1). Using imaging plate detectors and a set of tantalum filters, the spectrometer working range is 20-400 keV. The attenuated signal was fitted by a Maxwellian energy distribution with two effective temperatures to retrieve conversion efficiencies (CEs) from laser energy to x-ray emission into the 70-200 keV range. Source sizes were determined using a gold knife-edge imaging setup with 1 µm spatial resolution.

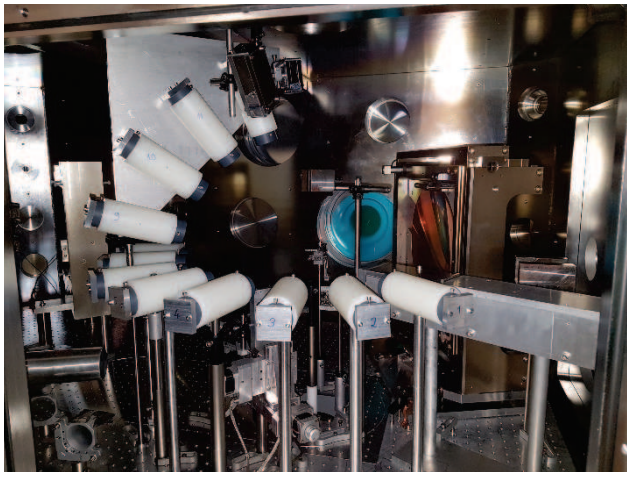

Figure 1: Hard x-ray spectrometer array to determine the emission distributrion of the laser-driven x-ray source.

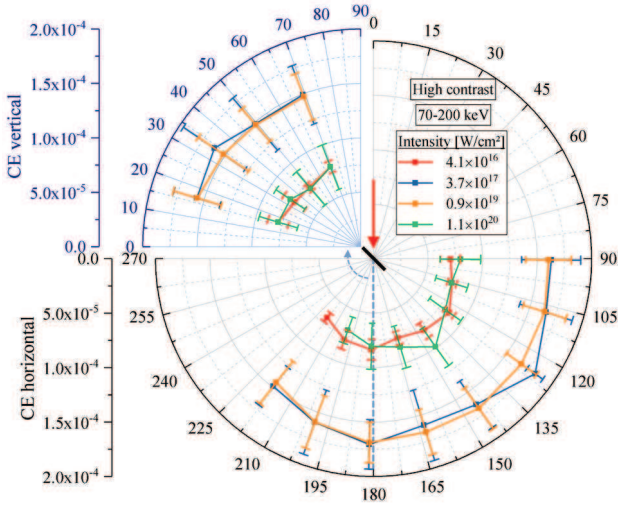

Figure 2: Angular dependency of the CE

We find that bremsstrahlung up to 400 keV is emitted isotropically, independent of laser intensity and contrast (see Fig. 2) and target type. The CE however rises between the lower two intensities used, then drops again for the highest by a factor of around 2. The CE is systematically higher for the low contrast laser pulses by up to a factor of 2. On average, we determined a CE into the 70-200 keV interval of $(1.5\pm0.2)\times10^{-4}$ at 0.9×10^{19} W/cm² and high contrast using gold foil targets.

The source sizes measured in the thin direction of the foil targets varied between 3.7-12.0 µm. On average, wire targets at high contrast showed 5 µm source size, exactly their diameter. In a follow-up experiment, this laser-generated x-ray source has enabled x-ray phase contrast imaging of laser-driven shock waves.

References

[1] R. Tommasini *et al.*, Physics of Plasmas. **18**, 056309 (2011)

[2] L. Antonelli *et al.*, GSI Scientific Report 2017

* also published in 'GSI Scientific Report 2017'

Cone Compression of a Pulsed Plasma Sheath*

T. Manegold[1], *S. Faik*[1], *C. Benzing*[1], *P. Tavana*[1], *J. Wiechula*[1], *M. Iberler*[1], *and J. Jacoby*[1]
[1]Goethe University of Frankfurt, Frankfurt am Main, Germany

Introduction

Coaxial plasma accelerators (CPA's) have been investigated in the past in different experimental configurations, with several applications, such as space propulsion [1] or as a high voltage switch [2]. The purpose of the presented project is the application as an intense UV/VUV back lighter source. The wavelength spectrum of the emitted light depends on the excited states, whereas the intensity is in correlation to the electron density. The plasma sheath of the utilized CPA has been characterized in [3]. To increase electron density and to extend the emitted spectrum to lower wavelengths, the plasma is compressed by a glass cone after acceleration phase.

Experiment and Results

The experiment is driven by a CPA, whose pulse forming network has a total capacitance of $27\,\mu$F with a maximum voltage of $10\,$kV. Due to the high current of up to $150\,$kA, the Lorentz force accelerates the plasma to velocities in the $10\,\frac{\mathrm{km}}{\mathrm{s}}$ range. The electron density determination of the uncompressed plasma has been performed time and spatially integrated by the common method of linear Stark-broadening of the H_β line. This method is however only applicable at the beginning of the compression. Then, due to the high electron densities, this line is broadened too widely to be utilized. As an alternative, the broadening according to the quadratic Stark-effect of a copper line at $479.40\,$nm was applied. It was possible to cross calibrate this line with the H_β line. Doing so, we obtain

$$n_e\,[\mathrm{cm}^{-3}] = (3.07 \pm 0.475) \cdot 10^{18} \cdot \Delta\lambda_S\,[\mathrm{nm}] \qquad (1)$$

In a first cone, which is characterized by an opening at the tip of $5\,$mm and a tapering angle of $26.5°$, the electron density could be increased from initially several $10^{15}\,\mathrm{cm}^{-3}$ in the uncompressed plasma cloud to about $10^{18}\,\mathrm{cm}^{-3}$ at the tip of the cone at a charging voltage of $9\,$kV and a Helium gas pressure of $15\,$mbar.

Two-dimensional hydrodynamic simulations of the compression have been performed with the RALEF-2D code. According to these simulations (Fig. 1), the electron density can even be increased by changing the cone parameters to a tiny opening of $0.5\,$mm and a tapering angle of $12°$. The discrepancy of the density values between simulation and experiment is assumed to be unobserved by the highly time dependant changes and radiation losses, not taken into account in the code. The experimental results of the electron density at $U = 5\,$kV and $p = 5\,$mbar are depicted in

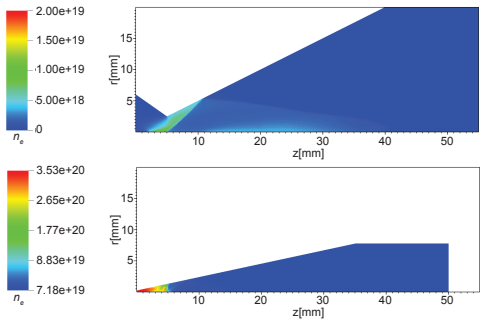

Figure 1: Simulation of electron density at the time of maximum value in first cone (top) and optimized cone (bottom).

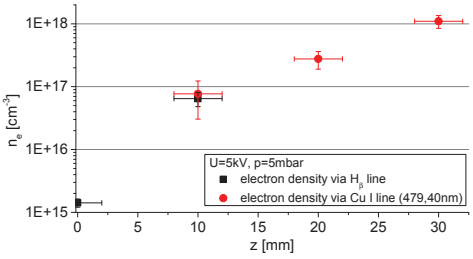

Figure 2: Electron densities in the optimized cone

Fig. 2 in dependence of the position z. As can be seen, although voltage and gas pressure are reduced, an optimized cone compressed the plasma to electron densities comparable to the values of the first cone at $9\,$kV and $15\,$mbar. Compared to the uncompressed values, the compression increases the electron density by about a factor of 630.

Additionally, the observed emitted wavelength has expanded at higher densities from wavelengths above $97.25\,$nm to a wavelength range starting already at approximately $53.70\,$nm. Our next step is to replace the fragile glass by a different material to be able to perform the compression at higher voltages and pressures to increase electron density even more. According to the RALEF-2D simulations, this could increase the compressed density by a further order of magnitude.

References

[1] D. Y. Cheng, "Application of a deflagration plasma gun as a space propulsion thruster", AIAA Journal, vol. 9, no. 9, pp. 1681-1685, Sep. 1971.

[2] M. Iberler, et al., "Optical and electrical investigations of a high power Lorentz drift based gas discharge switch", IEEE ICOPS, June 2008, p. 1.

[3] T. Manegold, et al., "Generation and characterization of a pulsed dense plasma with Helium", IPMHVC, pp. 580584, July 2016.

* This report is also submitted to the GSI Scientific Report 2017

Generation and transport of heavy ion beams at LIGHT*

J. Ding[1], D. Schumacher[2], D. Jahn[1], C. Brabetz[2], F.E. Brack[3,4], F. Kroll[3,4], R. Leonhardt[1], I. Semmler[1], U. Schramm[3,4], T.E. Cowan[3,4], A. Blazevic[2], V. Bagnoud[2], M. Roth[1,6]

[1]TU Darmstadt, Darmstadt, Germany; [2]GSI, Darmstadt, Germany; [3]TU Dresden, Dresden, Germany; [4]HZDR, Dresden, Germany; [5]HI Jena, Jena, Germany; [6]FAIR, Darmstadt, Germany

The LIGHT collaboration has been founded to provide a testbed for Laser Ion Generation, Handling and Transport [1]. The laser ion generation is based on the Target Normal Sheath Acceleration (TNSA) mechanism and is driven by the PHELIX 100 TW beam line at GSI. A pulsed solenoid captures and collimates a divergent ion beam coming from the TNSA-driven ion source. By means of chromatic focusing one can cut out a part of the exponentially decaying energy spectrum. The resulting collimated beam can be compressed in phase or energy in a radiofrequency (rf) cavity which is situated two meters behind the ion source. The resulting ion beam is then diagnosed with a diamond detector for a temporal analysis of the achieved phase focus at a distance of six metres from the target.

After a successful first demonstration of the generation, handling and transport of fluorine ions in 2015 [2] and a subsequent campaign in 2016 [3] with small optimizations for the resulting ion beam, two campaigns in 2017 were dedicated to the generation and characterization of a TNSA-driven carbon ion source and the transport and bunching of the resulting ion beam. Figure 1 depicts the energy spectrum of the central part of the carbon ion beam, measured with a Thomson Parabola 0.6 m behind the target.

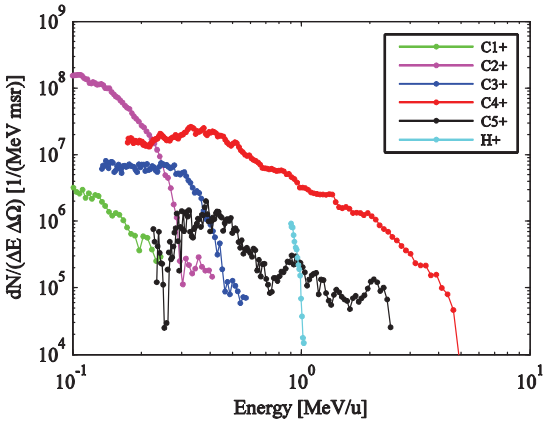

Figure 1: Energy spectrum of TNSA-driven carbon ion source. C4+ dominates the spectrum from 0.5 MeV/u on.

By heating the target up to around 1000 °C one successfully removed most of the hydrogen contaminations on the target surface and enabled efficient acceleration of heavy ions. In the process carbon ions of all charge states, barring 6+, were accelerated together with the remaining hydrogen. From figure 1 it is obvious, that carbon ions with charge state 4+ dominated the beam, from 0.2 MeV/u up to the cut-off energy at around 3.5 MeV/u.

Collimation and transport of the carbon ion beam was achieved with a pulsed solenoid, capable of delivering up to 10 T. From the thin lens approximation in equation (1) one can derive, that all generated charge states are transported through the beamline at varying energies. With future applications such as energy loss measurements of heavy ions in hot and dense plasmas in mind, the transport energy was set to around 1.2 MeV/u. For this purpose the solenoid was pulsed with 8.92 kA, leading to a maximum magnetic field on axis of 6.72 T.

$$\frac{1}{f} = \frac{q^2}{m^2}\frac{1}{4\gamma^2 v^2}\cdot\int B^2 dz \qquad (1)$$

The ion beam was diagnosed with a fast diamond detector. The result is shown in figure 2, where the Time-of-Flight (ToF) data was converted to kinetic energy and the signal has been rescaled due to the related change of bin widths. This also causes a significant rise of the noise level at low ion energies. Simulations with TraceWin, taking space charge into account, show that mainly C4+ was transported with the previously described solenoid configuration and beamline setup. In the simulations the solenoid was modelled as a current-carrying coil. The good agreement of TraceWin simulations with ToF data serves as benchmark for future simulations.

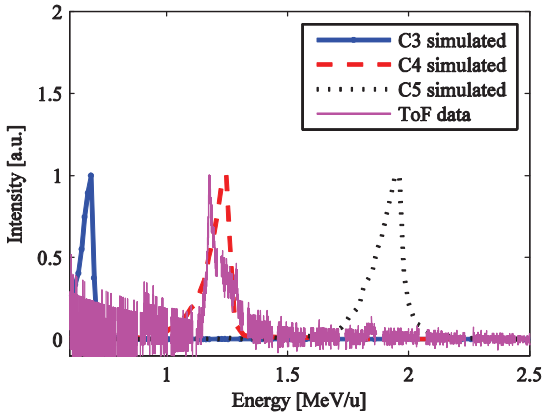

Figure 2: ToF data of diamond detector converted to energy spectrum of transported carbon beam at a solenoid current of 8.92 kA. For decreasing energy the noise per bin increases.

In two successful beam times in 2017, we were able to characterize an efficient TNSA-driven carbon ion source and demonstrate transport and energy collimation of carbon ions in our LIGHT beamline.

References

[1] S. Busold et al., NIMA 740, 94-98 (2014)
[2] J. Ding et al., HEDgeHOB annual report 2015
[3] J. Ding et al., HEDgeHOB annual report 2016

* This report is also submitted to “GSI scientific report 2017”

Final focussing of collimated proton beams with the laser-driven LIGHT beamline *

D. Jahn[1], *D. Schumacher*[2], *C. Brabetz*[2], *J. Ding*[1], *R. Leonhardt*[1], *F. Kroll*[3,4], *F.E. Brack*[3,4], *U. Schramm*[3,4], *A. Blazevic*[2,5], *and M. Roth*[1]

[1]Technische Universitt Darmstadt, Darmstadt, Germany; [2]GSI Helmholtzzentrum fr Schwerionenforschung, Darmstadt, Germany; [3]Technische Universitt Dresden, Dresden, Germany; [4]Helmholtzzentrum Dresden-Rossendorf, Dresden, Germany; [5]Helmholtz-Institut Jena, Jena, Germany

Laser-driven ion sources offer excellent beam properties (high particle numbers, low emittance) and have been intensely investigated in the past two decades. These sources deliver a exponentially decaying spectrum with a $\leq$30 deg divergence. As many applications require a monoenergetic, collimated beam, the LIGHT collaboration was founded to combine the advantages of laser-driven ion acceleration with conventional acceleration technology. A prototype beamline has been realized at the Z6 experimental area at GSI [1]. The target normal sheath acceleration source is driven by the Petawatt High-Energy Laser for Heavy Ion Experiments (PHELIX) 100 TW beam and delivers an exponential spectrum up to several tens of MeV. In the next step, a high-pulsed solenoid selects protons of (8$\pm$1) MeV via chromatic focussing directly 10 cm behind the thin target foil. In 2 m distance, the protons pass a radiofrequency cavity and are phase-rotated. Through the phase rotation the proton bunch can be energy-compressed to $\Delta E/E_0$ = (2.7$\pm$1.7) % or time-compressed into the subnanosecond regime [2]. Behind the cavity, a transport line leads the collimated proton beam to a second target chamber where diagnostics and applications can be placed. Inside this second chamber, a new final focussing system has been installed (6 m behind the target) for steep focussing. This part is necessary to prepare the beam for applications requiring a high intensity beam, e.g. for energy-loss measurements inside plasmas or to study fast processes inside materials. As a final focusing system a second high-field solenoid was placed in the second target chamber and operated at 7 T. As a detector a radiochromic film stack (RCF) was placed 10 cm behind the solenoid, shown in figure 1 . The protons penetrate deeper into the RCF stack, if they have a higher energy according to their characteristic Bragg peak behaviour. The protons deposit their energy inside the RCF films leading to a change in their colour which is analysed. The solenoid parameters haven been chosen in this way that 8.3 MeV protons are focussed in a 460 ps bunch length, shown in the 4th RCF film. The focal spot size is 1.3 x 2 mm^2 with 3 x 10^8 protons resulting in a current of 7.5 x 10^8 1/ns $\sim$ 121 mA. The focus profile is shown in figure 2. In 2015, we measured a focal spot size of 2.3 x 2.3 mm^2 [3]. In the next experimental campaign in 2018, these focussed proton bunches will be used for first application studies.

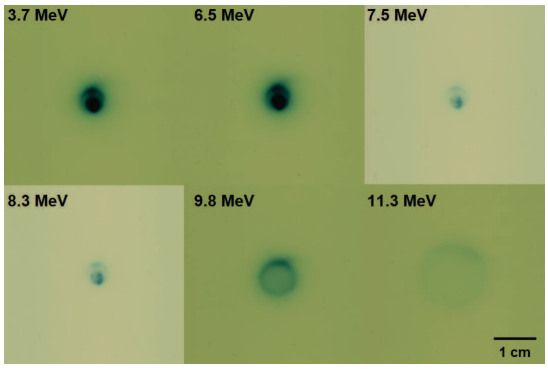

Figure 1: RCF stack detecting the final proton focus: The Bragg peak energy is shown. The 3rd and 4th RCF films are of the type HD-V2, the others are type EBT3. The solenoids setting focusses 8.3 MeV protons which is clearly seen in the 4th RCF film. On the other RCF films, the particular energies are diverge.

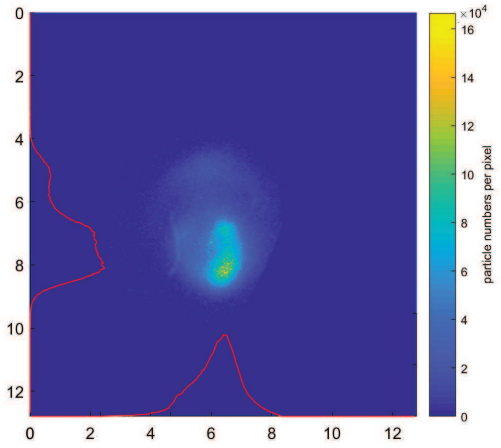

Figure 2: Proton beam profile measured with the 4th RCF film: The focal spot size is 1.3 mm x 2 mm at an energy of 8.3 MeV. The deposited energy is converted into particle numbers per pixel and shown.

References

[1] S. Busold et al., NIMA **740**, 94-98 (2014)

[2] S. Busold et al., Scientific Reports **5**, 12459 (2015)

[3] D. Jahn et al., GSI Scientific Report 2015 (2015)

* This report is also published in *GSI Scientific Report 2017.*

Ultra-high magnetic field generation in curved targets: A novel approach to laboratory astrophysics and laser-based applications*†

P. Korneev[1,2,#], J.J. Santos[3], M. Ehret[3,5], Y. Abe[6], F. Law[6], Y. Kochetkov[1], V. Stepanishchev[1], S. Fujioka[6], E. d'Humieres[3], V. Bagnoud[4], B. Zielbauer[4], G. Schaumann[5], M. Roth[5], V. Tikhonchuk[3]

[1]NRNU MEPhI, Russian Federation; [2]Lebedev Institute, Russian Federation; [3]CELIA, Université de Bordeaux, France; [4]GSI, Darmstadt, Germany; [5]IKP TU-Darmstadt, Germany, [6]ILE, Osaka University, Japan

Optical-based magnetic field generation is a convenient tool for applications, including particle guiding, laboratory based astrophysical-related studies and studies of matter behaviour in magnetic fields. The goal of this experimental campaign was a detailed study of a novel recently proposed scheme of such generation, in which a relativistic laser pulse interacts with a cylindrically shaped target [1], performing multiple reflections along the internal target surface (see Fig.1). In these conditions, the laser pulse generates relativistic electrons, propagating along the surface, and, consequently, return currents in the target bulk, which are responsible for the magnetic field generation.

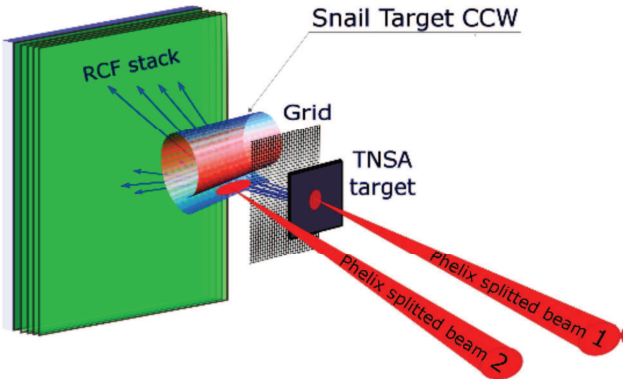

Figure 1: Principal experimental setup for generation of magnetic fields in snail-shaped target. Proton deflectometry diagnostic is shown; optical (polarimetry and interferometry) and Kα diagnostics are not shown.

In the experimental campaign, the PHELIX laser beam was splitted in two, one used as a target driver (CP1), and the other (CP2) as a TNSA proton generator when interacting with a gold foil with 4 μm thickness. Besides the main target and the foil, a fine mesh was aligned on the way of TNSA protons for better resolution of proton deflection in the diagnosed fields. Optical diagnostics (polarimetry and interferometry) was also performed.

About twenty successful shots gave the information about the generated field structure, its time-dependence, and strength. A sample RCF image with a preliminary analysis is presented in Fig. 2. The observed shape of detected diagnostic protons is in a good agreement with the test-particle modelling of deflected TNSA protons, assuming a ~500T magnetic field in the target generated by solenoidal-like currents. Preliminary analysis of the experimental data for different time delays between CP1 and CP2 shows that the magnetostatic structure is stable for ~ 80 ps, which is of the hydrodynamic scale of the target expansion.

The obtained experimental data are being processed yet, but already we can state several important results: the snail-shaped targets are efficient quasi-static magnetic field generators with the time-of-life of the magnetized structures being of the hydrodynamic time scale. The experimental study opens new perspectives for optical-based magnetic field generation and applications.

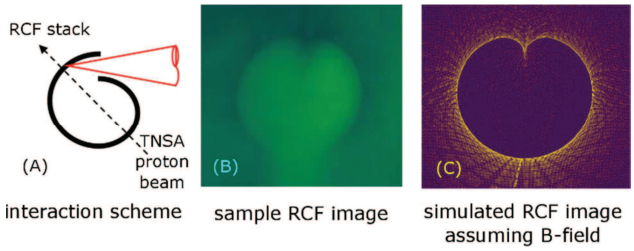

Figure 1: (A) sketch of the principal experimental set-up, (B) example of RCF image (from preliminary experimental results), (C) test-particle modelling of proton deflectometry image, assuming a solenoidal generated magnetic field of ~500T in the target.

References

[1] Ph. Korneev et.al., Phys.Rev. E 91, 043107 (2015)

* This work is supported by 2015-2019 grant of the Institut Universitaire de France obtained by CELIA, Russian Foundation for Basic Research (# 16-52-50019 ЯФ), Excellence program NRNU MEPhI (contract No. 02.a03.21.0005, 27.08.2013), Program of Increase in the Competitiveness of the National Research Nuclear University MEPhI. The EUROfusion Consortium and the Euratom research and training programmes 2014-2018 under grant agreement No 633053 and 2017-2018 under grant agreement No CfP-AWP17-IFE-CEA-02. The views and opinions expressed herein do not necessarily reflect those of the European Commission.

† This text is also submitted to GSI's annual report.

e-mail: korneev@theor.mephi

Investigations on laser-based neutron sources for possible applications*

M. Zimmer[1] , A. Kleinschmidt[2,3], S. Aumüller[1], V. A. Schanz[1], D. Jahn[1], J. Hornung[2], M. Roth[1,4]

[1]Institut für Kernphysik, TU Darmstadt, Germany, [2]Helmholtz-Institut Jena, Germany
[3]GSI Helmholtzzentrum für Schwerionenforschung, Darmstadt, Germany
[4]FAIR -Facility for Antiproton and Ion Research, Darmstadt, Germany

Introduction

The demand for compact neutron sources is rapidly growing in the last years. To meet this growing need, laser-based neutron sources will play a major role in the upcoming development. These sources can provide neutron beams with maximum energies of several 10s of MeV depending on laser intensity and energy. For many applications, like Neutron Resonance Spectroscopy (NRS) or Neutron Resonance Imaging (NRI), the neutron energy needs to be decreased into the regime of a few eV. This can be done with multiple scattering inside a moderating material. The moderator must be composed of elements that have a low mass for rapid slowing down, while at the same time must have a low neutron absorption cross section. Hydrogen has the lowest mass, but a high absorption cross section, carbon on the other hand has a high mass but a low absorption. Therefore, a moderator out of High Density PolyEthylene (HDPE) is used which consist of C and H atoms in a ratio 1:2.

Experiment

To test the capabilities of a laser-based neutron source for NRS and NRI, an experiment was designed and conducted at the PHELIX laser as a succession of a beamtime at the Trident laser facility at the Los Alamos National Laboratory, USA[1]. The intended goal was to test a new moderator design and two new neutron detectors.

New moderator design

Fluka Monte Carlo simulations have shown that a new moderator design could enable a gain of up to 30% more epithermal neutrons into the direction of the detector. This gain is achieved by two modifications to the previous moderator design of earlier experiments [1]. The width of the rear part in the direction of the detector, was decreased by two centimetres to 5 cm as seen in Figure 1. This reduces absorption by hydrogen during moderation and minimizes the neutron Time of Flight (ToF) pulse width which is mainly limited by the time neutrons diffuse inside the moderator before they reach the HDPE surface. The second modification is the addition of two HDPE wings at the front of the moderator. These wings are able to capture and moderate neutrons, that are emitted with an angle between 90° and 146° towards the TNSA axis, which otherwise would have been lost for experimental purposes.

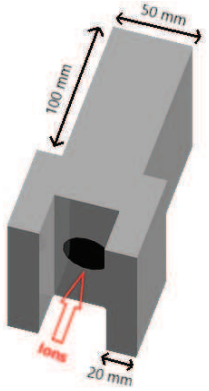

Figure 1: New moderator design with rear part reduced to 50 mm width and including two wings at the front side for moderating additional neutrons.

Testing of new neutron-ToF detector

The ToF detector is made of two 100x100mm borated Multi Channel Plates (MCP) in chevron configuration and an anode. Boron has a high cross section for (n,α) reactions. The emitted α-particles produce electrons in the MCP which are amplified and can be detected as a current on the anode. With this detector it was possible to distinguish between single neutron absorption events with a 10 ns temporal resolution. For higher neutron fluxes, the current can be seen as proportional to the amount of counted neutrons. Experiments have shown, that a high amount of neutron shielding around the detector is necessary to prevent scattered neutrons from the camber walls from interfering with the ToF measurement.

NRI detector

In addition to the NRS detector, a NRI detector consisting of a lithium glass scintillator and a fast gateable camera system was tested. The detector was placed in a distance of 1.1 m from the moderator in 90° towards laser forward direction. Scattered neutrons in this direction were shielded by a collimator made out of borated HDPE. In front of the scintillator several materials with high neutron absorption cross sections and absorption resonances were placed with the intent to distinguish between different samples in the image. As a result of this beamtime, it is possible to say that the detector can distinguish between a blocked and a free neutron flight path but for neutron resonance imaging, the signal to noise ratio has to be advanced and the neutron flux improved. For instance this can be done by using a larger light capturing system, decreasing the distance between scintillator and camera or by cooling the imaging system to reduce the camera noise.

References

[1] GSI Scientific Report 2016, DOI: 10.15120/GR-2017-1 RESEARCH-APPA-PP-11 P281

* This report is also submitted to “GSI scientific report 2017”

5 Accelerator and Beam Physics

Accelerator Driven High Energy Density Science - Activation of structural components of high intensity accelerators

Peter Katrík[1], Dieter H.H. Hoffmann[2,3], Edil Mustafin[1], Ivan Strašík[1]
[1]GSI Helmholtzzentrum für Schwerionenforschung, Darmstadt, Germany
[2]Xi'An Jiaotong University, School of Science, Xi'An, China
[3]National Research Nuclear University MEPhI, Moscow, Russia

High intensity accelerators are under construction for High Energy Density Physics experiments, Accelerator Driven Advanced Nuclear Energy Systems and nuclear waste incineration and other applications. They all have in common to require high intensity pulsed or continuous particle beams. We report on our investigations of activation processes of heavy ion accelerators due to beam loss during operation. This a crucial prerequisite to optimize the choice of construction materials and maintenance procedures [1]. Significant optimization of the operation schedule can be achieved if the accumulated residual activity is properly controlled and predicted. Radiation may cause detrimental changes of the functional properties of the structural components and materials, which will possibly lead to a significant shortening of their lifetime. Replacing activated accelerator components is regulated by dose-rate restrictions for the "hands-on" maintenance. Handling and final disposal of the accelerator parts after several years of usage is also an important issue directly related to the activation. We report results of Monte Carlo codes calculations simulating situations with various levels of activation and different induced nuclides. In order to test the reliability of the method, we carried out activation experiments to verify and benchmark the simulation codes and improved the widely used FLUKA code by supplying additional data. The target was subdivided into a stack of separated foils. This rendered the possibility to determine the radioactivity induced by the produced nuclides at a certain position of the target by measuring the gamma activity of each foil respectively. In all of our experiments we assembled the foils (disk shaped) into the so-called stacked-foil geometry. The total thickness of the targets as well as the number of the foils the target consisted of, varied according to the expected range of the primary particles in the bulk of the target material. The targets were designed in order to locate the end of the range position approximately into the middle of the target body. Since the highest depth resolution is necessary at the end of the penetration range, the thinnest foils were ordered along whole length of the target with the increasing density around the centre position. The thickness of individual foils varied between 0.1 mm and 1.0 mm. In some cases a grouping of a few thin foils into a measurement sample was applied in areas downstream and upstream of the range area, where a high depth-resolution was not necessary. The targets T_1 and T_2 were irradiated by ^{238}U with the initial energy of 200 MeV/u and 125 MeV/u, respectively. The third target T_3 was irradiated by a ^{124}Xe beam with the initial energy of 300 MeV/u. The synchrotron accelerator SIS-18 was operated in the fast-extraction regime with the beam pulse repetition rate from 2 up to 3 seconds. Information about provided irradiation is collected in the Table 1.

Target	Beam	Beam charge state	Energy [MeV/u]	Total number of ions	Irradiation time [s]	Number of foils	Thickness of the target [mm]	Diameter [mm]
T_1	^{238}U	+73	200	2.861×10^{12}	14313	70	7.0	100.0
T_2	^{238}U	+89	125	1.183×10^{12}	8037	16	1.6	100.0
T_3	^{124}Xe	+48	300	2.486×10^{12}	5220	73	25.3	50.0

Table 1: The parameters of the aluminium targets and the irradiation conditions

The experiments presented here were supported by several preliminary calculations in order to achieve a most precise prediction of the range area of the primary particles. Three different codes were used: FLUKA 2011, SRIM-2013, ATIMA. SRIM and ATIMA codes are less complex with relative low CPU demand. Therefore it is frequently chosen for calculating the physical quantities related to the interaction of the ions with the matter, such as stopping power, energy loss, and range and an energy-loss or an angular straggling. Figure 1 shows the distribution of the beam energy deposition in the bulk of the target material, calculated by FLUKA. Due to nuclear reactions, fragmentation occurs and this is clearly observed by a smeared out Bragg-Peak region [2].

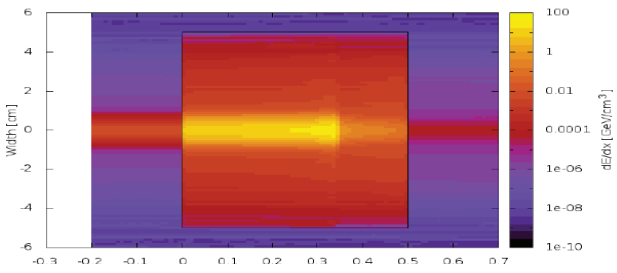

Fig. 1: An example of the stopping power distribution in the horizontal plane calculated by FLUKA for the case of 238U ions with the nominal energy of 200 MeV/u penetrating through the air gap and the aluminium target

References

[1] Peter Katrik (2017) D17, Dissertation TU-Darmstadt
[2] Submitted for publication to Matter and Radiation at Extremes (open access)

High Intensity Stored Beams of ^{229m}Th and the Nuclear Clock Perspective

Zenke Dou[1], Shihao Ru[1], Kun Xue[1], Shizeng Zhang[1],Yongtao Zhao[1], Dieter HH Hoffmann[1,2]
[1]Xi'An Jiaotong University, School of Science, Dept. Laser and particle Beams, Xi'An 710049, Shaanxi, P.R. China
[2]National Research Nuclear University MEPhI, Moscow, Russia

The International System of Units (SI) uses the transition of two hyperfine levels of the ground state of the caesium atom to define the time standard of 1s. Atomic clocks based on this electronic transition can keep the time as precise as 1 second within the current age of the universes, which is approximately 13 billion years. Can this precision be improved? Since the characteristics of atomic transitions are subject to the environment like electromagnetic fields particle density, plasma environment, the precision can obviously be improved when the time standard is based on a nuclear transition. Due to technical reasons such a level must be within reach of available lasers to set up a frequency comb. At the moment the only nuclear level known and predicted by theory is the M1 nuclear transition between the low-energy isomeric state and the ground state in the ^{229}Th nucleus. The energetic position of this level at approximately 7.6 eV is known from spectroscopy experiments [1], however with an uncertainty which is many orders of magnitude higher than the line width. Thus more knowledge about this level is necessary. We propose a broad band excitation using virtual photons to excite this level.

$$N(\varepsilon) = \frac{2\alpha Z^2}{\pi\beta^2\varepsilon}\left(\ln\left(\frac{1.123\beta\gamma}{\varepsilon b_{min}}\cdot\hbar c\right) - \frac{\beta^2}{2}\right)$$

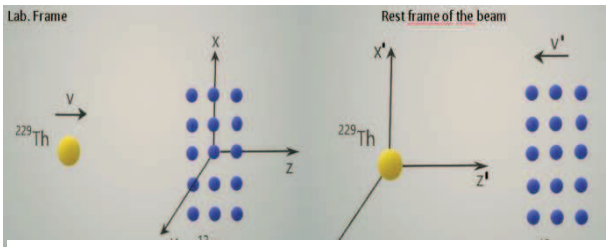

Fig. 1: A ^{229}Th ion moving towards a solid ^{12}C target in the laboratory frame and the rest frame of the projectile

We do envision - as shown in fig. 1- a beam of ^{229}Th circulating in a storage ring with a ^{12}C Target inserted. Due to the relativistic velocity of the fast charge particles an intense electromagnetic pulse is generated, when the particles pass each other. This electromagnetic pulse can be described by an equivalent spectrum of virtual photons. The resulting spectrum as an example is shown in fig. 2 giving the number of photons as a function of the photon energy in the low frequency limit.

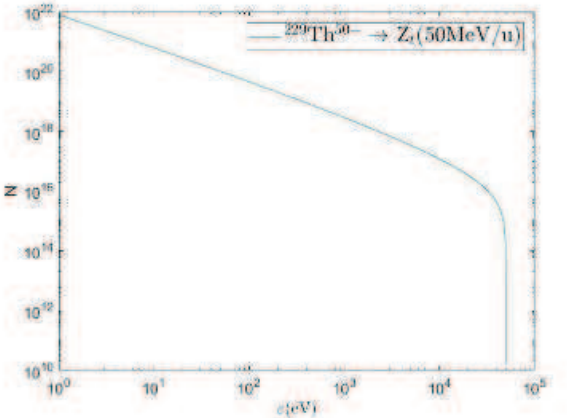

Fig. 2: Virtual photon spectrum of ^{229} **Th^{+50}** at 50MeV/u

From fig. 2 it is obvious that there is a high number of low energy photons. Since outer shell electrons are removed, these photons are not available to excite electronic transitions. In the de-excitation process the emitted photons are subject to Doppler shift. This allows to shift the observed transition energy into a range of optimum detector efficiency and low background.

The major problem of the proposed experiment is the intensity of stored ^{229}Th in a storage ring. It is in principle possible to start with a ^{229}Th ion source. Currently radiation safety issues make this possibility unlikely and we are in the process of simulating the experiment with 10^4 stored particles**.**

References

[1] B. R. Beck et al., Phys. Rev. Lett. 98, 142501 (2007)

6 Theory for HED/WDM in Plasma -, Laser - and Atomic Physics

Two-body formation mesonic bound states in ultradense plasmas of fusion catalysis concern*

C. Deutsch
LPGP, CNRS, Université Paris-Sud, Université Paris-Saclay, 91405 Orsay, France

It is pretty well documented that mesics atoms with keV ground state binding energy can easily survive in a 100 eV-1 keV temperature dense plasma. It is also highly likely that N-body effects could facilitate the in-situ production of those exoatoms. So, we herein envisage the presently considered 2-body approach as providing a lower bond to the resulting contribution of several possible and distinct recombination paths [1].

A most obvious mechanism for implementing a 2-body radiative recombination between the in-situ stopped nega-tive muon and ion D/T+ is proposed by Oppenheimer [2], with m_μ replacing m_e in the expression,

$$\sigma_0 = (2^7\pi e^2 h/3m^2c^3g^2)e^{-(4/g)tan^{-1}g} \star(1+g^2)^{-2}(1-e^{-2\pi/g})^{-1} \quad (1)$$

in terms of g ratio of μ^- initial translational energy to ionization energy of D/T-μ in excitation state n, i.e.

$$g = 18786.78\left(\frac{nV}{c}\right)^2 \quad (2)$$

Eq.(1) is mostly effective in the low velocity limit [12]

$$\sigma_0 = \frac{2^8\pi^2e^2\hbar}{3e_1^4m_\mu^2c^3}g^{-2}, \qquad e_1 = 2.718$$
$$= \frac{3.948\times10^{-27}}{g^2}cm^2 \quad (1a)$$

which involves the consideration of a cumulative distribution function (CDF) with a muon velocity smaller than the thermal one

$$a = 9.79\times10^5\sqrt{8.88\,T(eV)}\;cm/sec, \quad (3)$$

explicited by

$$\bar{\sigma}_0 = 1.1185\times10^{-33}\times\int_0^a \frac{dV\,V^{-2}e^{-\frac{V^2}{2a^2}}}{a^3}\;cm^2. \quad (4)$$

Putting Eq.(1a) into (4) yields a diverging quadrature featuring a catastrophic 2-body process illustrating so to speak the diving muon on the much heavier D/T ion.

In order to evaluate realistically this phenomenon, we pay attention to the smallest muon velocity compatible with the duration of the high density targets displayed previ-ously. More detailed investigations of μ slowing down to complete stop given in Table I, demonstrate clearly the WDM target ($N_{D/T}$ = 5.64 10^{23}/cc) as the most efficient one in securing that process on a psec time scale.

Hyperdense FIS targets (Table II) should be allowed to persist during a longer 10 psec scale to exhibit equivalent performances. - With those provisos in mind, it is possible to extract a finite quadrature from Eq.(9) by choosing a very small but nonzero final muon velocity, presently fixed at 10^{13} V (V_{th} designates μ thermal velocity). By so doing, we can approach a rather accurate estimate for the rate of 2-body recombination $\mu_{D/T}$

$$\tau_\mu(sec^{-1}) = N_{D/T}\bar{\sigma}_0 V, \quad (5)$$

featured in Table II. Given data display the largest for n=1, hydrogenic ground state and steadily decrease with increasing n, in conformity with Holtsmark continuum depression (1).

WDM ($N_{D/T} = 5.64\times10^{23}/cc$)				FIS($N_{D/T} = 10^{26}/cc$)	
T(eV)= 1.75	10	50	100	100	1000
T_{stop}(psec)= 0.665	0.135	0.0471	0.0363	63.32	9.97
R(μ m)= 1.317	0.22	0.078	0.0662	672	92.3

Table I: Stopping time T_{stop} (psec) and Range (μm) for muons stopped from $v_m = \sqrt{v_F^2 + v_{eth}^2}$ down to zero velocity

n	WDM ($N_{D/T} = 5.64 \times 10^{23}/cc, T = 1.75eV$)	FIS($N_{D/T} = 10^{26}/cc$)	
		100 eV	1 keV
1	5.847 $\times 10^{17}$	3.17 $\times 10^{16}$	3.17 $\times 10^{14}$
2	3.647 $\times 10^{16}$	1.98 $\times 10^{15}$	1.98 $\times 10^{13}$
3	7.204 $\times 10^{15}$	3.91 $\times 10^{14}$	3.91 $\times 10^{12}$
4	2.270 $\times 10^{15}$		
5	9.336 $\times 10^{14}$		
6	4.502 $\times 10^{14}$		

Table II: D/T ions - μ two-body recombination rates τμ(sec−1) = ND/T $\bar{\sigma_0}$v in terms of exoatom main quan-tum number n and Maxwell averaged $\bar{\sigma_0}$ (Eq.(4)) taken down to $10^{-13}V_{th}$

Again the WDM case highlights the most performing option, the more so when its lifetime gets lengthened to 500 psec.

References

[1] C. Deutsch, GSI - 2016 - 2 Report p. 66

[2] J. R. Oppenheimer, Phys. Rev. 31, 349 (1928), also H.A. Bethe and E.E. Salpeter, Quantum Mechanics of one - and two - electron atoms, Plenum Publ. Corp., New York, 1977, p. 322

Two-body diagnostics mesonic bound states in ultradense plasmas of fusion catalysis concern

C. Deutsch[1]

[1]LPGP, CNRS, Université Paris-Sud, Université Paris-Saclay, 91405 Orsay, France

For the purpose of illustration, we focus attention of the Ly_α line, possibly emitted in a FIS plasma with $n_{D/T} = 10^{26}/cc$ and a T = 1 keV temperature , permitting a quasi-classical treatment of target electrons colliding with exoatom hydrogenic sublevels (n,l) influenced by the quasi-static target ion electric field (Holtsmark).

Then, we are allowed to adapt the standard Baranger-Griem impact formalism [1], as follows. Then the light intensity polarized along a unit vector eˆ may be written

$$I(\omega,\hat{e}) = \pi^{-1}\mathrm{Re}\int W(\vec{F})d\vec{F}\sum_{i,j,k,l}\langle n_i|\hat{e}\cdot\vec{R}|n_j\rangle \qquad (1)$$

$$\times\langle n'k|\hat{e}\vec{R}|nl\rangle\langle n_i|\langle n_j|\{i[\omega-\hbar^{-1}(H_n-H_{n'})]-\phi_{nn'}\}^{-1}|nl\rangle|n'k\rangle$$

with $\vec{R}$ the optical electron position vector. $H_n[H_{n'}]$ is the atomic Hamiltonian taking into account the full static electromagnetic perturbation operating on the sublevels $|n_i\rangle$ and $|nl\rangle$ of the upper |state (n)[$|n_j\rangle$ and $|n_k\rangle$ of the lower state (n′)] of the line. $\varphi_{nn'}$ denotes the electron collision (or relaxation) operator.

The static Stark pattern in presence of the low frequency microfield reads as

$$\xi^2\left[\xi^2 - 9\frac{A^2}{Z_N^2}\right] = 0, \quad \text{for eigenvalues } \xi \qquad (2)$$

with $Z_N = 1$, ion charge, $A = e\,a_0\,E_0$, and E_0 denotes the static Holtsmark ion field

$$E_0 = \frac{e}{r_0^2} \quad \text{with} \quad \frac{4}{15}(2\pi)^{3/2}n_e r_0^2 = 1.$$

On the other hand, the electron collision operator is explained ($\alpha = \frac{1}{137.036}$) with

$$\frac{\Phi_\alpha}{2\pi} = \frac{5.00\times10^{-21}}{206.77}\left\{19.28 - Ln\left[\frac{1}{Z_N}\left(\frac{n_e}{T_e 206.77}\right)^{1/2}\right]\right\}$$

$$\times\frac{1}{Z_N^2}\frac{n_e}{T_e^{1/2}} \qquad (3)$$

in Ryd $= \frac{1}{2}\frac{\alpha^2 m_\mu c^2}{1+\frac{m_H}{m_{DT}}}$, $m_{DT} = 2.5\,m_p$ with $T_e(K)$.

The given Lyα line electron profile is then (Δv, frequency shift, $Z_N = 1$)

$$S^\alpha_{\vec{O}Z} = \frac{1}{2\pi}\frac{1}{Z_N^2}\frac{1}{\Phi_\alpha}\sum_{i=1}^{4}\frac{1}{1+[\frac{\Delta\nu-\xi_i/2\pi\hbar}{\Phi_\alpha/2\pi}]^2}. \qquad (4)$$

Corresponding global line broadening is then displayed on Fig.1. In same target plasma conditions, a Lyα Aine pertaining to $\mu - He^+$ Aon would yield a very similar bell-shaped curve with abscissa running from -0.006 to +0.006 Ryd, with energy unit Ryd $= 2\alpha^2 m_\mu c^2/(1+m_\mu/m_+)$.

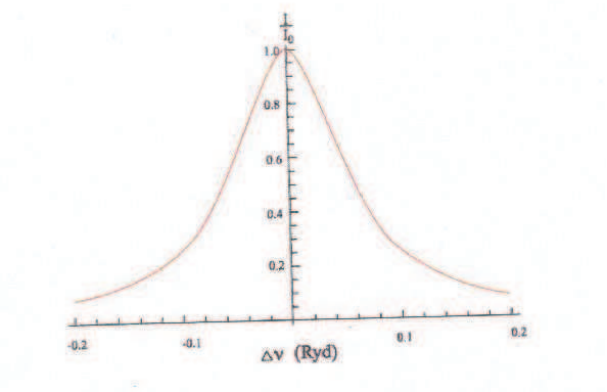

Figure 1: X-Ray (Stark) line profile emitted by D/T-μ exoatoms in FIS plasmas (Ne = 10^{26}/cc, T = 1 keV). Energies are in Ryd = 2812.35 eV (muon a.u.), Lyman α with unperturbed λ=6.146 $\mathring{A}$ [2].

References

[1] C. Deutsch, GSI - 2016 - 2 Report p. 66

[2] G. Bekefi, C.Deutsch and B. Yaa'kobi in Principles of Laser Plasmas, Ed. G. Bekefi, Wileys and Sons, New York, 1976, p. 549

Warm-Dense-Matter State of Iron Generated by Intense Heavy Ion Beams

L. Zhang[1], J. Ren[1], Y. Zhao[1,2, #]

[1]Xi'an Jiaotong University, Xi'an China; [2]Institute of Modern Physics, CAS, Lanzhou, China

Introduction

Warm Dense Matter (WDM) exists in the interior of planets and determines planetary characteristics, and is the intermediate state of matter in inertial confinement fusion. Therefore, it is important to investigate Warm Dense Matter with as many methods as possible, for reasons of basic science, novel applications and to enhance the perspectives of inertial confinement fusion (ICF). Heavy ion beams are regarded as an attractive complementary driver to generate WDM states. Due to their specific characteristics, e.g., the precise control of beam-energy deposition, the large sample size, the potential to heat any target material, and last but not least the high repetition rate of beam pulses from accelerators. In China, the High Intensity heavy ion Accelerator Facility (HIAF) will be built in Huizhou and generate highly energetic and highly bunched heavy ion beams focusing on heavy ion applications [1]. In this study, the compression performance of a LAPLAS type target, where the inner cylinder of the multilayered target consists of iron, has been studied theoretically by using the code MEDUSA. We comprehensively conducted simulations with a variety of conditions. Different outer-shell materials, e.g., gold, lead and platinum were assumed, the radial position of the annular beam center was varied and we studied the result on compression of iron sample.

Simulation Model

The simulation is done based on MEDUSA, which was initially developed for laser plasma interaction and laser fusion. Later the code was modified to allow the treatment of energy deposition of ion beams into matter. the target is of cylindrical geometry, consisting of two layers. Iron constituting the inner core is enclosed by the either of three different outer shell high-Z materials, namely gold, lead and platinum. The ion beam with an annular focal spot irradiates the target from its right face. The radius of inner core iron (Ri) is 0.2 mm and the radius of outer shell material (R_0) is 3.0 mm. In this study, the beam parameters are based on the performance of the HIAF booster ring. The assumption is, that this ring will deliver a uranium beam of Gaussian distribution with the intensity, ($N_u = 1.5 \cdot 10^{11}$) at an energy of 800 MeV/u. The full width at half-maximum (FWHM) is 1 mm and the beam duration is 150 ns.

Results

Figure 1(a)-(c) shows the variations of the pressure, temperature, and density of the whole target with respect to the radius R, respectively. The black-solid, red-dashed and blue-dotted curves show the results of the outer shell material of gold, lead and platinum at the maximal compression of the inner iron. It can be seen that when the outer shell material is platinum, the iron pressure is higher, which reaches about 8 Mbar and the density is higher, up to around 100 g/cm^3, while the temperature is as low as 1.8 eV. From these equations it is clearly seen that the pressure of ions and electrons is determined by the temperature of ions and electrons, density and mass number. Therefor the reason for the pressure of the outer shell is attributed to its ratio of density and mass number. Overall, the outer shell material has a larger the ratio of density and mass, allowing for higher compression of the inner iron.

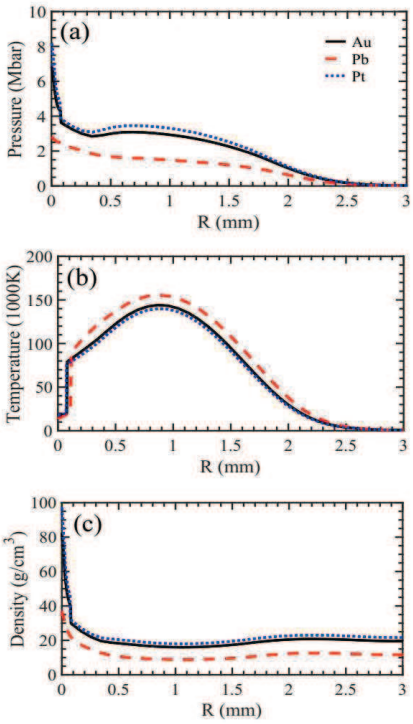

Figure 1: the variations of the pressure, temperature, and density of the iron target with respect to the radius R, respectively. The black-solid, red dashed and blue-dotted curves show the results of the outer shell material of gold, lead and platinum at the maximal compression of the inner iron, respectively.

References

[1] J. Ren et al., "Hydrodynamic response of solid target heated by heavy ion beams from future facility HIAF, Nuclear Instruments and Methods in Physics Research B 406 (2017) 703–707.

* Work supported by Science Challenge Project No. TZ2016005
#zhaoyongtao@xjtu.edu.cn

Simulations of Beam-Plasma Interactions Using WARP Particle-In-Cell Framework*

Kookjin Moon and Moses Chung †
Ulsan National Institute of Science and Technology, Ulsan 44919, Korea

Introduction

In recent decades, it has been needed to construct much powerful accelerators to challenge the new physics in the energy frontiers. To save the cost and reduce the footprint of such accelerator projects, novel acceleration mechanisms have been proposed. For example, plasma wakefield acceleration can be realized by injecting a high intensity laser pulse or charged particle beam into the plasmas. This method guarantees a much higher acceleration gradient than any conventional acceleration structures, however it has several problems such as substantial energy spread, inconsistent loading efficiency, instabilities of the drivers, limited amount of energy delivered to the witness beam from the driver beam (for the beam-driven plasma wakefield, BD-PWFA), and not long enough Rayleigh length (for the laser-driven plasma wakefield, LWFA). In this paper, we introduce two topics that have been actively investigated recently to solve the above problems using particle-in-cell (PIC) code WARP [1]. The WARP is an extensively developed open-source PIC Python package designed for simulation of plasmas and high current particle beams in a wide range of applications.

Self-Modulation Instability

The greater the energy of the driver beam, the greater the expected energy gain of the witness beam. High energy proton beams from hundreds of GeV to tens of TeV are already available at CERN, but the bunch length is too long. Therefore, the self-modulation instability (SMI), which occurs when the driver beam length is much longer than the plasma wavelength ($\lambda_p \ll L_b$), has been intensively studied to harness the beams ($\sim$10 cm) from the Super Proton Synchrotron (SPS) of CERN after the first theoretical modeling work was published [2]. Of the studies for SMI, seeding the instability should be the first problem to be investigated. One of the methods is to use the sharply rising head of a flat top beam which is made by stacking several short, Gaussian pulses as in Fig. 1.

Trojan Horse Scheme

It is not easy to control the size and emittance of the witness beam inside the plasma wakefield. In 2012, an idea was reported to create a witness beam by ionizing the residual gas using a very small and weak laser pulse in the blow-out region of the wakefield generated by an electron beam [3]. The radial size and emittance of the witness beam caused by a laser depend on the focal waist and power of the laser, and the plasma density. Assuming that the driver beam does not evolve inside the plasma, the physics of the driver and witness beam can be decoupled in the system (see Fig. 2). Possible oscillations and instabilities of the witness beam, which occur when the beam radius is not matched to the system, should be studied for consistent beam loading.

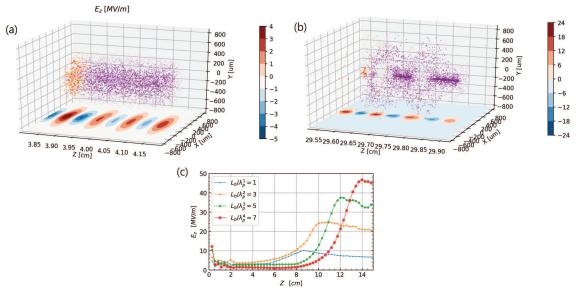

Figure 1: Simulations of a flat top electron beam (a) before and (b) after the propagation in the plasma, and (c) the evolution of the longitudinal wakefields.

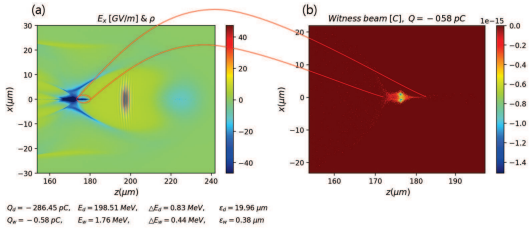

Figure 2: Simulation of (a) the driving electron beam with a laser pulse ionizing residual Helium gas. (b) Zoomed view of the witness beam ionized from the laser pulse.

References

[1] A. Friedman, R. H. Cohen, D. P. Grote, S. M. Lund, W. M. Sharp, J.-L. Vay, I. Haber, and R. A. Kishek, IEEE Trans. Plasma Sci. 42, 1321 (May 2014)

[2] N. Kumar, A. Pukhov, and K. Lotov, Phys. Rev. Lett. 104, 255003 (2010).

[3] B. Hidding, G. Pretzler, J. B. Rosenzweig, T. Konigstein, D. Schiller, and D. L. Bruhwiler, Phys. Rev. Lett. 108, 035001 (2012).

* Work supported by the National Research Foundation of Korea (NRF) Grant (No. 2015R1D1A1A01061074).

† mchung@unist.ac.kr

Relativistic stopping power for alpha particles in hot plasmas

Y. Zhang[1, 2], B. He[2,#] and Y. Zhao[1,#]
[1]Xi'an Jiaotong University, Xi'an, China; [2]Institute of Applied Physics and Computational Mathematics, Beijing, China

The stopping of ions in plasma is the key process in fusion science, such as DT-alpha heating, ion-driven inertial confinement fusion and fast ignition. In particular, it is of great significance to study the energy loss of alpha particles with 3.54 MeV in hot plasma of deuterium and tritium (D-T) mixture, where the relativistic effect of free electron's thermal motion probably shouldn't be ignored. We theoretically calculated the stopping power of MeV alpha particles in hot plasma (~ 200 keV). The relativistic Vlasov equation [1] is applied to investigate the stopping power due to the collective response of the plasma. The stopping power depends on the dielectric function ε(ω, k) and can be expressed as:

$$-\frac{dE}{dx}=\frac{Z^2}{\pi v^2}\int\frac{dk}{k}\int_{-kv}^{kv}\mathrm{Im}[\frac{1}{\varepsilon(\omega,\mathrm{k})}]\omega d\omega$$

where Z and v represent the charge and velocity of incident particle respectively, k means the wave number and ω means plasma frequency.

The real and imaginary parts of dielectric function were plotted in figure 1 for relativistic and non-relativistic velocity distribution of free electrons. Obvious difference was observed, which indicates the importance of relativistic effect in the stopping process of alpha particles with plasma electrons.

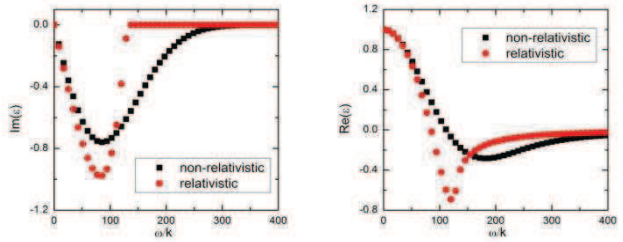

Figure 1: Real and imaginary part of the dielectric function when considering relativistic effect or not in electron's velocity distribution, where the plasma temperature is 200keV.

The stopping power due to the electron component with included (R) relativistic effect and not (NR), and the ion component in plasmas are shown in table I respectively, when the energy of the incident alpha particles varies from 0.05 MeV to 3.54 MeV. The total results of the two components are also calculated with relativistic effect included or not, which are denoted by Total(R) and Total(NR), respectively. The plasma temperature T_e is still 200keV, and the electron density n_e is $10^{26}/cm^3$. In the table the stopping power is in the unit of MeV/cm. From Table I, it can be seen that, the stopping power due to the interaction with plasma ion is around 8 times larger than that due to the interaction with plasma electrons. Namely, the stopping process of 0.05-3.54 MeV alpha particles in DT plasma is dominated by the interaction of alpha particles with plasma ions.

From the above results, it could be concluded that for 3.54 MeV alpha particles moving in 200keV DT plasma, although the relativistic effect is important in the interaction of alpha particles with electrons, the interaction with plasma ions plays the dominant role in the stopping process. Namely, the electron's relativistic effect could be ignored when calculating the slowing down of 3.54 MeV alpha particles in such hot plasmas.

Ep /MeV	Electron(R)	Electron(NR)	Ion	Total (R)	Total (NR)
0.05	8.14	7.17	675.69	683.83	682.86
0.1	11.57	10.20	887.22	898.79	897.42
0.5	26.82	23.64	1108.90	1135.72	1132.54
1.0	38.56	33.99	836.99	875.55	870.98
1.5	47.32	41.70	623.01	670.33	664.71
2.0	54.55	48.08	486.56	541.11	534.64
2.5	60.87	53.64	397.61	458.48	451.25
3.0	66.55	58.65	336.29	402.84	394.94
3.54	72.18	63.61	288.67	360.85	352.28

Table I: Stopping power for alpha particles in DT plasmas when T_e = 200keV and n_e =$10^{26}/cm^3$. Here R and NR mean the relativistic velocity distribution of electrons considered or not, respectively. Electron and Ion denote the compo-nent of the stopping power due to the electron and ion, respectively.

References

[1] Prentice A J R, Plasma Physics 9(1967), 433

* Work supported by Science Challenge Project JCKY201612A501 and No. TZ2016005 and NSFC U1532263 11574034, 11575032, U1530142.
# hebin-rc@163.com, zhaoyongtao@xjtu.edu.cn

Stopping power of warm dense electron plasmas*

I.M. Tkachenko[1,#], Yu.V. Arkhipov[2], A.B. Ashikbayeva[2], A. Askaruly[2], A.E. Davletov[2], D.Yu. Dubovtsev[2], S.A. Syzganbayeva[2]

[1]Universitat Politècnica de València, Valencia, Spain; [2]Al-Farabi Kazakh National University, Almaty, Kazakhstan

Phenomena related to the interaction between beams of charged particles with condensed matter and plasmas have been widely studied using different methods of diagnostics. In addition, beams of heavy fast ions are considered as a perspective driver for the inertial fusion.

The plasma polarizational stopping power of heavy ions projectiles is described by the Lindhard formula [1]:

$$\left[-\frac{dE}{dx}\right]^{pol} = \frac{2(Z_p e)^2}{\pi v^2}\int_0^\infty \frac{dk}{k}\int_0^{kv}\omega^2\left(-\mathrm{Im}\frac{\varepsilon^{-1}(k,\omega)}{\omega}\right)d\omega, \quad (1)$$

whose high-velocity asymptotic form was found by Bohr, Bethe, and Larkin [2-4]:

$$\left[-\frac{dE}{dx}\right]^{pol}_{v\to\infty} \cong \left(\frac{Z_p e\omega_p}{v}\right)^2 \mathrm{Ln}\frac{2m_e v^2}{\hbar\omega_p}. \quad (2)$$

The plasma inverse dielectric function (IDF), $\varepsilon^{-1}(k,\omega)$, was determined in [5] within the moment approach [6] complemented by some physical observations which permitted to express it in terms of only two characteristic frequencies, which are the ratios of the frequency power moments of the IDF imaginary part:

$$\varepsilon^{-1}(k,\omega) = 1 + \frac{\omega_p^2\left(\sqrt{2}\omega_1\omega + i\omega_2^2\right)}{\sqrt{2}\omega_1\omega\left(\omega^2-\omega_2^2\right) + i\omega_2^2\left(\omega^2-\omega_1^2\right)}. \quad (3)$$

The frequencies ω_1 and ω_2 in (3) can be calculated rigorously as soon as we know the static structure factor (SSF) of the system [5, 6]. Here we employ the following interpolation expressions [7,8]:

$$\omega_1^2 = \omega_1^2(k) = \omega_p^2\left(1 + k^2k_D^{-2} + k^4k_q^{-4}\right), \quad (4)$$

$$\omega_2^2 = \omega_2^2(k) = \omega_p^2\left(1 + \frac{\langle v_e^2\rangle k^2}{\omega_p^2} - \frac{v_{int}^2k^2}{\omega_p^2}\right). \quad (5)$$

The interpolation and fitting parameters introduced here are the following:

$$v_{int}^2 = -\frac{4}{15}\frac{\Gamma^{\frac{3}{2}}}{\beta m_e}\left(\frac{-0.9052}{\sqrt{0.6322+\Gamma}} + \frac{0.27243}{1+\Gamma}\right),$$

and k_D^{-1} is the Debye radius, $\Gamma = \beta e^2/a$, $k_q^4 = 12r_s/a^4$ $r_S = a/a_B$, a and a_B are the Wigner-Seitz and Bohr radii, $\beta = 1/k_BT$, k_B is the Boltzmann constant, and T is the temperature. Under the thermodynamic conditions we deal with here, the system is practically a classical plasma so that all magnitudes can be expressed in terms of the plasma coupling parameter Γ, and we may use for the average electron thermal velocity the Vlasov classical form: $\langle v_e^2\rangle = 3k_BT/m_e$.

We have compared the polarizational losses of heavy projectiles in electron gas calculated within the simplified interpolation version of the modified method of moments [5] to the results of the latter and to the PIC simulation data [9] in classical systems, see the Figures 1-4.

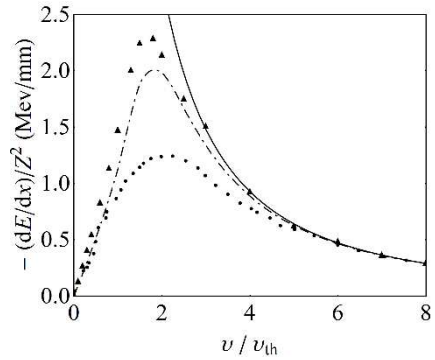

Figure 1: The electron gas stopping power (*-dE/dx*) as a function of the projectile velocity v normalized to the thermal velocity $v_{th} = \sqrt{k_BT/m_e}$ for a positively charged ion and different coupling strengths $Z\Gamma^{3/2}$; the circles display the simulation data, the solid line represents the asymptotic form (2), the dash-dotted line stands for the results of the interpolation model, while the triangles correspond to the complete method-of-moments results with the SSF determined in the hyper-netted chain approximation. The plasma conditions and charge state Z are: $k_BT = 10$ eV, $n = 10^{21}$ cm^{-3}, $Z = 2$ for $Z\Gamma^{3/2} = 0.23$.

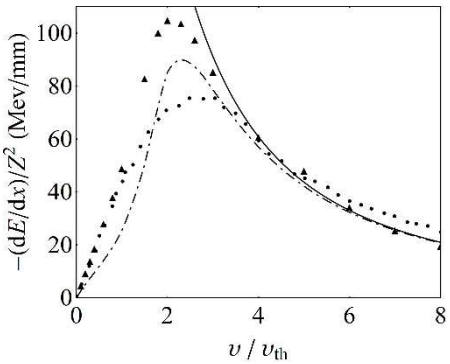

* Work supported by Ministry of Education and Science, Kazakhstan Grants AP05132677, AP05132333 and BR05236730/PTsF.

imtk@mat.upv.es

Figure 2: As in Fig. 1 but for $k_B T = 20$ eV, $n = 2.1 \cdot 10^{23}$ cm^{-3}, $Z = 2$ and $Z\Gamma^{3/2} = 1.1$

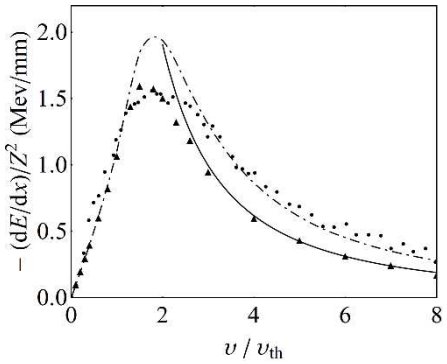

Figure 3: As in Fig. 1 but for $k_B T = 10$ eV, $n = 10^{21}$ cm^{-3}, $Z = 1$ and $Z\Gamma^{3/2} = 0.11$

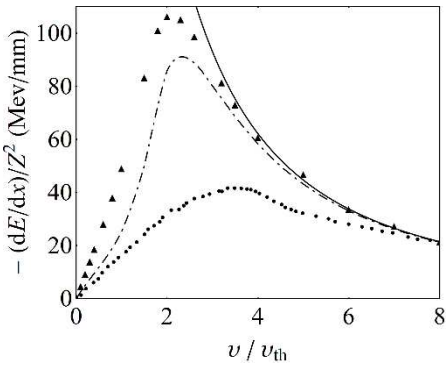

Figure 4: As in Fig. 1 but for $k_B T = 20$ eV, $n = 2.1 \cdot 10^{23}$ cm^{-3}, $Z = 8$ and $Z\Gamma^{3/2} = 4.6$

Under the above conditions the interaction contribution $|U(q)|$ to the frequency ω_2 is at least an order of magnitude smaller than the kinetic one, $K(q)$, so that the simplified random-phase interpolation form for the frequency $\omega_1(q)$ is perfectly applicable [10].

We observe that the suggested simplified interpolation approach based on the modified method of moments is capable of describing the energy losses of a charged particle in warm dense effectively classical electron plasmas with a fairly good precision. Notice that no adjustable parameters were used, and the interpolation-model calculation is practically algebraic. Last year the same interpolation approach was applied to describe the stopping power of two-component plasmas, and we are planning to carry out a comparative study. Our results imply the physical applicability both of the interpolation and the complete modified moment approach.

References

[1] J. Lindhard, K.Dan.Vidensk.Selsk,Mat.Fys.Medd. 28 (1954) 3.
[2] N. Bohr, Phil. Mag. 25 (1913) 10.
[3] H. Bethe, Ann. Phys.(Lpz.) 5 (1930) 325.
[4] A.I. Larkin, Zh. Eksp. Teor. Fiz. 37 (1959) 264 [Sov. Phys. JETP 37 (1960) 186].
[5] Yu. V. Arkhipov et al., Phys.Rev.Lett., 119, (2017) 045001.
[6] Igor M. Tkachenko, Yu.V. Arkhipov, A. Askaruly. The Method of Moments and its Applications in Plasma Physics (Lambert, Saarbrücken, 2012) 125 pp.
[7] V.M. Adamyan, I.M. Tkachenko, High Temp., 21 (1983) 307; J. Ortner, I.M. Tkachenko, Phys. Rev. E 63 (2001) 026403.
[8] G. Chabrier, A. Y. Potekhin, Phys. Rev. E 58 (1998) 4941.
[9] G. Zwicknagel, Laser and Particle Beams, 27 (2009) 399.
[10] Yu. V. Arkhipov et al., Contr. Plasma Phys., 56, (2016) 403.

Interaction of Intense Laser Pulses with Quantum Plasma

Punit Kumar, Shiv Singh and Nafees Ahmad
Department of Physics, University of Lucknow, Lucknow, Lucknow-226007, India

The growing interest in investigating new aspects of high density (quantum) plasmas is motivated by its potential applications in modern technology e.g., quantum well and quantum dots, quantum plasma echoes, metallic nanostructures, microelectronics devices, thin metal films, metal clusters, nano-plasmonic devices, quantum x-ray free electron lasers, in high intensity laser produced plasmas, in nonlinear quantum optics, in metallic nanostructures, in super dense astrophysical environment (e.g. in the interior of Jupiter, white dwarfs, and neutron stars), in dusty plasmas and in next generation of laser based plasma compression experiment (LBPC), etc. The studies involving interaction of intense laser beams with quantum plasma were carried out by the quantum plasma group. The interaction models were developed on the recently developed quantum hydrodynamic (QHD) model which consists of a set of equations dealing with transport of charge, momentum and energy in a plasma. The effects of quantum Bohm potential, the Fermi statistical pressure and the electron spin were incorporated.

Studies using QHD Model

Harmonic Generation by Whistler Pulse in Magnetized Quantum Plasma

Study of second harmonic generation resulting from propagation of whistler pulse in homogeneous high density quantum plasma immersed in an externally applied magnetic field was carried out. The oscillatory electron velocities, perturbed density and non-linear current density for the propagation of whistler in high density plasma were setup. The field amplitude of second harmonic of the whistler with respect to fundamental wave and the conversion efficiency for phase-mismatch was analyzed and higher conversion efficiency was observed in degenerate plasma for lower values of static magnetic field as compared to classical plasma.

Acceleration of Electrons in Quantum Dusty Magnetoplasma

A detailed study of ponderomotive acceleration of electrons in magnetized quantum dusty plasma was performed. A simple energy exchange solution in electron acceleration was established. It is noticed that the electron acceleration by circularly polarized laser pulse is significantly affected by presence of magnetic field, laser field amplitude and dust charge grains. It is found that an electron gains energy during rising part and losses energy during trailing part of laser pulse and presence of dust grains increase the growth of ponderomotive acceleration in quantum dusty plasma as compare to quantum plasma.

All the prevalent models considered electrons as a single fluid of macroscopically averaged spin-1/2 plasma. The earlier papers did not show a full picture and didn't took spin-up and spin-down interaction force into account. Very recently, a modified separate spin evolution (SSE) treatment of electrons in accordance with Pauli equation has been developed.

Studies using SSE-QHD Model

Two Stream Instability in Magnetized Quantum Plasma

The two-stream instability for a circularly polarized electromagnetic wave propagating through a high density magnetized quantum plasma using the modified SSE-QHD model was studied. The dielectric constant tensor using which the dispersion relation of two-stream as well as the beam-plasma instability was obtained. The results indicate that quantum effects and thermal effects play important roles along with the spin polarization produced by the spin interaction of spin-up and down species of the electron. The critical wave number for beam-plasma instability in magnetized quantum plasmas has also been evaluated and effect of spin polarization has been analyzed.

Parametric Decay of X-mode Radiation in Quantum Magnetoplasma

The study of parametric decay of an X-mode pump into a short wavelength electron Bernstein wave and a lower-hybrid wave while propagating through magnetized quantum plasma by using modified SSE-QHD model has been analysed. Spin-up and spin-down electrons have been taken to be separate species of particles and spin-spin interaction picture has been developed. The kinetic theory has been used to obtain the response of magnetized electrons. The parametric coupling has been studied and growth rate has been evaluated. The effects of spin polarization and other quantum effects have been analyzed and the results have been compared with earlier studies.

Laser induced Electron Acceleration

The electron acceleration by intense laser pulse is significantly affected by presence of spin polarization, density perturbation and magnetic field. It is noticed that the electron energy rises with increase in the magnetic field strength as well as the normalized frequency increases and energy gain is large for large spin polarization. The electron gains more energy in polarized than in unpolarized quantum plasma. It is also noticed that as well as

plasma density increases electron energy gain reduces due to quantum diffraction effects.

Surface Plasma Wave in Semiconductor Quantum Plasma

A scheme of stimulated SPW excitation in magnetized quantum plasma via stimulated electron-hole recombination in the proximity of the guiding surface was proposed. The dispersion and pointing flux of the surface plasma wave in quantum magnetized plasma was evaluated. It was found that the dispersion and pointing flux properties differ slightly in spin-polarized and unpolarized plasmas. The electron-hole instability of semiconductor in quantum plasma with the spin-polarization can be a problem of interest but we left for a future work. This result may be important for the ultra small electronic devices like travelling wave amplifier and solid density plasmas.

Filamentation of a Short Laser Pulse

Filamentation of a short laser pulse in a magnetized quantum plasma was studied. The direction of the external field has been taken to be along the direction of electron beam propagation in the first case and oblique in the second case. The dispersion for both the cases have been obtained and growth rate evaluated. The numerical analysis for growth rate has been carried out. The results of both the cases have been compared and analysed. Comparison has also been done with earlier studies and the difference is critically analysed and interpreted. The Filamentation instability of a short pulse laser in magnetized quantum plasma is significantly enhanced by the ambient magnetic field. The growth rate is increase with spin polarization in case of longitudinal wave, but in case of oblique the growth rate is reduced with the increase angle. The growth rate increase with magnetic field strength and the laser intensity. The growth rate in fully polarized plasma is about 18-24% more than that in unpolarized quantum plasmas.

Oblique Propagation of E.M. wave

We have briefly described dispersion and growth rate of the e.m wave at oblique propagation. The spin-polarization modifies the dispersion and growth rate dependencies due to the Fermi pressure. The dispersion and growth rate is reduce as the enhance the angle $(0 \to \pi/2)$ at spin polarization for various value, but the dispersion and growth rate increase with both the spin-polarization and angle. In quantum plasma the dispersion and growth rate is about 17% and14% respectively more than that in classical at $(\theta = \pi/4)$, and the quit distinctive in spin-polarized and non-polarized plasmas. The present study may be important for linear case of small perturbation amplitude, astrophysical bodies, non-linear phenomena and instabilities of the electromagnetic waves.

Simulation studies

QED cascade structure in the field of a standing linearly polarized wave was studied in collaboration with Prof. A. V. Kim and A. Bashinov from Institute of Applied Physics, Nizhny Novgorod, Russia. Plasma structures formed as a result of a QED cascade development in the field of linearly polarized standing wave are considered. In view of the inhomogeneous spatiotemporal cascade dynamics and complex particle motion it is proposed to analyze integral structures, which are spatial plasma structures averaged over half-period of the wave. Based on the study of integral structures with and without allowance for a QED cascade as well as on particle trajectories, different plasma structures and their amplitude thresholds are revealed. It is shown that the integral structures maxima can arise not only at the electric field nodes or antinodes, like in a circularly-polarized field, but also between them.

Analysis of the probability of intranuclear transitions in the nucleus of ^{186}Re in the laser plasma of the laser facility "Iskra-5"

M.A. Kulikov, D.E. Larin, G.V. Tachaev, A.A. Yes'man
FSUE "All-Russia Research Institute of Experimental Physics – Russian Federal Nuclear Center", Sarov, Russia

This work is a follow-up of a joint research effort [1] of the Radium Institute and VNIIEF, in which formation of a nuclear isomer substance of hot plasma driven by a high-power laser pulse is used to cause nuclear de-excitation. The main idea of the experiment is to observe the disturbance of the radioactive equilibrium between the metastable state of the isomer ^{186m}Re (half-life $2\cdot10^5$ years) and the unstable ground state of the same isotope (half-life 90.64 hr) in response to a high-intensity laser pulse of "Iskra-5" [2].

For ten months, from March 2016 through January 2017, the irradiated target with ^{186m}Re was subject to spectrometry studies, and the effect has been observed. To explain the effect, we suggest the following model:

– the nucleus of ^{186}Re has an unknown energy level (above the known excited one), to which part of nuclei of the excited state go over during their interaction with laser plasma in the "Iskra-5" laser beam;

– the life-time of a nucleus at this hypothesized level is longer than in the ground state, which disturbs the radioactive equilibrium in the absence of replenishment of the short-lived ground state by the known excited state.

By solving the simple system of equations we obtain:

$$\begin{cases} x(t) = \dfrac{z_0\lambda_y\lambda_z}{\lambda_z-\lambda_y}\cdot\left(\dfrac{e^{-\lambda_x t}-e^{-\lambda_y t}}{\lambda_y-\lambda_x}-\dfrac{e^{-\lambda_x t}-e^{-\lambda_z t}}{\lambda_z-\lambda_x}\right)+ \\ +\dfrac{y_0\lambda_y}{\lambda_y-\lambda_z}\cdot\left(e^{-\lambda_x t}-e^{-\lambda_y t}\right)+x_0e^{-\lambda_x t}; \\ y(t) = \dfrac{z_0\lambda_z}{\lambda_z-\lambda_y}\cdot\left(e^{-\lambda_y t}-e^{-\lambda_z t}\right)+y_0e^{-\lambda_y t}; \\ z(t) = z_0e^{-\lambda_z t}, \end{cases}$$

where x, y, z are the relative numbers of nuclei occupying the ground, the excited and the hypothesized levels, respectively;

λ is the decay constant of a nucleus at a respective level

the x_0-to-y_0 ratio is determined from the secular equilibrium condition $x_0\cdot\lambda_x = y_0\cdot\lambda_y$, so the system has two free parameters: the fraction of laser-driven nuclei jumping to the hypothesized level, z_0, and the decay constant of this level, λ_z.

Fitting the free parameters for the best match between experiment and theory gave the following estimates: $z_0 = 0.1$, $\lambda_z = 10^{-6}$ s^{-1}, which corresponds to a half-life of 400 hours.

Data comparison plots are shown in figure 1. Uncertainties are given for the 1σ level.

Using single-nucleon model, one can estimate the following parameters of the hypothesized level: spin-parity is 7^+ and energy is 3.2 keV.

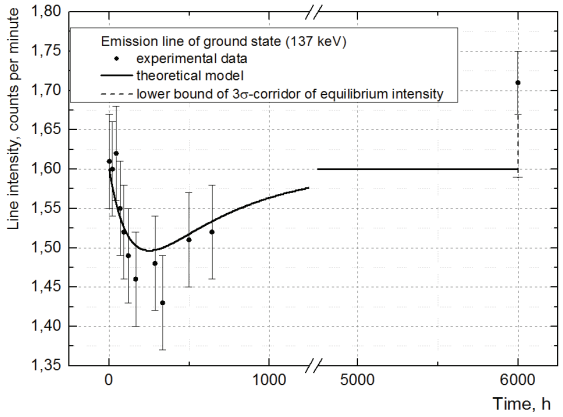

Fig. 1: Line intensity of the ground state as a function of time

The intensity of x-ray emission that is supposed to stimulate gamma-decay of isomer was assessed by a one-dimensional Monte-Carlo calculation of the problem [3]; the calculation shows that the intensity is too low to accelerate the decay. However, in the atom of rhenium the electron binding energy on the $M1$-shell is 2.932 keV, which is very close to our estimates of intranuclear transition energies in ^{186}Re. Thus, the electron conversion factor can reach a value of the order 10^{20}.

In any case, the mechanism of energy transition stimulation in atomic nuclei remains unclear for the time being. So, one of the evident ways to make the hypothesized effects more measurable is to enrich the preparation in the isomer in further experiments to improve the statistical confidence of the measurements.

References

[1] Vatulin V.V., Zhidkov N.V., Rimsky-Korsakov A.A., et al. Search for induced discharge of the isomeric state of the nuclei of ^{186m}Re in the plasma of the laser facility "Iskra-5". // Izvestiya RAN. Ser. fiz. 2017. Vol. 81, no. 10, p. 401. [In Russian]

[2] Annenkov V.I., Bagretsov V.A., Bezuglov V.G., et al. 120-TW pulsed laser "Iskra-5" // Kvantovaya elektronika. 1991. 18, no.5. P. 536-537. [In Russian]

[3] Morenko L.Z., Ryabikina N.A., Kibkalo A.A. Monte-Carlo simulations of spectral radiation transport under non-equilibrium burning conditions in the code MIMOZA (MIMMK) // Voprosy atomnoi nauki i tekhniki. Ser. Matematicheskoe modelirovanie fizicheskikh protsessov. 2003. Issue 2. P. 48-51. [In Russian]

Stretcher simulation for temporal laser pulse profile optimization*

V.A. Schanz[1,2], V. Bagnoud[1], and M. Roth[2]
[1]GSI, Darmstadt, Germany; [2]TU Darmstadt, Darmstadt, Germany

The temporal pulse profile of a high-intensity laser pulse is very relevant for laser-plasma experiments. Parts of the pulse interacting with a target are already intense enough to create a pre-plasma prior to the arrival of the main peak. The rising slope of the laser pulse, which persists hundreds of picoseconds, influence the pre-plasma conditions the most. Several publications in the past conclude noise in the CPA-systems stretcher as the prime reason for this slow rising slope. For further investigation, we developed a MATLAB based ray tracing code, simulating stretcher geometry with the possibility to generate noise at the optics of the stretcher. In this report, we present the status quo of this ray tracing simulation.

Temporal pulse contrast

Up to the present day, all short-pulse high-intensity laser systems have one issue in common: the need to improve and understand their temporal contrast, which is defined as the ratio of the maximum intensity to the intensity of the pulse at a certain time before the maximum. Especially, the rise time at the leading edge of the main peak, which is depicted in figure 1, is much longer than a Fourier-transform limited pulse dictates.

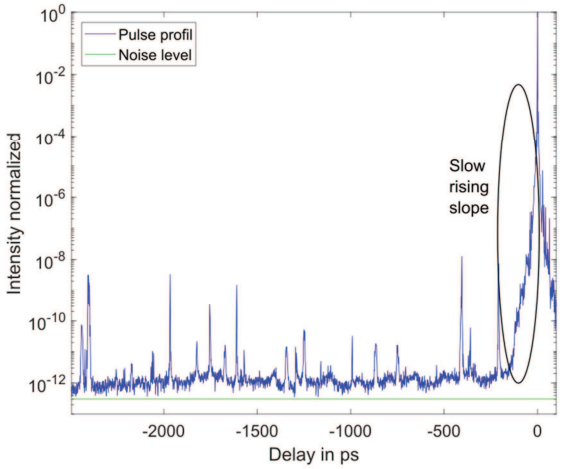

Figure 1: Temporal pulse profile of the PHELIX laser, measured with a specially designed detector [1,2]. The detection limit is shown in green and the leading edge, which will be improved with the development presented in this report, is highlighted in black.

Almost all high-intensity short-pulse laser systems are based on the chirped pulse amplification (CPA), where the pulse is temporally stretched, amplified and afterwards recompressed. Stretching and compression are done by the arrangement of dispersive optics, e.g. gratings, whereby a wavelength dependent optical path is achieved. Today's conventional wisdom expects the main reason for the shape of the leading slope in amplitude and phase modulations in the stretcher.

Ray tracing CPA system analyzation

To investigate this topic, we created a MATLAB based ray tracing code and simulated the propagation of a beam through a stretcher- compressor setup (fig. 2), resulting in zero dispersion after propagation through the whole system.

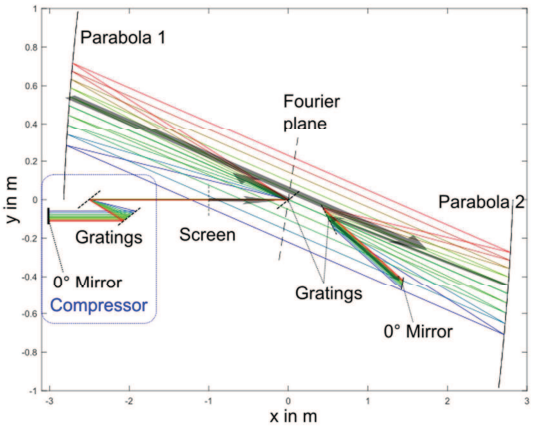

Figure 2: Visualization of a simulated beam path, generated with a self-written ray tracing code. Different colours represent beams with different wavelength. Rays start at the screen, propagating to the right, following the indicated grey arrows. After hitting the 0° mirror, they propagate back on the same path, passing the screen and entering the compressor. For clarity reasons, no arrows are shown for the second pass (back) in the stretcher and the passes in the compressor.

Randomly distributed scattering objects, with densities corresponding to clean room definitions, are defined on the gratings and the Fourier plane. When hit, such an object will attenuate the intensity of an incoming ray and apply an additional phase. At a defined screen the spectrum and spectral phase of the resulting pulse after propagation through the system is determined. This allows the calculation of the resulting temporal pulse profile.
Parameter studies will be carried out this year to investigate the influence of different distortions at different optics, followed by experimental verification.

References

[1] V.A. Schanz et al., “Noise reduction in third order cross-correlation by angle optimization of the interacting beams”, Opt. Express 25, 9252-9261 (2017)
[2] V.A. Schanz et al. EP 16 188 142.0, EPO, patent pending

* This report is also submitted to the GSI Scientific Report 2017

Transient band occupation in laser-excited gold

P. D. Ndione[1], *S. T. Weber*[1], *D. O. Gericke*[2], *and B. Rethfeld*[1]

[1]Fachbereich Physik und Landesforschungszentrum OPTIMAS, Technische Universität Kaiserslautern, Germany;
[2]Centre for Fusion, Space and Astrophysics, Department of Physics, University of Warwick, UK

Over many decades, several theoretical studies have been carried out in order to better understand how matter reacts in presence of laser light. Yet, some questions still remain; especially with respect to changes of the optical properties such as reflectivity and transmission. The laser pulse drives the material out of equilibrium, due to absorption of photons by the electrons. Then, excited electrons redistribute their energy among themselves and, later, also transfer it to the initially cold lattice [1, 2]. During excitation and relaxation, several kinetic processes are involved which happen on different timescales. To trace optical properties, several analytical models have been proposed such as Lindhard and Mermin dielectric function [3, 4]. The latter require the full distribution as input parameter.

Under nonequilibrium, Boltzmann collisions integrals seem to be suitable to obtain the electron and phonon distributions [1, 2]. However, such calculations are extremely complicated and time consuming. In addition, the knowledge of the distributions is not of major importance on a timescale of a hundred of femtoseconds. Both Lindhard and Mermin functions, which are wavevector and frequency dependent, converge in the optical limit ($\boldsymbol{q} \to 0$) to the well known Drude dielectric function,

$$\varepsilon_r^L(0,\omega_L) = 1 - \frac{4\pi e^2}{{\omega_L}^2} \sum_{\ell,\ell'} |\langle \boldsymbol{k}+\boldsymbol{q}, \ell' | \exp(i\boldsymbol{q}.\boldsymbol{r}) | \boldsymbol{k}\ell \rangle|^2 \times \int dE_{\boldsymbol{k}_\ell}\, f(E_{\boldsymbol{k}_\ell}) D(E_{\boldsymbol{k}_\ell}) \frac{\partial^2 E_{\boldsymbol{k}_\ell}}{\partial \boldsymbol{k}_\ell^2}, \tag{1}$$

where we sum over all wave numbers in all bands. $f(E_{\boldsymbol{k}l})$ denotes the electron distribution function, $D(E_{\boldsymbol{k}l})$ is the density of states and the second energy derivative represents the effective mass. The knowledge of the bands occupation should be sufficient to calculate the optical properties. However one should keep in mind that terms accounting for interband transitions are needed.

For metals excited with optical photons, we may trace the transient band occupation by solving rate equations. In our model, we consider two active bands: sp and d, corresponding to conduction and valence bands, respectively. We assume a joint electronic temperature for both bands. Then the equations for the occupation and energy read

$$\frac{dn_{sp}}{dt} = \frac{\alpha_{\text{inter}}}{\hbar\omega_L} I_L - \frac{1}{\tau_{\text{relax}}} \left(n_{sp} - n_{sp}^{eq}(T_e, \mu(T_e)) \right), \tag{2a}$$

$$(C_{sp} + C_d) \frac{\partial T_e}{\partial t} = (\alpha_{\text{intra}} + \alpha_{\text{inter}}) I_L. \tag{2b}$$

The laser mostly excites electrons from d to sp shells. The dynamics of sp electrons is described in Eq. (2a). There, excitation of electrons is determined by the energy absorbed from the laser. This is governed by interband absorption coefficient α_{inter} and photon energy $\hbar\omega_L$. Later, the system relaxes to an equilibrium density $n_{sp}^{eq}(T_e, \mu(Te)) = \int dE\ f(E, T_e, \mu(T_e)) D_{sp}(E)$. We assume that the system relaxes to that density with a relaxation time τ_{relax}. The electrons' temperature T_e is traced in Eq. (2b) with C_{sp} and C_d being the heat capacity of sp and d electrons, respectively. Fig. 1 illustrates time-dependent sp density in gold. One may attribute the density increase to the contribution of interband transitions and its decay to the relaxation process.

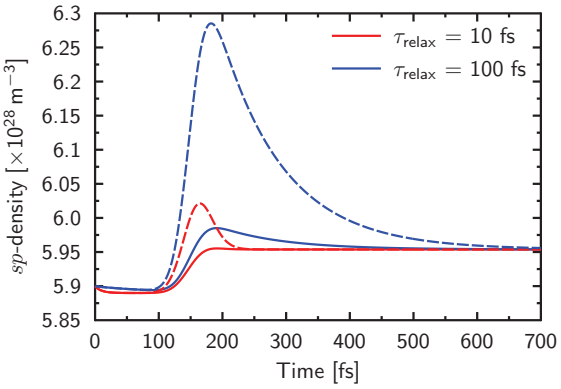

Figure 1: Transient sp-density in gold for different absorption parameters and relaxation times. d-band electrons are excited to states above the Fermi level with a 50 fs laser pulse centered a three times the pulse duration and with a maximum intensity of $I_{\text{max}} = 6.8 \times 10^{14}$ W/m^2 and photon energy $\hbar\omega_L = 1.5$ eV. Then, electrons relax to an equilibrium density with a relaxation time τ_{relax}. Solid and dashed lines stand for, α_{inter} being 10% and 50% of total absorption coefficient.

Advances in laser technologies provide diverse light sources such as VUV or X-ray pulses. With these radiations, excitation of deeper bands is possible. That involves more kinetic processes and also more than two bands are required to properly describe such systems.

References

[1] S. T. Weber and B. Rethfeld, *ASS*, **417**, 64 (2017).
[2] B. Y. Mueller and B. Rethfeld, *PRB*, **87**, 035139 (2013).
[3] J. Lindhard, *MFM*, **28**, 8 (1954).
[4] N. D. Mermin, *PRB*, **1**, 2362 (1970).

Magnetic mirror simulation to boost electron beam heated HED

B. Fathinejad[1], J. Jacoby[1]

[1]Institute for Applied Physics, Goethe University, Frankfurt am Main, Germany.

Introduction

The properties of warm dense matter and high energy density matter (HED) are important in planetary science, astrophysics and for inertial fusion science. The effective heating of a dense target to high temperatures is a major challenge here. It has been shown that intense laser pulses can produce high-current relativistic electrons with significant efficiency [1, 2]. Shortcomings for an effective heating with intense electron beams are a big initial emission angle and a large energy spread of the emitted relativistic electrons. With an imposed axial magnetic field it should be possible to channel electron beams into the target. Recently, a magnetic field of 600 T was produced by laser driven coils to compress and guide these electron beams [1]. Electron beam heated cone targets with magnetic guidance achieve core temperatures of about 1.7 keV [2], where about 5 keV are required to initiate burning in a pellet. To improve the heating, it has been suggested [3] to use magnetic mirrors to enhance the temperature in a dense target.

Simulation and Results

A magnetic mirror reflects any charged particle beam entering an increasing magnetic field, if the emission angle at beginning is big enough (1). The physical reason for this reflection is basically angular momentum conservation of the beam particles.

$$\frac{v_{\parallel}}{v_{\perp}} < \sqrt{\frac{B_{max}}{B_{min}} - 1} \qquad (1)$$

E.g. for an emission angle of α=45° the reflection condition $B_{min} < B_{max}/2$ is derived. This reflection is not energy dependent.

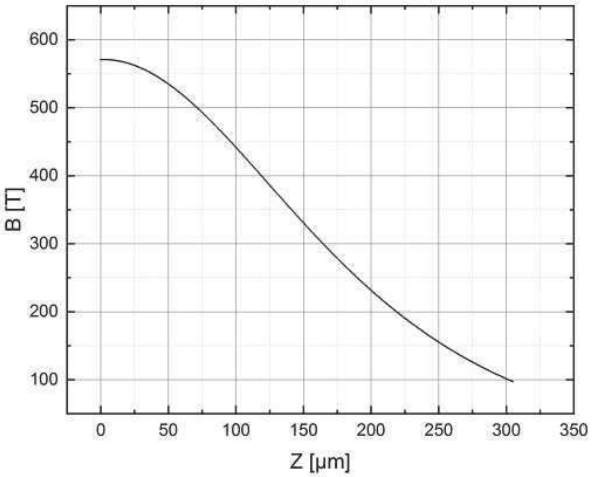

Figure 1: The magnetic field distribution of a single coil with R= 250 µm at the axis of this coil.

The magnetic field of a single coil with the radius R=250 µm was simulated with currents of 250-300 kA using CST particle studio (Fig. 1). The obtained trajectories of the simulation are shown in Fig. 2. The beam trajectories are cut off shortly after reflection. The source of the electrons was assumed to have an emission angle of α=35° to the axis with a 10 µm surface diameter and at a distance of 250 µm to the coil center. The distance between the reflection and the coil center remains about 65µm. The resulting gyro-diameter at the mirror-point is about 30 µm for the assumed 2 MeV electron beam. Energy and emission angle are simulated without spread. Also not considered are space charge effects of the emitted electrons and a possible pinching of the beam due to high currents even if this in principle could be included with CST particle studio.

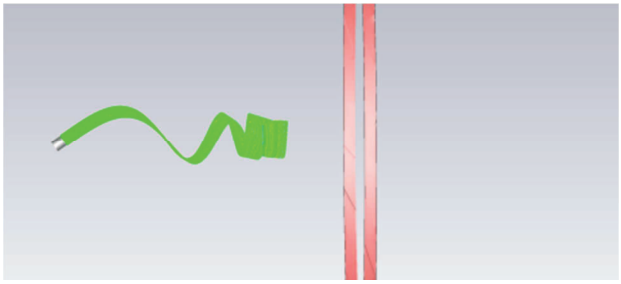

Figure 2: A projection of the trajectory of the 2 MeV electron beam moving towards the coil centre. The beam trajectories are cut off shortly after reflection.

Discussion

The achieved temperature heated by a particle beam depends from the deposited energy in the target which for high energies is proportional to the path length in the medium. If we assume that the reflected beam performs two turns at a short distance instead of just passing through then the deposited energy and in turn the temperature should be enhanced by about a factor 2 π. This might be just the missing factor to boost a pellet towards ignition. The field strength and the shape of the reflecting field will of course be influenced by the dynamic compression of the hot pellet shell, which however may even allow enhancing the magnetic field by factors higher than directly produced by a laser driven coil. This may further minimize the heated area and enhance the temperature by reducing the gyro-diameter at reflection.

References

[1] M. Bailly-Grandvaux et al., Nature Communications 9 (2018) 102

[2] Y. Sentoku et al., Demonstration of REB Drive Fast Ignition with Assistance of External Magnetic Field in FIREX Project, 10th IFSA, St. Malo, Sep. 2017

[3] J. Jacoby, Plasma Jets and Magnetic Mirrors to Boost Ignition, 37th HED Workshop, Hirschegg, Feb. 2018

Twisted light modes and their influence on relativistic electron dynamics

C. Baumann[*1] *and A. Pukhov*[1]

[1]Institut für Theoretische Physik I, Heinrich-Heine-Universität Düsseldorf, 40225 Düsseldorf, Germany

Introduction

Allen *et al*. discovered in 1992 that Laguerre-Gaussian (LG) laser beams carry a well-defined orbital angular momentum (OAM) [1]. These laser modes have helical phase fronts (see, for instance, Fig. 1) and are often referred to as twisted light modes. According to a wide range of possible applications, studies about twisted light-matter interaction are currently conducted extensively (see [2] and references therein). In the present work, it is therefore discussed how electrons behave when they are subjected to twisted light pulses of relativistic intensities.

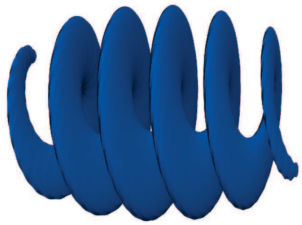

Figure 1: The phase front of a LG mode, characterized by the mode indices $p = 0$ and $m = -1$, is shown. The reader can find more information about LG modes in [3].

Results

The results are obtained by performing three-dimensional particle-in-cell (PIC) simulations with the code VLPL [4]. A series of four simulations has been conducted in which a circularly polarized LG laser pulse of relativistic intensity ($I = 2.47 \times 10^{21}$ Wcm^{-2}) irradiates a cylindrical plasma target ($L = 30$ μm and $R = 10$ μm) at normal incidence. The several runs differ by the used twisted light mode ($m = -1, -2$) and the chosen helicity ($s = \pm 1$) of the laser. The p-index of the LG mode is always set to 0. The laser has a Gaussian temporal profile with a FWHM duration of roughly 25 fs and a beam waist of $w_0 = 8$ μm. The initial electron density of the target is much less than the critical density.

Figure 2 finally shows the three-dimensional electron distribution at a fixed moment in time. It can be seen that the electron dynamic strongly depends on both the twisted light mode itself and on the helicity of the laser pulse. In the first case ($m + s = 0$), one generates ultra-short ($\sim$ 200 as) disk-like electron bunches that are separated in the longitudinal direction by the laser wavelength. In all other cases ($m + s \neq 0$), electrons are distributed on $|m + s|$ spiral-shaped orbits.

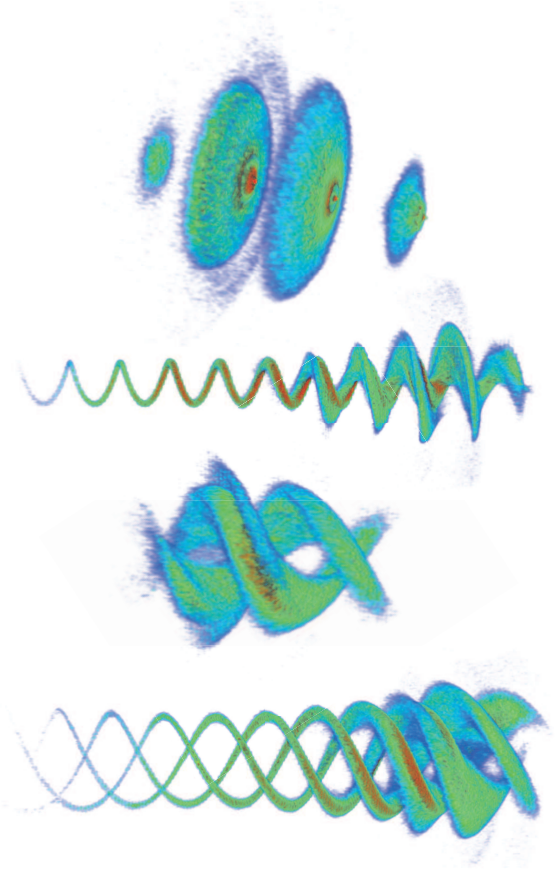

Figure 2: The electron distribution of four different runs is shown. The parameters are as follows: $m + s = 0$, $m + s = -1$, $m + s = -2$ and $m + s = -3$. The propagation axis of the laser coincides with the symmetry axis of each subplot.

References

[1] L. Allen *et al*., Phys. Rev. A 45, 8185 (1992)

[2] J. P. Torres and L. Torner, Twisted photons: Applications of Light with Orbital Angular Momentum, John Wiley & Sons (2011)

[3] P. F. Goldsmith, Quasioptical systems: Gaussian Beam Quasioptical Propagation and Applications, Wiley-IEEE Press (1998)

[4] A. Pukhov, J. Plasma Phys. 61, 425 (1999)

* Christoph.Baumann@tp1.uni-duesseldorf.de

Effect of Lattice Temperature on the Ion Track Kinetics in Alumina

A.E.Volkov[1,2,3#], S.A.Gorbunov[2], N.A. Medvedev[4,5], R. A. Rymzhanov[3]
[1]NRC KI, Moscow, Russia; [2]LPI of RAS, Moscow, Russia; [3]JINR, Dubna, Russia; [4]Institute of Physics of CAS, Prague, Czech Republic; [5]IPP, Prague, Czech Republic

A new version [1] of the Monte-Carlo code TREKIS [2,3] is used to investigate an effect of a target temperature on lattice excitation by the relaxing electron ensemble in a swift heavy ion (SHI) track.

Collective responses of the electronic and ionic systems to their subpicosecond excitations in SHI tracks are taken into account without unnecessary macroscopic assumptions and fitting parameters. The cross sections applied in TREKIS are constructed within the dynamic structure factor ($S(\omega,\boldsymbol{q})$, DSF) and complex dielectric function ($\varepsilon(\omega,\boldsymbol{q})$, CDF) formalism:

$$\frac{d^2\sigma}{d(\hbar\omega)d(\hbar q)} = \frac{2\left(Z_e(v)e\right)^2}{n_{sc}\pi\hbar^2v^2}\frac{1}{\hbar q}\left[1-e^{-\frac{\hbar\omega}{k_BT}}\right]\mathrm{Im}\left(\frac{-1}{\varepsilon(\omega,q)}\right) \quad (1)$$

Here $Z_e(v)$ is the effective charge of a projectile as a function of the velocity v; e is the electron charge; $\hbar\omega$ and $\hbar q$ are the transferred energy and momentum respectively; k_B is the Boltzmann constant, and T is the temperature of the sample; n_{sc} is the spatial density of scattering centers.

The DSF of a lattice is modelled via molecular dynamic simulations which enables taking into account: (a) all modes of lattice collective response; (b) dependence of this response on the initial lattice temperature [1].

The exponential term in Eq.(1) appears due to the asymmetry of the lattice DSF dependence on the temperature, $T_{lattice}$

$$S(\boldsymbol{q},\omega) = \exp\left(\frac{\hbar\omega}{k_BT_{lattice}}\right)S(-\boldsymbol{q},-\omega) \quad (2)$$

In order to demonstrate the effect of such an asymmetry, excitation of the alumina lattice by an SHI is investigated for two different irradiation temperatures: at 80 K, which is lower than the energies of most acoustic phonons ($k_BT_{lattice} << \hbar\langle\omega_{acc}\rangle = 0.11$ eV), and at 300 K ($k_BT_{lattice} \sim \hbar\langle\omega_{acc}\rangle$).

A considerable increase of the elastic mean free paths of electrons and valence holes in alumina at 80 K in comparison to those at 300 K is detected, since less intensive scattering of electrons and holes on phonons [1].

Electrons can not only transfer energy *to* the atoms, but also receive it *from* the lattice. An especially significant difference in the phonon emission mean free paths is observed [1] at 80K vs. 300K due to the asymmetry of DSF. At 80 K the lattice receives energy much more often than returns it back to scattering electrons and valence holes. This leads to higher levels of lattice excitation occurring in the vicinity of SHI trajectories in crystals irradiated at 80 K in comparison to that at 300 K (fig.1).

The excess energy of lattice atoms is shown in terms of the temperature in fig.1 in order to compare the excitation level with the initial lattice state, whereas in fact the lattice is not thermalized during such ultrashort times [1].

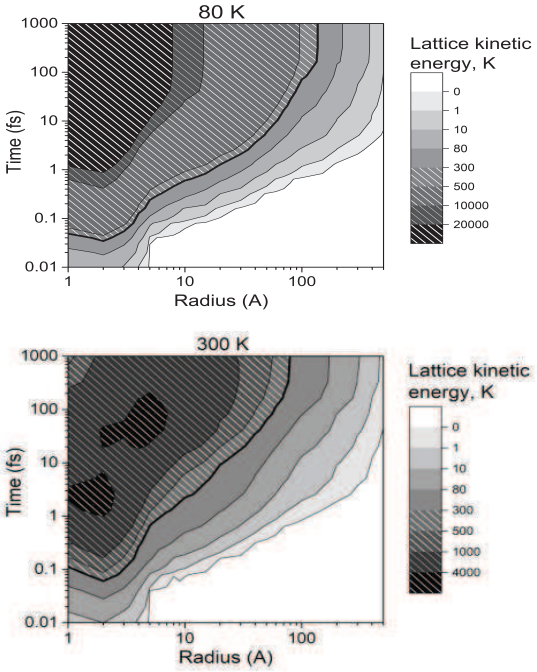

Figure 1: Spatial and temporal dependencies of the excess lattice energy in tracks of Xe 167 MeV ions in Al_2O_3 irradiated at 80 K and 300 K. Shaded areas indicate significant energy increase at which evolution of the cross sections need to be included.

It should be noted that the used initial lattice DSF is valid only at times before the energy deposited into the lattice overcomes the initial temperature. At longer times evolution of the cross sections needs to be included. In the shaded areas in Fig. 1, more sophisticated effects can be expected, such as fast changes of the momentum distribution function of lattice atoms frozen in their positions, as well as nonequilibium processes in the lattice.

References

[1] S.A. Gorbunov, N. Medvedev, R.A. Rymzhanov, A.E. Volkov. Nucl. Instr. Meth B (2018) DOI: 10.1016/j.nimb.2018.01.005
[2] N. Medvedev, A.E. Volkov, J.Phys.D **50** (2017) 445302
[3] R.A. Rymzhanov, N.A. Medvedev, A.E. Volkov, Nucl. Instr. Meth. B 388 (2016) 41

a.e.volkov@list.ru

Simulated swift heavy ion tracks in Al_2O_3

R. A. Rymzhanov[1,#], N.A. Medvedev[2,3], and A.E.Volkov[1,4,5]
[1]JINR, Dubna, Russia; [2]Institute of Physics of CAS, Prague, Czech Republic; [3]IPP, Prague, Czech Republic; [4]LPI of RAS, Moscow, Russia; [5]NRC KI, Moscow, Russia.

Structural changes, formation threshold and overlapping of swift heavy ion (SHI) tracks in Al_2O_3 are studied using a combined start-to-end numerical model. The asymptotic trajectory Monte Carlo code TREKIS (Time-Resolved Electron Kinetics in SHI Irradiated Solids) [1] is used to determine the initial parameters characterizing an excited state of the ensemble of electrons as well as energies transferred to lattice atoms via electron lattice coupling in an ion track. The model is based on the dynamic structure factor - complex dielectric function formalism which takes into account collective responses of the target lattice and electronic ensemble to excitation by a projectile and fast electrons generated in a track.

TREKIS simulates: (a) penetration of an SHI resulting in ionization of a target and appearance of primary electrons (δ-electrons) and holes; (b) scattering of δ-electrons on lattice atoms and target electrons as well as the kinetics of all secondary generations of electrons arising during relaxation of the electron subsystem; (c) Auger decays of core holes, also resulting in production of secondary electrons; (d) radiative decays of core holes, following photon transport and photoabsorption exciting new electrons and holes; (e) valence holes mobility and their interaction with target atoms.

The results of Monte-Carlo simulations (radial distribution of the energy transferred into the lattice) are then used as input data for classical molecular dynamics simulating subsequent lattice response and structure transformations near the ion trajectory.

Application of this model demonstrated a good agreement with experiments. For example, simulations of Xe 167 MeV ion impacts showed that relaxation of an excess lattice energy results in formation of a cylindrical discontinuous disordered region of about 2 nm in diameter. The threshold of an SHI track formation was estimated to be ~6.1 keV/nm (Fig. 1a). Recent transmission electron microscopy observations confirmed these predictions [2]. Calculated X-ray diffraction patterns of irradiated material demonstrated more pronounced damage of the Al atoms sublattice near SHI trajectories [3].

Qualitatively different effects of overlapping of tracks of Xe 167 MeV (S_e=25 keV/nm) vs Bi 700 MeV (S_e=42 keV/nm) ions were revealed in alumina. The subsequent Xe ion induced recovery of the first track when the second track is within a radius of 6.5 nm. This thermal-like annealing seems to be the mechanism of the saturation of the number of tracks observed in the experiments. For the higher stopping power (Bi ion), both simulations and experiment demonstrated an effect of formation of a damaged region connecting Bi ion tracks (Fig. 1b). Only at higher fluences of Bi ions (shorter distances between ions trajectories) partial recovery of tracks starts [3].

References

[1] N.A. Medvedev et al. J. Phys. D 48 (2015) 355303
[2] R.A. Rymzhanov et al. J. Phys. D, 50 (2017) 475301
[3] R.A. Rymzhanov et al. Nucl. Instr. Meth B, (2017) DOI: 10.1016/j.nimb.2017.11.014

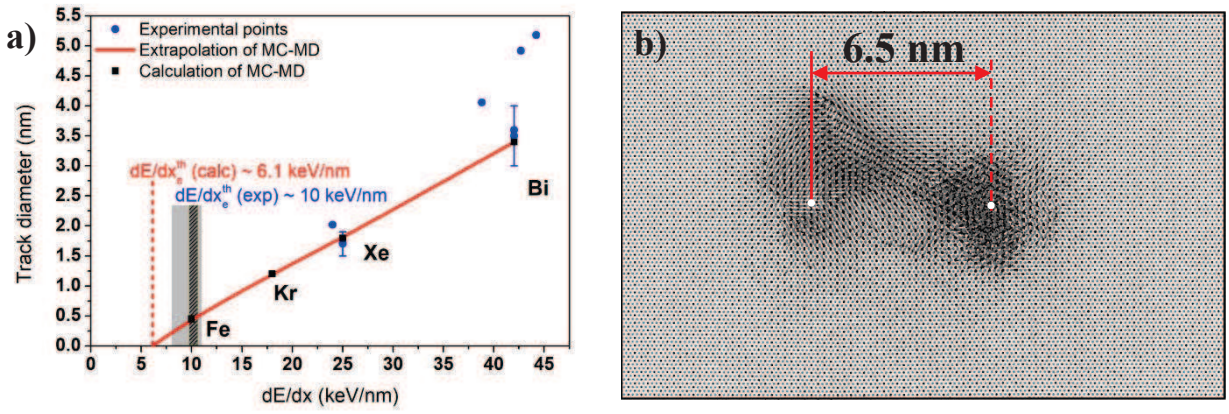

Figure 1: a) Dependence of the track diameter on the energy loss of an ion (dE/dx) in alumina; b) Results of a simulation of two subsequent impacts of Bi 700 MeV ion in Al_2O_3.

#rymzhanov@jinr.ru

XTANT: X-ray-induced Thermal And Nonthermal Transitions modelled with a hybrid approach

N. Medvedev[1,#], V. Tkachenko[2,3], V. Lipp[3], Z. Li[3,4], B. Ziaja[3,5]

[1]Institute of Physics and Institute of Plasma Physics, Czech Academy of Sciences, Prague, Czechia; [2]Institute for Laser and Optics, Hochschule Emden/Leer - University of Applied Sciences, Emden, Germany; [3]CFEL, DESY, Hamburg, Germany; [4]Max Planck Institute for the Structure and Dynamics of Matter, Hamburg, Germany; [5]Institute of Nuclear Physics, Polish Academy of Sciences, Krakow, Poland

Our recently developed hybrid code XTANT (X-ray-induced Thermal And Nonthermal Transitions [1–4]) describes transitions win solids and molecules under X-ray free-electron-laser (FEL) irradiation. It combines a few different approaches, interconnected and executed in parallel:

(a) Monte Carlo module tracing X-ray photon absorption, high-energy electrons kinetics, and core holes decay;

(b) module describing evolution of the low-energy electrons, using rate equations and a thermodynamic approach;

(c) the Boltzmann collision integral module following nonadiabatic electron-ion energy exchange;

(d) transferable tight binding module for calculations of the transient electronic band structure and atomic potential energy surface;

(e) molecular dynamics module to trace atomic motion.

In order to make direct comparison with experimental results, XTANT provides transient optical coefficients of the irradiated target [5], as well as the corresponding diffraction patterns.

With this approach, we studied various damage mechanisms and temporal evolution of X-ray irradiated silicon [3], diamond [1,5], amorphous carbon [4], C_{60} crystal [4], and GaAs [6] under high energy density deposition by an FEL pulse. We examined the irradiation conditions leading to thermal melting of targets as a result of electron-lattice energy exchange [3,4]; nonthermal phase transitions due to modification of the interatomic potential [1]; Coulomb explosion due to accumulated net charge in finite-size systems [4]; spallation or ablation at higher fluences due to a detachment of sample fragments [4].

Comparisons with the experimental data, whenever available, confirmed the predictivity and accuracy of our combined approach. For example, in Refs. [1,5] we described an ultrafast phase transition of diamond into an overdense graphite state within 150-200 fs, in a perfect agreement with the experiment [5]. The atomic snapshots from the simulation are shown in Fig. 1.

We demonstrated that such nonthermal graphitization of diamond proceeds via multiple steps [5]. The initial electronic excitation occurs during the FEL pulse, after which photoelectrons relax to the bottom of the conduction band via collisional processes and the resulting electron cascading. Electronic excitation triggers a band gap collapse [1]. This occurs within ~50 fs after the pulse maximum of the FEL pulse, at the time instant when the density of conduction band electrons overcomes the threshold value of ~1.5% [1]. It is followed by the atomic relocation towards new positions corresponding to graphite (occurring at ~150-200 fs). Simultaneously, electronic density in the conduction band increases further, leading to an irreversible phase transition [1,5].

The success of the hybrid code XTANT applied up to now to various FEL-irradiated materials confirms the validity of the underlying physical models and, in general, demonstrates the predictive power of hybrid approaches.

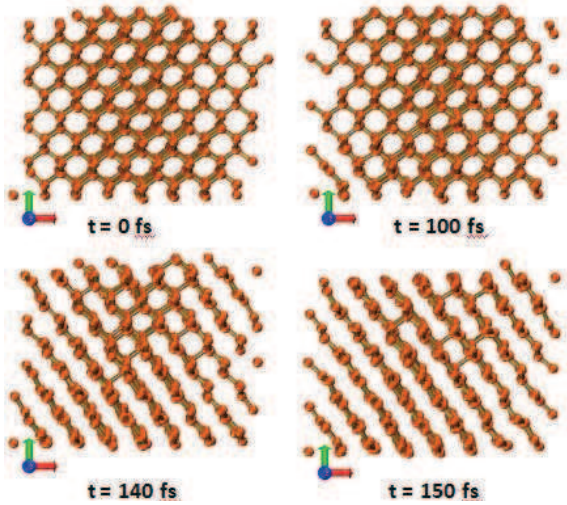

Figure 1: Atomic snapshots of nonthermal graphitization of diamond irradiated with 10 fs FEL pulse (92 eV photon energy, 0.85 eV/atom dose); reproduced from [7].

References

[1] N. Medvedev, H. O. Jeschke, B. Ziaja, New J. Phys. **15**, 15016 (2013).

[2] N. Medvedev, A. E. Volkov, B. Ziaja, Nucl. Instrum. Meth. B **365**, 437 (2015).

[3] N. Medvedev, Z. Li, V. Tkachenko, B. Ziaja, Phys. Rev. B **95**, 14309 (2017).

[4] M. Toufarová *et al.*, Phys. Rev. B **96**, 214101 (2017).

[5] F. Tavella *et al.*, High En. Dens. Phys. **24**, 22 (2017).

[6] V. Tkachenko, N. Medvedev, V. Lipp, B. Ziaja, High En. Dens. Phys. **24**, 15 (2017).

[7] N. Medvedev, V. Tkachenko, B. Ziaja, Contrib. Plasms Phys. **55**, 12 (2015).

nikita.medvedev@fzu.cz

Ab-initio modeling of Al_2O_3 lattice instability under extreme excitation of the electronic system

R.A. Voronkov[1,#], N. Medvedev[2,3], R.A. Rymzhanov[4], A.E. Volkov[1,4,5]

[1]Lebedev Physical Institute of the Russian Academy of Sciences, Leninskij prospekt, 53,119991 Moscow, Russia; [2]Institute of Physics, Czech Academy of Sciences, Na Slovance 2, 182 21 Prague 8, Czech Republic; [3]Institute of Plasma Physics, Czech Academy of Sciences, Za Slovankou 3, 182 00 Prague 8, Czech Republic; [4]Joint Institute for Nuclear Research, Joliot-Curie 6, 141980 Dubna, Moscow Region, Russia; [5]National Research Center "Kurchatov Institute", Kurchatov Sq. 1, 123182 Moscow, Russia

Swift heavy ions (SHI) or free-electron laser beams interacting with solids excite primarily the electronic system of a target within a few tens of femtoseconds. The electronic temperature under conditions of such irradiations reaches several electron-volts and above [1,2]. Apart from exchanging energy with the lattice via electron-ion coupling, such high electronic temperatures modify the interatomic potential of the solid that can induce lattice instability. It may result in unusual phase changes via nonthermal structure transformations (e.g., nonthermal melting) [3,4].

Realization of the nonthermal effect depends on a material and an excitation level of the electronic system. Thus, a dedicated analysis is required to determine how the electronic excitation affects the interatomic forces in a particular material of interest.

We applied Quantum Espresso simulation package [5], based on the density functional Car-Parrinello molecular dynamics [6], to study an effect of the elevated electronic temperature on nonthermal structure instability in Al_2O_3 – a candidate material for inert matrices for the nuclear fuel.

We demonstrated that nonthermal structure transformations due to modification of the interatomic potential by electronic excitation may start in an Al_2O_3 crystal for the electronic temperature above ~2.5 eV [7]. It is shown that for the electronic temperatures higher than $T_e = 4$ eV, nonthermal damage of alumina occurs within ~ 0.5–1 ps, i.e. a typical timescale for X-ray free-electron laser spots. An example of the simulated atomic snapshots is shown in figure 1. This damage manifests itself as order-order phase transition of the lattice into the final state resembling a coexistence of alpha and gamma alumina [7]. These levels of excitation are realistic for FELs, thus nonthermal phase transitions can be expected in experiments.

At the temporal scale of ~50-100 fs, relevant for SHI tracks, the electronic temperature at least above T_e ~ 6-10 eV is required during these times to trigger nonthermal phase transition. At such electronic temperatures, the damage proceeds as amorphization of an Al_2O_3 crystal. However, such levels of excitation are not expected to persist in SHI tracks for the necessary time lapse [1,2]. Thus, we concluded that nonthermal melting is not expected to play a major role in damage induced by swift heavy ion irradiation of alumina [7].

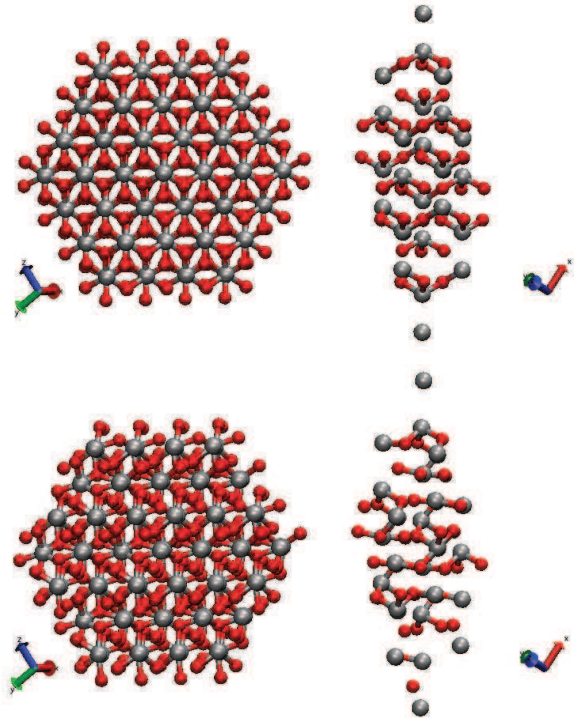

Figure 1: Atomic snapshots of an Al_2O_3 supercell at the initial instant (top panel) and after 1 ps (bottom panel) at the electronic temperature $T_e = 4$ eV. Large grey balls show aluminum atoms; small red balls are the oxygen atoms. Interatomic bonds are colored correspondingly [7].

References

[1] N. Medvedev, A. E. Volkov, and B. Ziaja, Nucl. Instrum. and Meth. B **365**, 437 (2015).
[2] N. Medvedev and A. E. Volkov, J. Phys. D **50**, 445302 (2017).
[3] C.W. Siders, Science 286 (1999) 1340–1342.
[4] S.K. Sundaram, E. Mazur, Nat. Mater. 1 (2002) 217.
[5] P. Giannozzi *et al.*, J.Phys.:Condens.Matter 21 (2009) 395502.
[6] R. Car, M. Parrinello, Phys. Rev. Lett. 55 (1985) 2471.
[7] R.A. Voronkov N. Medvedev, R.A. Rymzhanov, A.E. Volkov, Nucl. Instrum. and Meth. B (*submitted* 2017).

roman.a.voronkov@gmail.com

Monte Carlo simulation of the non-equilibrium spin dynamics

J. Briones * *and B. Rethfeld*
Department of Physics and OPTIMAS Research Center, Erwin Schroedinger Str. 46, 67663 Kaiserslautern, Germany.

When a ferromagnetic film is excited by an ultrafast laser pulse it experiences a partial demagnetization within the first hundreds of femtoseconds (fs) followed by a remagnetization on a larger time scale. During laser excitation the photons primarily excite electrons, bringing the system out of equilibrium. Afterwards, these excited electrons will undergo changes on their spin-angular momenta causing the de- and remagnetization [1, 2]. Many possible scattering mechanisms [3, 4, 5] , as well as superdiffusive transport [6] are under discussion to explain the origin of ultrafast magnetization dynamics.

Magnetization can be calculated from the difference of electron population between two bands of spin-up and spin-down electrons, respectively. In non-equilibrium, not only the change of the spin-dependent population due to the dynamic two bands contributes to the demagnetization, but also the spin-flip scattering (sf) of electrons to quasiparticles, a mechanism related to the transfer of angular momentum from the electronic system to another. Here we will use an ad hoc parameter to describe this spin-flip probability.

We use a particle-based Monte Carlo technique [7] to study the non-equilibrium dynamics. The simulation will have three well defined stages. The first stage occurs during laser excitation. An electron is randomly selected based on the population of the bands. The more populated the area within an energy range of the filled bands, the more probable is an electron to be excited. The second stage takes places immediately after the electron is excited by the laser pulse. We assign for each interaction a probability distribution function and randomly decide which interaction is more probable to occur. For our simulation we have two possibilities, either the excited electron excites another electron by electron impact ionization or it remains unperturbed. We trace all electrons individually with spin resolution, as well as those newly excited. The third stage is related to the convergence of the model. The Monte Carlo technique requires repetition to achieve small relative uncertainty, this means that the process must be repeated several times.

The demagnetization from the equilibrium magnetization, for different values of spin-flip probabilities within the first femtoseconds, is shown in Fig. 1. Remagnetization is not observed since the electron-phonon interaction is yet to be implemented.

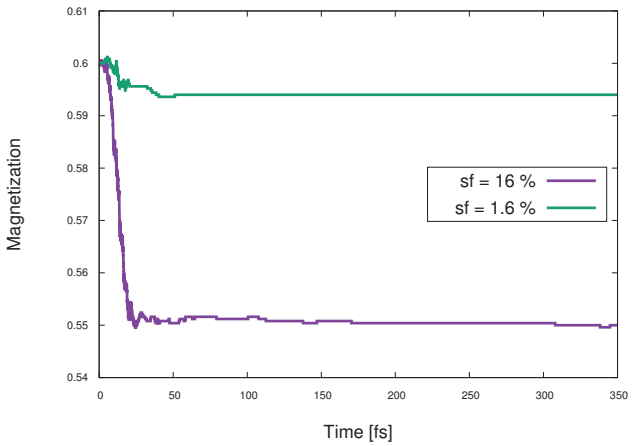

Figure 1: Demagnetization of Nickel for different spin flip probabilities (sf).

References

[1] E. Beaurepaire, J.-C. Merle, A. Daunois, and J.-Y. Bigot, "Ultrafast spin dynamics in ferromagnetic nickel," *Phys. Rev. Lett.*, vol. 76, pp. 4250–4253, May 1996.

[2] B. Y. Mueller, A. Baral, S. Vollmar, M. Cinchetti, M. Aeschlimann, H. C. Schneider, and B. Rethfeld, "Feedback effect during ultrafast demagnetization dynamics in ferromagnets," *Phys. Rev. Lett.*, vol. 111, p. 167204, Oct 2013.

[3] M. Haag, C. Illg, and M. Fähnle, "Role of electron-magnon scatterings in ultrafast demagnetization," *Phys. Rev. B*, vol. 90, p. 014417, Jul 2014.

[4] B. Koopmans, G. Malinowski, F. Dalla Longa, D. Steiauf, M. Faehnle, T. Roth, M. Cinchetti, and M. Aeschlimann, "Explaining the paradoxical diversity of ultrafast laser-induced demagnetization," *Nature Materials*, vol. 9, Dec 2009.

[5] M. Krauß, T. Roth, S. Alebrand, D. Steil, M. Cinchetti, M. Aeschlimann, and H. C. Schneider, "Ultrafast demagnetization of ferromagnetic transition metals: The role of the coulomb interaction," *Phys. Rev. B*, vol. 80, p. 180407, Nov 2009.

[6] M. Battiato, K. Carva, and P. M. Oppeneer, "Superdiffusive spin transport as a mechanism of ultrafast demagnetization," *Phys. Rev. Lett.*, vol. 105, p. 027203, Jul 2010.

[7] K. Huthmacher, A. Herzwurm, M. Gnewuch, K. Ritter, and B. Rethfeld, "Monte carlo simulation of electron dynamics in liquid water," *Physica A: Statistical Mechanics and its Applications*, vol. 429, pp. 242 – 251, 2015.

* briones@physik.uni-kl.de

Spatially resolved ultrafast demagnetization dynamics

S. Ashok, S. T. Weber, J. Briones, and B. Rethfeld*
Fachbereich Physik und Landesforschungszentrum OPTIMAS, Technische Universität Kaiserslautern, Germany

Over the past few decades there has been unprecedented development in the speeds at which machines can perform calculations and process data. Unfortunately the technologies for storing and reading the information are yet to catch up. This creates the urgent need for faster data storage devices. Very promising direction appears to be from an experiment performed by Beaurepaire et al. in 1996. They discovered the manipulation of the magnetization of a thin nickel film on a picosecond timescale when excited with an ultrashort laser pulse [1]. This opened up the possibilities for ultrafast magnetic data storage devices.

Promising models for ultrafast demagnetization dynamics include Elliott-Yafet spin flip process and super diffusive transport. In reality both the processes contribute to the observed ultrafast demagnetization dynamics. Due to the complexity of the phenomenon, various temperature based models such as Three-Temperature model [2] and Microscopic-Three-Temperature models [3] have been proposed. Those models assume spin and charge seperation, which seems questionable for itinerant ferromagnets.

Kinetic calculations have shown that the driving force behind ultrafast demagnetization dynamics is the nonequlibrium between of the chemical potentials of up and down electrons [4]. On that basis, a μT-modelhas been proposed [5] which traces the dynamics of temperatures and chemical potentials of the up- and down-electron subsystems simultaneously. In addition, the temperature of the lattice and the magnetization are taken into account as transient variables. The equations can be simplified into a general matrix formulation of a time- and space-dependent coupled transport equation:

$$\mathcal{C}\frac{d\vec{X}}{dt} = \nabla\mathcal{K}\nabla\vec{X} + \mathcal{G}\vec{X} + \vec{S}, \qquad (1)$$

where $\vec{X}$ is a vector of up- and down- electron temperatures $T_e^{\uparrow,\downarrow}$, lattice temperature T_p chemical potentials of the up- and down-electron subsystems $\mu^{\uparrow,\downarrow}$ and magnetization m. $\mathcal{C}$ is the matrix of capacities, $\mathcal{K}$ is the matrix of transport coefficients and $\mathcal{G}$ is the matrix of coupling between various subsystems. $\vec{S}$ denotes the energy input due to laser pulse. For a thin ferromagnetic film of nickel (where heat and charge transport can be neglected) the demagnetization dynamics was obtained in [4].

For a thick ferromagnetic film, eq. (1) was solved without (Fig. 1) and with (Fig. 2) considering the heat and charge transport. We were able to obtain magnetization profiles as shown in the figures below.

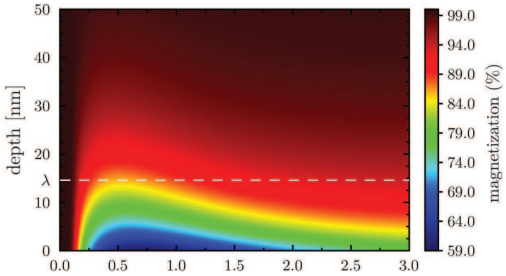

Figure 1: Demagnetization dynamics of nickel film, neglecting transport of heat and charge. λ being the penetration depth of the laser.

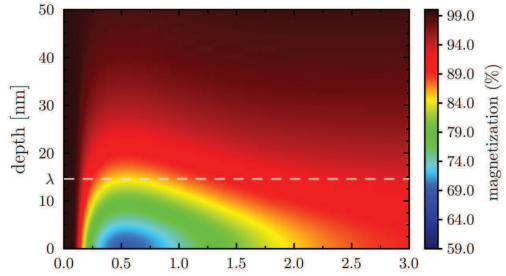

Figure 2: Demagnetization dynamics in nickel film considering transport coefficients from [6]

For thicker films, the de- and re-magnetization at the surface is considerably weaker when heat and charge transport is considered than in the case of neglected heat and charge transport. Also, the remagnetization is faster when transport effects are present. Both of the results can be understood by observing that the electrons that travel into bulk of the material transport energy in addition to energy carried by lattice modes, leading to faster thermalization.

References

[1] E. Beaurepaire, et al., *PRL*, **76**, 4250 (1996)
[2] A. Vaterlaus, et al., *PRL*, **67**, 3314 (1991)
[3] B. Koopmans, et al., *PRL*, **95**, 26207 (2005)
[4] B. Y. Mueller, et al., *NJP*, **13**, 123010 (2011)
[5] B. Y. Mueller and B. Rethfeld, *PRB*, **90**, 144420 (2014)
[6] L. Thesing, Diplomarbeit, Kaiserslautern (2015)

* ashok@physik.uni-kl.de

Adiabatic invariants from the Poincaré-Cartan integral invariant

P. Mulser* and G. Alber
Institut für Angewandte Physik, Technische Universität Darmstadt, D-64289 Darmstadt, Germany

In the case of an explicit secular time dependence adiabatic invariants replace the no longer valid energy conservation. Starting from the basic Poincaré-Cartan integral invariant a compact proof of the rules is given adiabatic invariances obey in the libration and rotation mode. As an important application the ponderomotive force in the longitudinal electric wave is determined and the condition for particle trapping in the wave is deduced. Adiabatic invariants play a central role in thermodynamics; they are entropy conserving.

Adiabatic invariants are of considerable importance in all fields of physics: charged particle motion in slowly changing magnetic fields, in nonlinear optics in inhomogeneous media, as WKB approximation for instance, parametric instabilities in the laser field, like resonantly driven Brillouin and Raman excitations, in fluid dynamics and in thermodynamics. There, they are entropy conserving. Finally, all ponderomotively grounded phenomena are reducible to the adiabatic conservation of action. In a time dependent Hamiltonian energy is no longer conserved owing to $dH/dt = \partial H/\partial t \neq 0$. Histor-ical examples of adiabatic invariances are the Einstein-Bohr pendulum of slowly varying length, conservation of the magnetic moment and the ball bouncing between two parallel plates changing their relative distance $l(t)$ from each other. In all cases energy $\times$ cycle time T is conserved. From the bouncing ball for example follows that the Fermi energy of the ideal gas is proportional to the density to power 2/3.

In the nearly periodic particle motion there are two classes of phenomena: *libration*, if the orbit is nearly closed in phace space like Galilei's pendulum, and *rotation*, if the orbit is quasi periodic and open like the overturned pendulum rotating around its horizontal axis. Other examples of the two modes are particles trapped in a wave and detrapped particles. There exist more or less convincing proofs for libration following $\oint \mathbf{p}d\mathbf{q} = \text{const}$ in phase space of momentum $\mathbf{p} = m\mathbf{v}$ and position $\mathbf{q} = \mathbf{x}$, however the law governing rotation does not seem to be common knowledge. We give a compact proof of both modi of operation based on the fudamental *Poincaré-Cartan invariant* (PCI) [1].

Motion in the extended phase space $\{\mathbf{p}, \mathbf{q}, t\}$ can be visualized by the directions $\dot{\mathbf{p}} = -\partial H/\partial \mathbf{q}$, $\dot{\mathbf{q}} = \partial H/\partial \mathbf{p}$ and direction 1 along t. They determine uniquely the orbits $\mathbf{p}(t)$, $\mathbf{q}(t)$, see Fig. 1. The PCI tells that the phase flow through an arbitrary cross section of a bundle of orbits emanating from L_0 is constant. Assume now that $H = H(\mathbf{p}, \mathbf{q}, t; \lambda(t))$ with λ slowly changing in time. We formulate the adiabatic theorem in 7 dimensionsional phase space:

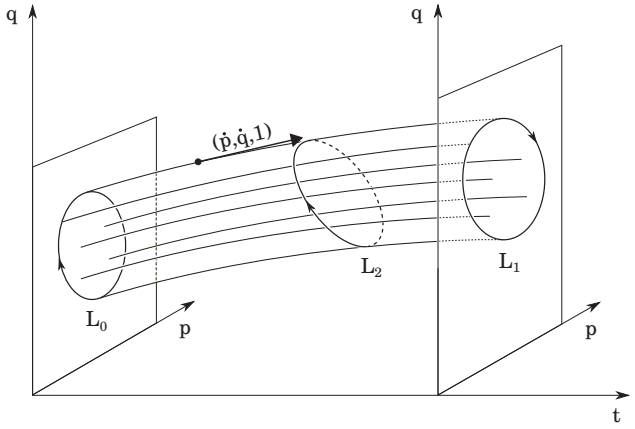

FIG. 1. Poincaré-Cartan integral invariant. The vectors $(\dot{\mathbf{p}}, \dot{\mathbf{q}}, 1)$ define a bundle of orbits emanating from a closed loop L_0 in the plain $t = t_0$ into the extended phase space $\{\mathbf{p}, \mathbf{q}, t\}$. By their projection onto the plane $t = t_1$ loop L_0 is mapped onto loop L_1 of the same area. In the case of a Hamiltonian $H(\mathbf{p}, \mathbf{q}, t; \lambda)$ strictly periodic in time $T = t_1 - t_0$ at λ held constant the fluxes of vortex lines through L_0 and L_1 are identical. In addition, an arbitrary cut across the flux tube generates the same flux $\oint(\mathbf{p}d\mathbf{q} - Hdt)$ through the surface encircled by L_2. Under λ varying adiabatically within T the orbits deviate only by a small amount from strict periodicity and L_1 nearly reproduces L_0.

(i) λ = const implies strict periodicity of motion, and time dependence, if any, fast with respect to the slow variation of $\lambda(t)$;
(**ii**) the variation of λ is such that the orbits are nearly closed, i.e., an oscillation/gyration center exists;
(**iii**) the variation of λ over several cycles is smooth.
Under these conditions holds

$$F = \oint(\mathbf{p}d\mathbf{q} - Hdt) = \text{const}_a \qquad (1)$$

If N is the number of cycles and ΔF is the variation of F over one cycle adiabatic conservation, indicated by "const$_a$, is secured if $\Delta F = o(1/N)$ [2]. The meaning of

o is "at higher than first order in 1/N". All we have to show now is $dF/dt = 0$ in first order.

Proof. For the difference $F(t_0 + \delta t) - F(t_0)$ of the periodic orbits starting from t_0 and $t_0 + \delta t$ holds

$F(t_0 + \delta t) - F(t_0) \equiv F(t_0 + \delta t, \lambda_0 + \delta\lambda) - F(t_0, \lambda_0) =$
$[F(t_0+\delta t, \lambda_0+\delta\lambda) - F(t_0+\delta t, \lambda_0)] + [F(t_0+\delta t, \lambda_0) - F(t_0, \lambda_0)]$
The second square bracket is zero because PCI applies. The Jacobian $j_{t_0+\delta t}(\lambda_0, \lambda_0 + \delta\lambda)$ maps the first onto the second term in the first square bracket,

* peter.mulser@physik.tu-darmstadt.de.

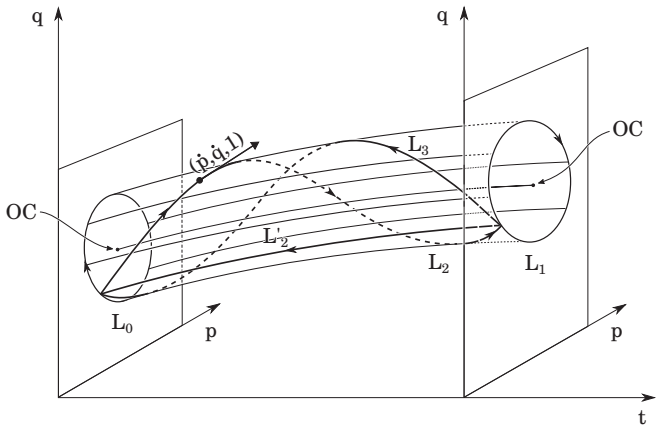

FIG. 2. The true particle orbits, here one in the rotation mode and another closed orbit indicating the separatrix towards trapping (libration mode), wind around the bundle of associated oscillation/gyration center trajectories. OC - OC marks the oscillation/gyration center. The libration mode consists of the forward loop L_2 and the backward loop L_3, each of them of periodicity T . Rotation mode: open loop L_2 ending at $t = t_0 + T$. If it is closed by L_2' along (p = const, q = const) the flux through L_2+L_2' equals half the flux through the libra-tion loop L_2+L_3 and L_0, here separatrix with $\mathrm{const}_a' = \mathrm{const}_a$ and peaked edges.

$$F(t0+\delta t, \lambda_0+\delta\lambda) - F(t0+\delta t, \lambda_0)$$

$$= \oint \{[j_{t_0+\delta t}(\lambda_0, \lambda_0+\delta\lambda) - 1](\mathbf{p}d\mathbf{q} - H(\mathbf{p},\mathbf{q},\lambda_0)dt\}$$

The unit Jacobian $j = 1$ stands for $j_{t+\delta t}(\lambda_0, \lambda_0)$. In first order the Jacobian greatly simplifies, $j_{t+\delta t}(\lambda_0+\delta\lambda)-1 = \nabla\dot{\mathbf{z}}\,\delta t = 0$, $\dot{\mathbf{z}}$ taken at $t = t_0+\delta t, \lambda = \lambda_0+\delta\lambda$. Thus

$$j(t_0, t_0+\delta t)-1 = j(t_0, t_0+[\partial\lambda/\partial t]\,)(\delta t)-1 = \nabla\,\frac{\partial\dot{\mathbf{z}}}{\partial\lambda}\frac{\partial\lambda}{\partial t}(\delta t)^2$$

$$\Rightarrow \frac{dF(t_0)}{dt} = \lim_{\delta t\to 0}\frac{1}{\delta t}\oint \nabla\frac{\partial\dot{\mathbf{z}}}{\partial\lambda}\frac{\partial\lambda}{\partial t}(\delta t)^2(\mathbf{p}_0 d\mathbf{q}_0 - Hdt) = 0$$

Cycle averaging $H(\mathbf{p},\mathbf{q},t;\lambda = \mathrm{const})$ with the decomposition $\mathbf{p} = \mathbf{p}_0 + m\mathbf{w}$, $\mathbf{x} = \mathbf{x}_0 t + \boldsymbol{\xi}(t)$, $W = T^{-1}\int \mathbf{w}^2 dt/2$ goes over into the slowly varying oscillation/gyration Hamiltonian $H_0(\mathbf{p}_0^2/2m + Z(\mathbf{x}_0); \lambda(t))$. Specializing to a lonngitudinal electron plasma wave of potential $V(x') = \hat{V}\cos kx'$ in the wave frame $x' = (x - \omega/k)t$ follows

$$\oint H'dt = H_0(v_0, x')T = (\frac{1}{2}v_0^2 + W + \overline{V})T = ET,$$

$$E = \mathrm{const},\ T = \int\frac{dx}{v(x)},\ v_0 = \frac{\lambda}{T},\ \overline{V} = \int\frac{V(x)}{v(x)}dx \quad (2)$$

Libration and rotation are determined from the two loops sketched in Fig. 2. Under $\lambda = \mathrm{const}$ the straight orbits emanating from L_0 are all identical and coincide with the motion of the invariant oscillation center $OC(t_0) \to OC(t_0+T)$ positioned at the virtual "center of mass". The true orbits of $\oint v_0 dt = 0$ over period $2T$ are closed and wind around the bundle of straight orbits forth and back. The flux $F = \oint pdq$ through them equals the area of the loop L_0. The open loops of the rotation mode wind around the same bundle L_0 of straight orbits and yield $\int(pdq - Hdt)$ over the period T and can be closed by the trajectory (p, q = const) along $-[(t_0+T) - t_0]$. With $E_0 = v_0^2/2$ the two adiabatic invariants follow

$$\text{libration}: \oint_{L_0}\mathbf{p}d\mathbf{q} = 4T(E_0+W) = 2\mathrm{const}_a;\ v_0 = 0 \quad (3)$$

$$\text{rotation}: \int_T \mathbf{p}d\mathbf{q} - Hdt = T(E_0+W-\overline{V}) = \mathrm{const}_a' \quad (4)$$

Explicit evaluation of $V(x') = \hat{V}\cos kx'$ in terms of the elliptic integrals of the first and second kind $\mathrm{K}(\alpha), \mathrm{E}(\alpha)$, and of (2) and (4),

$$v_0 = \pi\left(\frac{\hat{V}}{\alpha}\right)^{1/2}\mathrm{K}^{-1}(\alpha),\ E_0 = \frac{\pi^2\hat{V}}{2\alpha}\mathrm{K}^{-2}(\alpha);\ \alpha = \frac{2\kappa}{1+\kappa}$$

$$\kappa = \frac{2\hat{V}}{v_i'^2},\ E_0+W = \frac{2\hat{V}\mathrm{E}(\alpha)}{\alpha\mathrm{K}(\alpha)},\ \overline{V} = \frac{1}{2}v_i'^2\left(1 - \frac{2\kappa}{\alpha}\frac{\mathrm{E}(\alpha)}{\mathrm{K}(\alpha)}\right) \quad (5)$$

yield the most general ponderomotive force and "potential" (which in reality is not a potential) through

$$\frac{2\kappa}{\alpha}E(\alpha) = K(\alpha) \quad (6)$$

including *uphill acceleration*, and particle trapping at $v_0 = 0$. It follows further that energy change of a particle crossing an electron plasma wave or reflected from it is only accomplished by temporarily trapping. The cycle averaged potential $\overline{V}$ dominates in the neighbourhood of trapping; only its presence makes trapping possible. In the opposite case of v_0 far from reducing to zero $\overline{V}$ becomes insignificant and the difference of polarization of the wave, transverse or longitudinal vanishes.

The adiabatic invariant (4) applies equally well to the transverse monochromatic laser wave in the relativistic domain, with the same result as obtained from the invariant averaging of the Lagrangian $L = \int\mathbf{p}d\mathbf{q} - H(\mathbf{p},\ \mathbf{q},\ t)$ over a full cycle T in [3]. $\overline{V}$ is absent.

References

[1] V.I. Arnold, *Mathematical Methods of Classical Mechanics* (Springer New York, 1978), p. 237

[2] V.I. Arnold, *Dynamical systems* (Springer Berlin, 1988), Vol. III, ch.5, 2

[3] D. Bauer, P. Mulser, and W.-H. Steeb, Phys. Rev. Lett. **75**, 4622 (1995)

Analytical Calculations for the Transfer of Ultrarelativistic Protons

D.E. Larin
FSUE "All-Russia Research Institute of Experimental Physics – Russian Federal Nuclear Center", Sarov, Russia

This paper describes the designed method of analytical computations for the transfer of protons with the energies of about dozens of GeV through the matter and the focusing magneto-optic system (MOS) comprising a quartette of quadrupole lenses.

Using Borelian function theorem from two random values we can get the following expressions [1]:

$$h_{x\cdot y}(t) = \int_{-\infty}^{\infty} f_x\left(t/\tau\right)\cdot g_y(\tau)\frac{d\tau}{|\tau|},$$

$$h_{x+y}(t) = \int_{-\infty}^{\infty} f_x(t-\tau)\cdot g_y(\tau)\,d\tau,$$

$$h_{y=g(x)}(t) = f_x\left(g^{-1}(t)\right)\cdot\frac{d\left(g^{-1}(t)\right)}{dt},$$

where *f*, *g*, *h* are the densities of the distribution of random values specified in the index of the function.

When passing through the layer of the matter with thickness *L* an ultra-relativistic proton undergoes multiple Coulomb scattering (MCS) at a random angle θ, the distribution of which has the following view [2]

$$\Theta(\theta) = \text{gauss}(\theta,\theta_0),\ \theta_0[\text{mrad}] \approx \frac{14{,}1}{E[\text{GeV}]}\sqrt{L/L_{rad}},$$

where *E* is the proton energy; L_{rad} is the radiation length of the matter.

Besides the angular dispersion the proton undergoes radial throw Δ*r* in the layer of the matter that is related to angle θ_0 [3], so the distribution of the protons due to MCS has the following view:

$$F_{coul}(r) = \text{gauss}\left(r,\theta_0 L/\sqrt{3}\right).$$

Besides MCS the protons in transfer also undergo dispersion due to the hadron interaction with nuclei of the surrounding matter. As it comes from Born theory, when the wavelengths of the particles are much less than the instantaneous radius, the particles undergo elastic (diffraction) scattering forward in a narrow cone with 1st-order Bessel angular distribution. Then the proton scattering due to the contribution of the hadron interaction is

$$F_{had}(r) = \frac{3\pi\vartheta}{8\lambda_{el}}\int_0^L e^{-\frac{t+L/2}{\lambda_{el}}}\cdot\frac{J_1^2\left(r/t\vartheta\right)}{r^2}\cdot t\cdot dt,$$

where the exponent is the probability density along the thickness of the object to probe hadron interaction with a proton; the term *L*/2 indicates that in most practical cases the object being irradiated with protons is located as a center in the focusing plane of the MOS; J_1 is Bessel function of the first order; the characteristic scattering angle is [4]

$$\vartheta = \hbar c/E\cdot\left(4\pi N_a\lambda_{tot}^2/A\cdot\lambda_{el}\right)^{1/2},$$

where λ is the total or elastic thickness of attenuation; *A* is the molar mass of matter.

The transformation of the radial coordinate in MOS, related to angle aberration of the proton ϕ, is for "thin lense" [5]

$$r' = -r + D\cdot\phi\cdot\Delta E/E,$$

where *D* is the length of the quartette; Δ*E* is the losses of the proton energy.

Energy loss distribution of the charges relativistic particles in the not thick layer of the matter is called Landau distribution [6]:

$$\varepsilon_{Land}(L,\Delta E) = \frac{\varphi(\lambda)}{\xi\cdot L},\ \lambda(\Delta E) = \frac{\Delta E}{\xi\cdot L} - \ln\left(\frac{\xi\cdot L}{\varepsilon'}\right) - 1 + C,$$

where *C* is the Euler's constant; ξ and ε′ are the parameters from the quantum-relativistic Bethe – Bloch formula; φ(λ) is a universal dimensionless function.

Extremely bulky probability calculation formulas will give us the desired convolution – the resulting distribution of a thin proton beam. To simulate the density distribution for the proton flux across the beam we need to integrate the thin beam distribution by the MOS aperture with the account for the loss of protons from the beam because of the inelastic interactions with the nuclei of the matter and a possible cut of the angular distribution of the beam with collimators installed in the Fourier plane of the magneto-optic system.

References

[1] Borovkov A.A. Theory of Probabilities. – Moscow: Nauka, 1986. – 432 p.

[2] Flash Radiography with 24 GeV/c protons. C.L. Morris, E. Ables and oths. Journal of Applied Physics, 109, 104905. 2011.

[3] Physical Review D. Particles and Fields. Pt.1, vol.66, n.1-I. The American Physical Society.

[4] Mukhin K.N. Experimental Nuclear Physics. Book 2. Particle Physics. – Moscow: Energoatomizdat, 1993. – 408 p.

[5] K. Steffen. Optics of High-Energy Beams. – Moscow: Mir, 1969. – 224 p.

[6] Landau L.D. Collection of Works, Vol. 1. – Moscow: Nauka, 1969. – pp. 482-490.

The full-scale Monte-Carlo simulation of shock-wave experiments at PRIOR-II facility*

A.V. Kantsyrev[1#], A.V Skobliakov[1], A.V. Bogdanov[1], A.A. Golubev[1], D.S. Kolesnikov[1], V.A. Panyushkin[1], A.N. Zubareva[2], N.S. Shilkin[2], D.S. Yuriev[2],V.B. Mintsev[2], D.V. Varentsov[3]
[1]Institute for Theoretical and Experimental Physics, National Research Center «Kurchatov Institute», Moscow, Russia
[2]Institute of Problems of Chemical Physics of the Russian Academy of Sciences, Chernogolovka, Russia
[3]GSI Helmholtzzentrum fur Schwerionenforschung, Darmstadt, Germany

It is expected that upgraded proton microscope PRIOR-II will be used at HHT for experiments of Phase "0" FAIR project. Electromagnetic quadrupole lenses will be installed in the imaging section of PRIOR-II for achievement of the best facility parameters.

The design (Fig.1) of ion-optic scheme of PRIOR-II has been already developed and described in [1]. It consists of 9 quadrupole magnetic lenses and two dipoles.

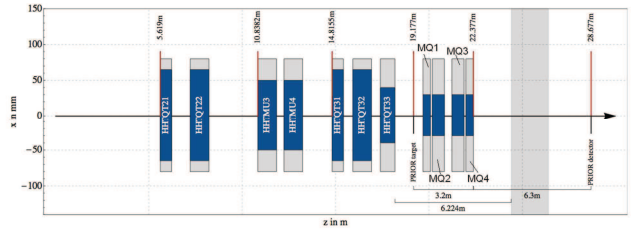

Fig. 1: The ion-optic scheme of PRIOR-II at GSI [1]. QT21, QT22, QT31, QT32, QT33 –lenses of matching system; MQ1-MQ4 – new electromagnetic quadrupole lenses of imaging section; MU3, MU4 – dipoles

The virtual model [2] of PRIOR-II facility was developed in Geant4 toolkit to perform a full-scale Monte-Carlo simulation of future experiments. The matching of the ion-optic scheme was performed by COSY infinity code (Fig. 2.). Five lenses of the matching section (QT21-QT33) provide optimal parameters of the proton beam in the object plane: the size and angular distribution of the proton beam. The MQ1-MQ4 lenses presented the imaging section with magnification factor of 3.5. A so-called Fourier plane is formed between MQ2 and MQ3 in the center of the imaging section.

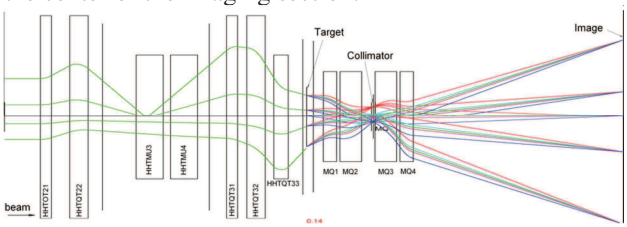

Fig. 2 The envelope of the proton beam.

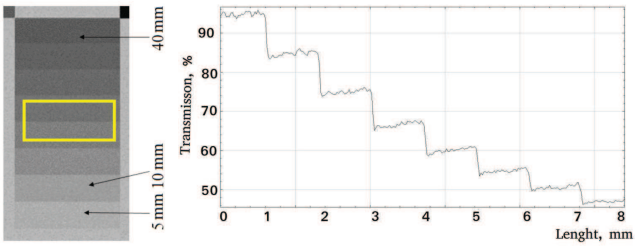

Fig. 3. Calculated proton-radiographic image (left) and vertical profile (right) of PMMA stepped wedges.

The full-scale numerical simulation was performed for a 4 GeV proton beam with energy spread $\Delta E/E = 10^{-3}$ and $5*10^8$ protons in the beam. Results of modeling of step wedges of copper and PMMA (organic glass) plates with different thickness are shown in Fig 3,4. The collimator with an angular capture of 1 mrad was used for PMMA object and 3.5 mrad for copper object. The spatial resolution along the yellow selections in Fig. 3 and Fig. 4 is 6 μm for the PMMA and 8 μm for copper wedges.

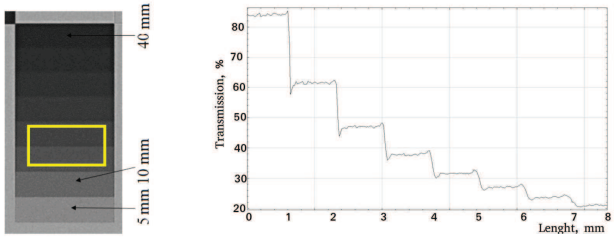

Fig. 4. Calculated proton-radiographic image (left) and vertical profile (right) of copper stepped wedges

It was earlier proposed to investigate anomalous compressibility of shock-compressed cerium [3] by proton radiography. The results of modeling this experiment at PRIOR-II are presented in Fig.5.

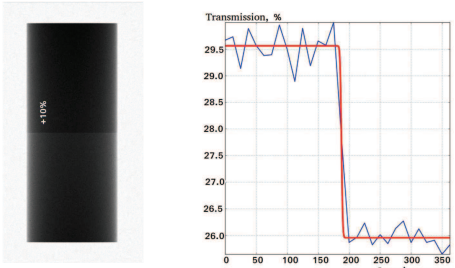

Fig. 5. Proton-radiographic image (left) and vertical profile (right) of cerium

The Cerium target was taken as a cylinder with a radius of 5 mm, divided into two parts. The right part represents shock-compressed cerium with a density 10% above cerium at normal density (left part of Fig.5). A 2.2 mrad collimator was chosen for this object. The spatial resolution is about 8–10 μm at the boundary of density change and transmission difference about 13%.

The developed model of PRIOR-II facility will be used for simulation of future dynamic experiments such as shock compressed porous materials or Xe gas.

References

[1] D. Varentsov et al., PRIOR - Proton Microscope for FAIR, Technical Design Report, October 2016

[2] A.V. Kantsyrev et al., J. Phys.: Conf. Ser. 2018, 946, 012019

[3] A.N. Zubareva et al., J. Phys.: Conf. Ser. 2014, 500, 032010

* Work supported by grant of FAIR-Russia Research Center and RFBR grant 18-38-00708
# kantsyrev@itep.ru

Multistage model of wet chemical etching of swift heavy ion tracks in olivine

S. Gorbunov[1#], R. Rymzhanov[2], and A. Volkov[1,2,3]

[1]P. N. Lebedev Physical Institute of the Russian Academy of Sciences, Leninskij pr. 53,119991 Moscow, Russia

[2]Joint Institute for Nuclear Research, Joliot-Curie 6, 141980 Dubna, Moscow Region, Russia

[3]National Research Center 'Kurchatov Institute', Kurchatov Sq. 1,123182 Moscow, Russia

Several classes of models of wet chemical etching (WCE) of swift heavy ion tracks (SHI, M>20 a.m.u., E>1MeV/nucleon) can be mentioned, but all of them, in fact, based on a number of calibration parameters from results of SHI-irradiation and etching experiments, e.g. track shape or lengthwise etching rate.

An approach [1] which is free from such fittings is presented. It consists of (a) Monte Carlo model TREKIS of SHI passage and secondary electron cascading [2]; (b) MD code simulating structure transformations during relaxation of the excited lattice in a track; (c) a module calculating the material-etchant reaction rates around the SHI trajectory, based on a transition state theory; (d) a model of WCE describing reaction-controlled and diffusion-controlled etching as well as transition between these two regimes when necessary.

In a framework of the transition state theory the ratio between material-etchant reaction rates for a damaged and an undamaged region (the relative reaction rate) can be written in this case as [3]:

$$\frac{K_{Track}}{K_{Bulk}} = \exp\left(-\frac{\Delta G}{RT}\right), \qquad (1)$$

where $\Delta G = G_{Bulk} - G_{Track}$ is difference between the Gibbs energies of the damaged (G_{Track}) and undamaged (G_{Bulk}) regions.

The multiscale model of SHI track formation [3] was used to calculate a change of free Gibbs energy of an olivine target. In the nanometric vicinity of the ion trajectory where structure transformations occur, ΔG was calculated as

$$\Delta G = \Delta(U+PV-TS), \qquad (2)$$

where U, P, V, T and S are subsequently the internal energy, the pressure, the volume, the temperature and the entropy of the atomic subsystem. These values were extracted from MD simulations of structure transformations in a track (see details in [3]). The Gibbs energy of Fe^+ vacancies was taken when calculating the reaction rate increase resulted from Fe^+ cation reduction stimulated by spreading electrons up to the micrometric distances from the ion trajectory [3].

These calculations demonstrated that diffusion-controlled etching is realized in the area of strong structure transformations [1], while the reaction rates [1] control etching of a part of the region of Fe^+ cation reduction as well as surrounding undamaged bulk olivine, see Figure 1.

s.a.gorbunov@mail.ru

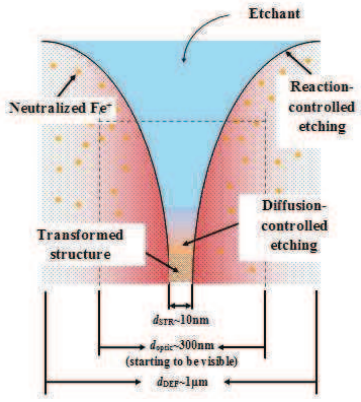

Figure 1: Scheme of SHI track etching in olivine

Figure 2 demonstrates the dependence of the lengthwise etching rate of olivine on the residual path length determined from the simulations of etching of tracks of 2,1 GeV Au ion (fixed losses) vs. the values got from the experiments [1].

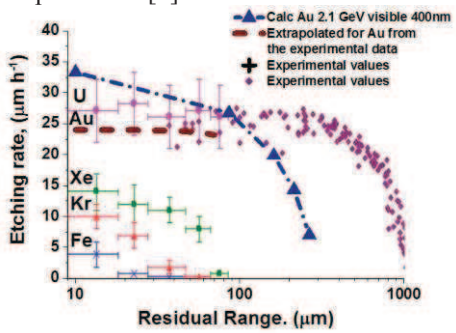

Figure 2: Lengthwise etching rates as functions of the residual ranges in olivine. Dashed line is the extrapolation of the experimental data for Au ions. Results of calculations are presented by triangles.

We supposed that tracks start to be visible by optical microscopy when their diameters overcome 0.4 μm. In this case the estimated lengthwise etching rate (33μm·h-1) is in a reasonable agreement with that detected in the experiments (24μm·h-1).

References

[1] S.A. Gorbunov, A.I. Malakhov, R.A. Rymzhanov, A.E. Volkov, J. Phys. D: Appl. Phys. 50 (2017) 395306.

[2] N.A. Medvedev, R.A. Rymzhanov, A.E. Volkov, J. Phys. D. Appl. Phys. 48 (2015) 355303.

[3] S.A. Gorbunov, R.A. Rymzhanov, N.I. Starkov, A.E. Volkov, A.I. Malakhov, Nucl. Instruments Methods Phys. Res. Sect. B. 365 (2015) 656–662.

Appendix: EMMI Workshop Report on Plasma Physics at FAIR, June 21th-23th, 2017

EMMI Workshop Report: Plasma Physics at FAIR

An update to the Scientific Case for Plasma Physics at FAIR

Editors: K. Schoenberg and V. Bagnoud
Contributors: P. Neumayer, O. Rosmej, A. Blazevic, S. Neff, D. Varentsov, T. Kuehl and A. Golubev

The plasma physics department of GSI organized a workshop on plasma physics at FAIR on June 21th-23th 2017. The Extreme Matter Institute (EMMI) sponsored the workshop. Participation from the international plasma physics community was solicited to discuss topics in plasma physics and high energy density science with a view to planning the plasma physics science program for phase "0" at FAIR. A summary of the main topics of the meeting follows.

Group picture of the workshop participants

Table of contents

1 Workshop Summary and Recommended Actions

High Energy Density Physics (HEDP), the study of matter under extreme conditions of temperature and density, is a developing multidisciplinary field that is expanding the frontiers of many scientific disciplines. HEDP cuts across many traditional fields of physical science, including astrophysics, cosmology, nuclear physics, plasma physics, laser science, and material science. It is a scientific enterprise where theory and experiment intersect to extend our conceptual framework of the universe. Potential applications range from improving our understanding of planetary structure, to creating new material states of matter, to fusion energy.

HEDP, along with atomic physics, biophysics and materials research, forms one of the 4 major scientific pillars for the Facility for Antiproton and Ion Research (FAIR) presently under construction at the GSI site in Darmstadt. These pillars will utilize the unique capabilities of FAIR to grow and develop forefront scientific understanding through the first half of this century. With these perspectives in mind, a workshop on HEDP and Plasma Physics at FAIR was held at GSI Darmstadt on June 21th-23th, 2017. The principal purpose was to assess the status of high energy density (HED) research worldwide with a view to identifying HED and plasma physics themes at FAIR. That is, areas of HED and plasma physics research where FAIR can provide unique capabilities to advance scientific understanding. The workshop was attended by 120 scientists representing a broad range of international HED research from 12 nations. The meeting was organized to provide an overview of international HED research with a view to building a collaboration of future FAIR scientific users.

The identified themes for FAIR HEDP and Plasma Physics research fall into the following areas:

- **Properties of materials driven to extreme conditions** of pressure and temperatures **relevant to planetary science** (earth and super-earth like planets, giant gaseous planets, brown dwarfs) by the FAIR heavy ion beams.
- **Shocked matter and material equation of state** (EOS) studies driven with FAIR heavy ion beams, laser drivers, gas-guns, electromagnetic drivers and explosive drivers, using advanced radiographic tools, in particular PRIOR.
- **Basic properties of strongly-coupled plasma** (energy/particle transport, radiation properties, particle stopping properties, etc.) created with heavy ion beams (e.g. HIHEX and LAPLAS) and lasers.
- **Nuclear Photonics**: excitation of nuclear processes in plasmas, laser-driven particle acceleration and neutron production, and neutron-based diagnostics with application to understanding FAIR-produced HED matter.

Prominent scientists were invited to give overviews of these scientific themes along with their views on where FAIR-based research can make unique contributions to HED physics in the future. A thematic synopsis of these talks follows.

Summary of Recommended Workshop Actions

- Developing FAIR Plasma Physics Collaboration
- Phase-0 Scientific Program
- FAIR commissioning and first experiments

Properties of materials driven to extreme conditions relevant to planetary science

David Riley summarized several outstanding HEDP questions in planetary science. For example, the postulated existence of diamond layers in large planets like Uranus [1], the generation of magnetic fields in large planets [2], and the metallization of hydrogen under extreme conditions of pressure and temperature. The motivation was to provide planetary science with the experimental data necessary for computational model development and validation and improve present theories to predict large-planet properties. The strong coupling between particles, the degeneracy of the plasma, and its partial ionization challenges the warm dense matter theory that underpins the models used to calculate planetary properties. Validation of computational models will require experimental data under the HED conditions present in large planet interiors.

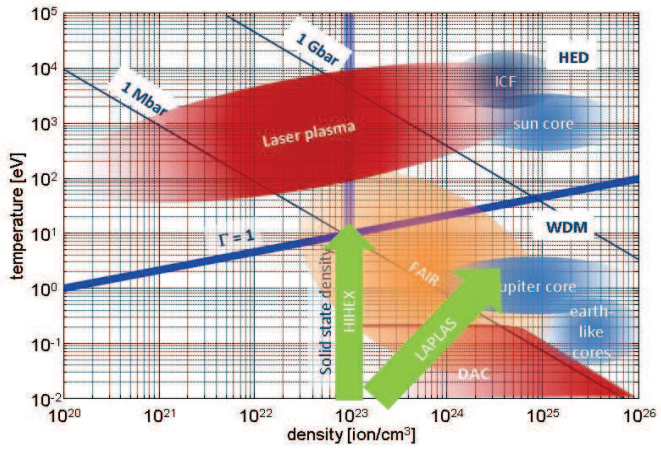

Figure 1: density-temperature diagram showing HED states achievable at FAIR, their relevance to planetary physics applications and complementarity with other drivers. The HIHEX and LAPLAS refer to two experimental schemes that will be developed at FAIR.

Accessing warm dense matter conditions in the laboratory presently utilizes a variety of techniques including shock drivers that are laser-driven, Z-pinch-driven or explosive-driven. These techniques reach pressures in the range of 1-10 Mbars and are well established. As an alternative, volumetric heating from highly penetrating photon (x-ray) sources and particle beams (electrons, ions) provide several advantages. This generates, for example, warm dense matter in local thermodynamical equilibrium and with samples large enough such that these systems are relatively uniform and evolve on the nanosecond to microsecond time-scale. These conditions enable accurate EOS determination and provide enough time for processes like superheating [3] to develop and become visible. Here, the use of heavy-ion beams at FAIR for creating WDM states offers a unique and complementary approach to the other WDM drivers , as shown in Figure 1.

Ronald Redmer focused on the specific topic of matter under planetary conditions. Warm dense matter, found in the interior of large planets or in man-made plasma like those of the National Ignition Facility (NIF) in the USA, share the same need for Equations of State in the 1 to 100 eV range, pressures in the megabar to gigabar range, and densities between 1 and 10 times solid-state density. Giant planets are relatively large astronomical objects with masses up to 10 000 times the mass of the earth and mass to density scaling laws that are dependent on their chemical composition. These giant planets are presently understood as complex systems where material behavior including conductivity, equation of state (EOS), and mass-flow are used to explain the generation of magnetic fields (dynamo effect). The materials found in large planets

[1] Ross et al., Nature **292,** 435 (1981)

[2] Stevenson et al., Rep. Prog. Phys. **46,** 555 (1983)

[3] Luo and Ahrens. Physics of the Earth and Planetary Interiors **143,** 369-386 (2004)

include H, He, C, N, O, Fe, Si along with molecular combinations of these elements. The simulation of the microscopic and mesoscopic properties of these materials, under planetary conditions, requires sophisticated simulation codes, like molecular dynamics (MD) codes, based on distribution function theory (MD-DFT), that predict parameters like viscosity, thermal and electrical conductivity etc.. These codes are essential to build planetary models but require experimental validation. Again, use of heavy-ion beams at FAIR offers a unique and complementary approach to the other WDM drivers to access these WDM conditions.

Shocked matter and material equation of state

Igor Lomonosov stressed that studying the equation of state of energetic materials has many applications in applied science and technology. Examples discussed included fission and fusion power plants, space debris mitigation, and meteoroid impact prediction and modelling. Dynamic experiments enable studying the temperature of materials in the eV range as a function of pressures in the 10-100 Mbar range, reaching the melting point or evaporation point conditions for these materials. Depending on the scheme used for dynamic compression, equations of state on the isentrope or isobar can be created and measured.

As discussed by **Ronald Redmer**, diamond anvil cells (DAC) can access modest pressures and temperatures (up to 2 Mbar) for material structure and EOS studies. For some cases, dynamic compression can reach up to 10 Mbar. Fourth-generation light sources employing free electron lasers (FELs) use coherent x-rays to probe the compressed DAC matter and provide data to benchmark molecular dynamics codes. The DAC technique, however, cannot access the WDM state.

Igor Lomonosov also presented the data range available through static DAC measurements and their relevance to WDM studies for conditions moderate in comparison to the other drivers. Dynamic compression using nuclear explosives have proven to be very effective in reaching ultra-high pressures above one gigabar in the second half of the nineteenth century. Nevertheless, creating and probing matter in the HED state remains an international scientific priority.

The FAIR facility will be able to generate the world's highest heavy-ion beam current. As such, this capability enables the creation of unique warm dense matter states for scientific investigation. The "Heavy Ion Heating and Expansion" (HIHEX) scheme, where matter is isochorically and uniformly heated by an intense heavy ion beam, is one FAIR-based technique for WDM EOS studies. This experimental scheme has already been tested at the GSI-HHT cave, although with lower beam intensities. Many groups in Russia and Germany have experience and interest in this technique for EOS studies, specifically utilizing the improved beam parameters at FAIR. Another use of the FAIR beams is to launch shock waves as reported by **David Riley**, where the ion beam is stopped in a high-Z material and the expansion creates a shock (compression) in a probe located at the side. This scheme, originally proposed by the HEDgeHOB collaboration, remains another potential shock-driver technique.

Given FAIR heavy ion beams will be used to create WDM or other extreme states of matter, a complete set of probes and diagnostics will also be required. FAIR HED and plasma physics experiments must operate in a "pump-probe" configuration and this will require a powerful backlighter source. As presently envisaged, the "Helmholtz Beamline", will provide the high-energy laser for backlighting and other probing. The Helmholtz Beamline is on the roadmap of infrastructure of the Helmholtz society but remains in the planning stage. Without a powerful laser backlighter, the HED research at APPA will be significantly impacted.

Basic properties of strongly-coupled plasma

Research on dense plasmas at FAIR will also, and particularly, allow addressing the fascinating fundamental aspects of correlated many-body quantum systems. Plasmas at warm-dense matter conditions pose a formidable challenge to theory. Due to strong coupling of the ion system the statistical framework of traditional plasma physics is no longer applicable and perturbative methods fail. In addition, partial degeneracy of the electron component requires a quantum mechanical treatment. Concomitantly, strong coupling and electron degeneracy give rise to the rich and exotic behaviour of these matter states, such as phase transitions and metallization. As example, **Ronald Redmer** elaborated on the still outstanding issue of the metallization of hydrogen. Recent experiments in shock-compressed D_2 suggested an insulator-metal transition at pressures significantly higher than predicted by DFT-MD calculations. The latter showed a strong sensitivity to the choice of the exchange-correlation functional. Accurate experimental data in the warm-dense matter regime thus help elucidate the role of assumptions in modern state-of-the-art dense matter theory. **Siegfried Glenzer** presented measurements of plasmon scattering from aluminium samples, rapidly heated by intense x-ray pulses. Plasmon shift and width are only poorly described by the usual Born-Mermin-approach and indicate a non-linear damping component and a non-Drude-like conductivity. Also here, the advanced HSE-functional provided a significantly enhanced agreement between theory and measurement. **Victor Mintsev** showed early measurements of electrical conductivity of noble gases in the WDM regime, where the classical Spitzer-theory fails, and now modern ab-initio methods are employed. He also presented one of the experimental proposals within the FAIR plasma physics collaboration, to study molecular fluids (such as H_2 and N_2) at Mbar pressures, where they are predicted to undergo phase transitions to various exotic (high-conductive, metallic, polymeric) phases. **Igor Lomonosov** reminded in his talk the problem of measuring the critical points of many metals. Theoretical predictions vary widely and experimental measurements are very difficult. Furthermore, the prediction of non-congruent phase transitions in composites is a topic of fundamental thermophysical interest.

The topic of the ionization potential depression (IPD) in strongly-coupled plasmas was addressed in the talk by **Tilo Döppner**. This topic has attained significant attention and motivated strong theoretical activities after experiments at isochorically heated aluminium samples at the first free electron laser LCLS at Stanford had shown significant discrepancies with the widely used IPD model. **T. Döppner** presented results from a campaign in the Discovery Science Program at the National Ignition Facility, measuring the ionization balance at ultra-high densities, exceeding 30 g/cc by spherical compression in a laser-driven hohlraum. Measuring the ionization balance by x-ray scattering indicates a significantly higher ionization than predicted by standard theories of IPD. This clearly shows the need for an improved understanding and treatment of atomic physics in such strongly coupled systems. Such strongly coupled degenerate plasmas, although at lower density, can be produced with very high quality (homogeneity, equilibrium conditions) by heavy-ion heating of tamped foils. **Dimitri Khaghani** showed on-going activities to prepare high-resolution x-ray transmission spectroscopy to measure continuum lowering in such plasmas in the FAIR phase-0 program.

Nuclear Photonics

Nuclear Photonics encompasses a rapidly evolving field of research enabled by high-power, short-pulse laser facilities together with targets designed for the production of intense particle or photon beams. The application of these intense beams promises significant advantages for the diagnosis of FAIR-generated matter at extreme conditions. For example, laser-generated protons, neutrons, and X-rays can be directly employed for

radiographic imaging. Intense laser-generated and moderated neutron beams can also be employed for measuring temperature of shocked or isochorically-heated matter using neutron resonance spectroscopy. Nuclear Photonics is an important area for collaboration with other facilities researching extreme matter worldwide. Several applications and opportunities for FAIR were discussed in the talks summarized below.

2 HED at GSI/FAIR

2.1 Status of the plasma physics collaboration

The collaboration for High-Energy-Density Science at FAIR (HED@FAIR) was founded on February 3rd 2017 during the 37th international workshop on Physics of High Energy Density in Matter in Hirschegg Austria.

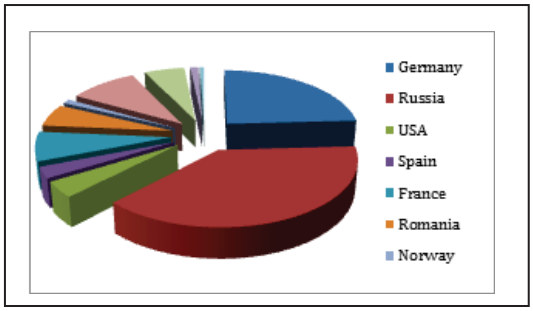

Figure 2: 178 members from 11 countries have joined the HED@FAIR collaboration as of August 2017

The HED@FAIR collaboration that focuses on the experimental program that will be conducted at the dedicated plasma physics beamline in the APPA cave of FAIR, is basing its program on the preliminary work of the HEDgeHOB and WDM collaborations and seeks to unify the effort of both groups into a single goal. The collaboration is organized around a collaboration board that is the steering body of the collaboration and an executive board, which is responsible for the representation towards the outside and the daily business of the collaboration. The collaboration board, chaired by V. Bagnoud, elected during the workshop Alexander Golubev as chair of the executive board and collaboration spokesperson.

The collaboration is open to any scientist that is interested in participating in the definition, development and realization of the HED program at FAIR. In addition, the collaboration HED@FAIR aims to play an ever growing role in the interim science program (the so-called phase 0) that breaches the gap between the present and the startup of FAIR in 2024. In this view, the collaboration will use the existing GSI facilities (PHELIX, the Z6 target station at the UNILAC, and the high-energy cave HHT at the SIS-18) to prepare the scientific program of the APPA cave.

2.2 FAIR facilities

The sessions of the workshop addressing the FAIR facilities covered the progress in the FAIR project as well as R&D contributions from collaborating universities around GSI and theoretical support from JIHT in Moscow.

At first, P. Giubellino, the scientific director of GSI and FAIR, reported on the status and current development at GSI/FAIR. The FAIR project is on track, as best illustrated by the ground breaking ceremony for the synchrotron tunnel on July 4th this year and the integrated project management plan, that includes planning for the FAIR buildings, the accelerator, as well as the detectors for experiments. According to this plan, the HED collaboration expects to start bringing first components in 2021 into the cave and do the commissioning without beam in late summer 2024. P. Giubellino emphasized the importance and uniqueness of synergistically exploiting ion and laser beams for dense plasma research. Plasma physics is about pump-probe experiments, hence the GSI SIS18 and the upcoming FAIR SIS100 synchrotron, in combination with bunch compression capabilities to produce intense, short (<70 ns) beam pulses, are ideal plasma physics

drivers matched to the current and future needs of the community. High-energy lasers, like PHELIX at GSI or the envisaged Helmholtz Laser Beamline at FAIR, offer powerful diagnostic tools for HED research. Therefore merging laser and accelerator technology is a highly strategic research direction for FAIR and also for Helmholtz.

Particular attention was paid to the upcoming beam time 2018/19, with the restart of the intensity-upgraded UNILAC/SIS18 facility including storage ring ESR and the newly installed CRYRING. PHELIX operation will continue on the present level. From 2018 till the start of commissioning of SIS100 synchrotron 2021, there will be about 3 months of beam time per year for the FAIR Phase 0 program.

Peter Spiller, leader of the subproject SIS100/SIS18 at FAIR, reported on the status of the accelerator, especially on the upgrade of the existing SIS18 and the progress in the realization of SIS100. The SIS18 upgrade program, as originally defined, will be completed beginning of 2018. Further upgrade measures to stabilize the dynamic vacuum in a 3 Hz operation mode have been proposed and need to be implemented. Additional effort has been taken to improve the operation for the user program in FAIR phase 0, e.g. a high harmonic micro-spill smoothing cavity will be tested in 2018. Civil construction for the „Link existing facility" is running and progressing well. Concerning the SIS100, contracts for major system components have been placed. The delivery and testing of accelerator components is underway.

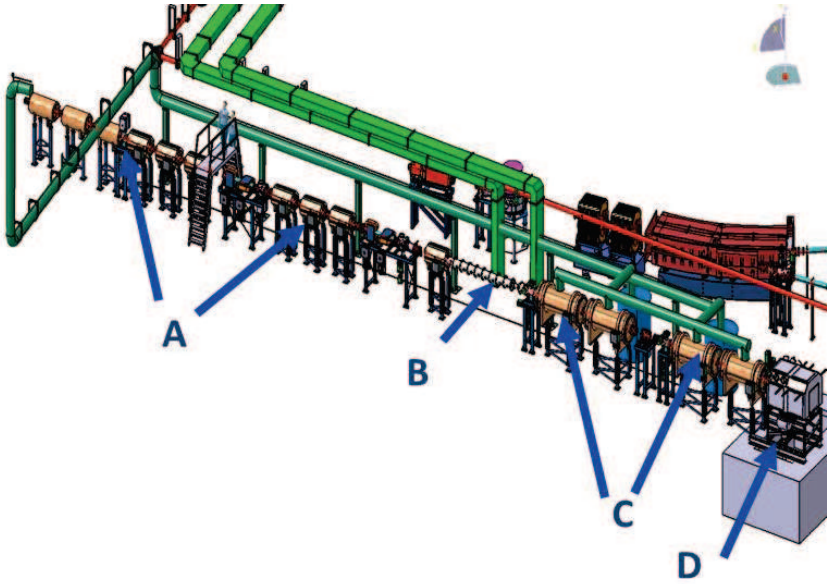

Figure 3: A 3-D model of the planned plasma physics beamline in the APPA cave at FAIR. A: beam-matching section and diagnostics; B: wobbler; C: focussing magnets; D: target chamber.

S. Neff, the resource coordinator of the HED@FAIR collaboration, presented the status of the facility for the HED experiments at FAIR. This facility is designed to exploit the world-wide unique capabilities for HED experiments at FAIR. The baseline design of a flexible ion beam line, as shown in Figure 3, is finished and approved by FAIR. This beam line will allow for a wide variety of experiments using uranium (HIHEX, LAPLAS) to protons (PRIOR) in the first phase of FAIR. All technical design reports, except for the matching beam section, are approved. The construction of the superconducting final focusing system has started at IHEP. Beyond the modular start version of FAIR, achieving the full performance of the experimental capabilities will, however, require additional funding.

To illustrate the foreseen experiments at FAIR in the APPA cave with annular beams, **Naeem Tahir** presented in his talk new theoretical results on generation of earth-like

planetary interior conditions at FAIR[4]. Simulations have been made for 75-100 ns, 1 GeV/u U-beam that will be available on Day 1 ($5 \cdot 10^{10}$ ions/bunch) and in the FAIR full operation mode (10^{11} -5. 10^{11}). These calculations show that the LAPLAS-scheme using hollow beams creates highly-compressed solid and liquid iron states. Measurement of transport properties like thermal and electrical conductivities, and viscosity of the iron samples under extreme conditions will be possible. In the frame of future experiments, studies of Richtmyer-Meskov and Rayleigh-Taylor hydrodynamic instabilities are also proposed.

M. Roth gave an overview about the R&D activities of the German universities within the frame of BMBF-Verbundforschung and concerning first-day experiment diagnostics at FAIR. His talk covered new development of photon and particle diagnostics. For PRIOR, high-performance scintillators and cameras and have identified and these components should be tested at HHT. The key questions will be temporal and spatial resolution, efficiency, radiation damage and EMP resistance. For the laser driven X-ray diagnostics, TU Darmstadt is working on two subjects: the development of an actively cooled main amplifier with a sandwich design, where a thin coolant layer flows between two glass slabs enabling an increase in the laser repetition rate to one shot every 10 minutes; and optimizing narrow band X-ray yield for XRTS by using micro-structured targets like needles, pillars or grooves. Experiments at different laser facilities have shown reduced reflected laser energy and enhanced Kα- emission from this class of targets.

N. Andreev gave an overview about the theoretical support of FAIR relevant experiments at the Joint Institute for High Temperature (JIHT) in Moscow. He presented a wide range of models starting with laser interaction with matter, laser electron acceleration for backlighting WDM, and the generation of Kα X-rays in foils at PHELIX. JIHT, in support of the HED research community, has developed a wide range of models for laser iteration with matter that can be used to better understand laser-plasma production, e.g. at PHELIX. For example, hot electron generation in low-density targets has been investigated as a high current source of accelerated electrons. Laser electron acceleration, where a short and intense laser pulse is at grazing incidence to a solid target, provides a bright source of fast electrons in a hundred MeV energy range. Models of electron temperature and Kα photon generation by hot electrons, produced by a sub-picosecond relativistic intense laser pulse, are in a good agreement with measurements.

Finally **A. Schönlein** from the Goethe-University Frankfurt presented some of the envisioned applications of high resolution X-ray fluorescence spectroscopy for HIHEX-experiments at FAIR. For the investigation of fundamental properties of matter under extreme conditions within the HIHEX scheme, the energy density distribution in the target, deposited by a heavy ion beam, is a key parameter for numerical simulations of hydrodynamic target response. Therefore they presented the development of a scintillator and fiber-based X-ray fluorescence detector for FAIR to measure the target expansion, the ion beam intensity distribution on the target as well as the number of interacting projectiles. First experiments at the UNILAC showed the applicability of the scheme, where the dependence of the X-ray fluorescence yield on the number of interacting projectiles and target material has been successfully investigated.

[4] N. Tahir et al., The Astrophysical Journal Supplement Series **232** (2017)

2.3 Phase 0 research at GSI

In 2018, GSI will complete the upgrade of the SIS-18 accelerator ring necessary for seeding FAIR. After this shut-down period, the SIS-18 will gradually be driven to higher and higher intensities. FAIR and GSI have decided to drive a limited research program during this start-up phase to exploit the improved capabilities of SIS-18 and test the necessary equipment from the FAIR collaborations. This period is called “Phase 0”. For HED@FAIR, the phase 0 means running experiments at GSI’s existing facilities: PHELIX, the Z6 target station of the UNILAC, and the high-energy cave at the SIS-18 – HHT.

Stefan Götte reported about the experimental capabilities of the PHELIX facility. Since its commissioning in 2008, PHELIX has developed into a well-established user- facility making a significant contribution to the field of plasma and atomic physics. He discussed the latest evolution of the laser parameters, the procedure of the experimental project application and the user support. For phase 0, in addition to user operation, parameters like the laser focus quality, the repetition rate operation, and the commissioning of a VISAR system at Z6 experimental area, for laser-driven shock experiments, will be improved. In the future, the construction of the beam lines to the HHT experimental areas, an upgrade of the facility at Z6, and the support to develop the nanosecond 100-J laser at FAIR are planned.
In addition to PHELIX, GSI plans to restart its experimental program at the HHT cave..
The GSI accelerator will provide beam time for the user community in limited amounts of about 3 months per year during phase 0. The HED@FAIR collaboration will use this opportunity to commission the second PRIOR prototype (PRIOR II), which is based on electromagnets (see section 0 of this document:

Proton microscopy, PRIOR, and the round table discussion). This technical implementation of the proton microscope is more robust against radiation than the one based on permanent magnets and therefore should perform for a longer time in the APPA cave environment without significant maintenance costs.

Finally, it is expected that ion intensities above 10^{10} ions/bunch will be obtained in the near future at SIS-18 and will be available at HHT. Such intensities will be sufficient to achieve quasi-isochoric heating of a dense target and isentropic expansion (HIHEX). This will enable the measurement of EOS and transport properties for non-ideal plasma and warm dense matter (WDM).. However, this requires volumetric diagnostics as discussed in details in section 5: Round table discussion: PHELIX at HHT.

3 Reports on HED research worldwide and its applications

Plasma physics research is being conducted at many facilities worldwide. Researchers active in the field came to the workshop to present the current activities and capabilities of these facilities, underlining the complementarity of approaches between theirs and FAIR.

3.1 Plasma Physics Research at other facilities

HEDP studies span a range of science that is highly interdisciplinary. As such, this requires numerous interconnections to existing and developing major facilities; no single facility can fully serve the HEDP broad research agenda. Creating and probing matter under extreme conditions, across many orders of magnitude in density, temperature, and temporal extent, necessitates tailoring said research to the specific capabilities of a given facility. So will be the case for FAIR, where the unique pump-probe characteristics of APPA will support a range of HED experiments.

The workshop session on plasma physics research at other HED facilities gave important input onto the relevance of the HED program at FAIR and its possible links to the international efforts at other laboratories. While it is beyond the scope of this report to fully assess international HED capabilities, the facilities represented herein provide a reasonable survey. Major facilities represented included the National Ignition Facility (NIF)-USA, the Linac Coherent Light Source (LCLS)-USA, Laser Megajoule (LMJ-PETAL)-France, NCDX-II and Bella-USA, HIAF-China, PALS-Czech Republic, ELI-Czech Republic, Titan-USA, PHELIX-Germany, LANSCE-USA, and MaRIE-USA. These facilities are shown on the world map of Figure 4.

Figure 4: HED facilities worldwide that offer a complementary approach to FAIR and that were represented at the workshop

The presentation by **Thomas Schenkel** from LBL Berkeley gave an account to present and planned activities at the NDCX-II induction linac and the Bella-i laser facility. Complimentary to the high-energy heavy-ion beams at FAIR the NDCX-II linac concentrates on low-energy but very intense beams on light ions (e.g. He+). Offering a pulse length of 2.5 ns and a peak current of ~2 A, a main emphasis is presently on the effects of high-flux, short ion pulses on solid state structures, and also energy loss under high-flux conditions. In the future, when higher intensities are reached, phase transitions and warm-dense mater will be in reach. Exciting perspectives also exist in the study of the synthesis of novel materials at the on-set of the warm dense matter regime. The Bella-I laser facility represents at present the highest repetition rate Petawatt laser. Operating at up to 49 J in 33 fs at 1 Hz, the laser can provide the most intense source of laser accelerated electrons (above 1 GeV) and ions. It will also deliver unprecedented intensities of Betatron x-rays for diagnostics. At present a phase 1 of experiments on ion acceleration is running. Combined with focusing devices it will provide a powerful tool for the preparation of warm dense matter. Once a beamline with short focal length will be commissioned intensities around 1022Watts per cm2 will be reached. This can open a new regime of laser acceleration as well as it can give the chance to see QED effects.

Dimitry Batani from the "Centre Laser et Applications" at the University of Bordeaux was concentrating on the complementarity and possible synergy between the projects at GSI/FAIR and the LMJ-PETAL project at Bordeaux. Despite the completely different characteristics of the laser and the ion beam driven plasmas a similarity was seen in the concepts of laser driven diagnostics. Development of laser driven secondary sources and novel techniques like XANES, X-ray radiography, and X-ray phase contrast radiography will be useful for both drivers. Short pulse and isochoric heating will address different aspects of the plasma phase diagram. It was stated that, as a complementary scenario heavy-ion prepared plasma in combination with laser diagnostic, acceleration and the creation of magnetic fields should "… write a new chapter in the HED physics"

Libor Juha from the PALS Research Center and the Institute of Plasma Physics of the Czech Academy gave a wide overview over present and future dense plasma physics at PALS and the ELI Beamlines facilities. Many excellent experimental results from the PALS laser (1kJ pulses with 300 ps duration at 315 nm) were shown. The importance of

advanced diagnostics and secondary sources was emphasized. The status and an outlook on the ELI beamlines facilities and experimental areas were given. With a suite of laser driven sources covering x-ray to THz, and a maximum power density exceeding 10^{23} Watt/cm^2, the facility is striving for ultra-high fields and new access to astrophysical problems as well as applications in technology and applied sciences.

Rui Cheng from IMP CAS at Lanzhou gave an overview on the Warm Dense Matter oriented program at the planned HIAF facility in China. The key parameters of the accelerator complex are similar to the FAIR scope. As at FAIR, the scientific program is supporting different subjects, including nuclear physics and nuclear astrophysics as well as atomic und plasma physics. The time scale of the project is similar to FAIR. In the science program questions related to ICF, particular in context with the Chinese inertial fusion program at the SHENGUANG project, has a strong role. A wide research activity directed towards a study of the physics of WDM has already started. Very remarkable is the effort towards a High Energy Electron Radiography (HEER). Experiments have reached prove of principal with a high resolution and density resolution. In the planning a pulse duration of ~10 ps seems possible. The test platform is set up is under construction at the IMP at Lanzhou. Proton radiography and other diagnostic schemes are also under development. With the additional diagnostics HIAF will be highly competitive to FAIR.

Kurt Schoenberg, from the GSI Extreme Matter Institute (EMMI) and Los Alamos National Laboratory, presented an overview of Neutron Resonance Spectroscopy (NRS). NRS is a promising technique for measuring temperature in shocked or high-energy-density matter at the proposed Los Alamo MaRIE facility and at FAIR. Time and spatially resolved measurements of bulk-temperature of experimental samples are a critical need in dynamic materials research. Specifically, a technique is sought with temporal resolution capabilities of order 1 ns (shock transit time over the dimension of a typical solid grain) and as small as ~ 10 μm, although lesser resolution would still be valuable given present alternatives. NRS utilizes a broad-energy-band neutron beam to excite a nuclear transition, typically of order 20 eV. The Doppler-dominated absorption-line width in the transmitted neutron beam yields the sample temperature. The penetrating power of epithermal neutrons and the ability to localize a suitable dopant within the sample readily enables spatial and temporal resolution, provided the neutron fluence is sufficiently high.

NRS has been demonstrated at the Los Alamos Neutron Science Center (LANSCE) using moderated neutrons from a ~ 1GeV proton-driven spallation source.[5] However, spallation neutrons must be heavily moderated to be useful. This moderation process leads to neutron pulses with durations longer than desired, and assembly sizes that are very large and costly. Moreover, even for an instantaneous neutron pulse of finite energy spread, the ultimate time resolution is dictated by the spread in time of flight through the doped/resonant part of the dynamic sample for the neutrons with energies spanning the resonance width. This time spread is proportional to the flight time from the moderated (epithermal) neutron source. At LANSCE, the NRS targets must be placed ≥ 1 m away, which makes the time spread ~ 200 ns for the resonance line used (~ 20 eV).

An intense neutron-beam source driven by laser-produced intense deuterium (D) beams shows promise of greatly improving temporal resolution. For example, the Trident laser has produced a neutron beam with ~10^{10} neutrons in approximately 1 ns and in ~ 1 steradian, with a quasi-Maxwellian energy distribution of ≈ 2.7 MeV average energy. Neutron moderation from these lower energies can be done much faster than in

[5] V. Yuan et. al., Phys. Rev. Lett. **94**, 125504 (2005).

spallation sources with a much smaller moderator, providing a path to meeting NRS requirements. Nevertheless, significant development of the NRS technique remains in order to meet the neutron flux/fluence requirements and general experimental design for MaRIE-class dynamic experiments. These development activities provide a foundation for collaboration between MaRIE and FAIR shock-driven thermometry development. Specific areas for collaboration include:

- Developing compact, laser-driven neutron sources relevant for specific FAIR or MaRIE experimental configurations.
- Modeling of the effects of thermodynamic states on the neutron resonance profile, including proper inference of bulk temperature.
- Design of NRS first experiments, including achievable spatial and temporal resolution.

3.2 Research on Ultrafast Plasma

The session on ultra-fast plasma physics began with a presentation by **A. Phukov** (U. Düsseldorf) on nano-structured targets irradiated with ultra-short relativistic laser pulses. Advances in short-pulse laser technology have led to generation of high-contrast laser pulses with a laser pre-pulse level over 10 orders lower than the laser peak intensity. This allows irradiation of delicate high-aspect ratio nano-structures with intense laser pulses, preserving the target structure until the arrival of the laser-pulse. Highly computing intensive 3D particle-in-cell simulations show that this allows the laser light to penetrate into the interstitial space between the nano-structure, thus delivering laser energy at average densities far above the critical density. This results in a very efficient absorption (near 100%) of laser energy and the generation of extreme energy densities, corresponding to 100's of Gbar pressures – conditions prevailing in the center of the sun, reached otherwise only in inertial fusion scenarios. These simulations also show that cooling of these extremely hot states is dominated by x-ray radiation, which could yield record high conversion efficiencies of laser energy to x-rays. First experiments have already shown significant enhancement of x-ray line emission from these targets. This shows a promising path towards ultra-bright x-ray sources, enabling many x-ray based applications. Furthermore, simulations of individual nano-wires irradiated by ultra-relativistic laser pulses show strong magnetic fields, generated by return currents drawn along the wire. These fields produce a strong inwards cylindrical compression and eventually lead to a nano-scale Z-pinch.

A. Korzhimanov from the Institute of Applied Physics in Nizhny Novgorod talked about the perspectives to generate matter at high energy density conditions by rapid isochoric heating using laser-accelerated protons. Given the parameters of current (such as PHELIX, Omega EP and others) and upcoming (e.g. ELI beamlines L4 or the XCELS facility in Russia) high-energy short-pulse laser facilities worldwide, ranging from few hundred joules of laser energy in picoseconds up to several kJ at pulse durations below 100 fs, already simple scaling relations indicate that matter states with keV temperatures at Gbar pressures could be attainable by proton-heating. This offers a very intriguing path towards efficiently generating homogenous samples of high-energy density. More detailed calculations were presented, showing modifications due to non-linear effects, which require a self-consistent treatment of the particle stopping and material heating. At even higher particle beam flux density, calculations indicate that non-linear beam-plasma-interaction may become a major effect. While this in itself is a fascinating field at the crossing of accelerator and plasma physics, this needs to be taken into account in the design HED experiments.

O. Rosmej presented results from experiments at the PHELIX and the Jeti40 (Jena) laser systems, where thin metal foils had been irradiated with intense laser pulses at the

highest available temporal contrast. Broadband spectroscopy was used to measure characteristic line emission of the entire K-shell spectrum, ranging from neutral K-alpha up to Ly-alpha, and further to the more energetic He-beta and He-gamma lines. The spectra indicate both heating to temperatures of order 1 keV, as well as high densities close to the density of solid. This heating can be explained by the interaction of energetic electrons, produced in the intense-laser matter interaction, while the target remains near solid density due to the high-contrast laser pulse. These findings were further corroborated by measurements of the escaping fast electrons by means of an electron spectrometer, and the emission bremsstrahlung radiation with hard x-ray spectrometers based on imaging plates, as well as on a highly-pixelated CdTe detector. The results are supported by particle-in-cell calculations, which show that besides hot electrons fractions at average energies of 10's of keV and MeV, a significant amount of energy is converted to electrons at only 1-2 keV. These electrons carry about 2 orders of magnitude more charge than the more energetic ones, and they are responsible for depositing up to 10MJ/g in a 100nm thick layer of the target.

S. Glenzer gave a broad overview of activities at the Linac Coherent Light Source (LCLS) x-ray free electron laser at SLAC. The FEL can be used both to generate matter at HED conditions by ultra-fast energy deposition by photoelectric absorption, and to probe dense plasmas, e.g. created by an optical laser, with x-ray techniques such as x-ray diffraction and scattering. A variety of recent experiments that have resulted in high-impact publications was presented, such as accurate ion-ion structure factor measurements on strongly shocked aluminium, formation of lonsdaleite diamond in shocked graphite, or the phase separation in low-entropy shock-compressed CH-targets relevant to the conditions in giant ice planets. Developments towards high rep-rate targets based on liquid jets, and results from first experiments measuring equilibration rates showed the need for quantum kinetic theories to explain the electron-ion energy exchange observed in these experiments. Furthermore, high-resolution x-ray scattering spectra in the collective regime on x-ray laser heated aluminium foils revealed plasmon resonances significantly narrower than predicted by calculations in the Mermin-approach, including collisions by means of the Born approximation. Also, ab-initio MD calculations using as exchange-correlation functional the widely used PBE-functional fail to reproduce, while the more sophisticated non-local HSE-functional achieves an almost perfect fit to the data. Finally, an outlook was given to upcoming experiments within the "Discovery Science"-program at the National Ignition Facility (NIF), where such x-ray scattering experiments will be performed at ultra-high densities, approaching conditions as found in brown dwarfs.

3.3 Laser-based Plasma

High-energy nanosecond lasers are used worldwide as plasma drivers because of the versatility of such drivers. One of the most prominent high-energy laser facilities is the National Ignition Facility (NIF) that allocates about 10% of its available beam time to a discovery science program that is dedicated to academic access. Thanks to the symmetric geometry of the NIF setup, spherical compression can be achieved to reach high pressures after illumination of a spherical sample with the laser. In a recent experiment aiming at reaching high-pressures, a group of researcher belonging in part to the HEDatFAIR collaboration led by P. Neumayer and R. Falcone, compressed CH and Be capsules to about 30 g/cm^3 and reached electron densities of $\sim 10^{25}$ cm^{-3} using the x-rays generated by converting the NIF energy in a hohlraum. This experiment, reported by **Tilo Doeppner** at the workshop, employed x-ray Thomson scattering (XRTS) as a diagnostic to quantitatively measure the elastic and inelastic components of the x-ray spectrum, from which one can infer the ionization state of the sample. In the conditions accessible at the NIF, where the electron temperature is similar to the Fermi energy, the preliminary analysis of the data shows evidence that the carbon atoms have a much

higher K-shell ionization. This effect is called ionization potential depression and is still a challenging effect for theory as the most widely used codes fail to predict the NIF measurements.

In his contribution, **Peter Mulser** reviewed the advantage of the x-ray radiation generated by laser-driven plasmas. In his view, plasmas generated by laser-intensities at or above 10^{22} W/vm^2 and the current experimental and theoretical work being done worldwide have many advantages and make a case for a powerful high-intensity laser as follow-on to PHELIX. Effects based on the very strong ponderomotive force generated at this intensity and the fast electrons that result from the laser-plasma interaction must be exploited. In addition, the coupling of the laser energy into the plasma, limited by the reflection of the laser at the critical plasma density, can be mitigated by the use of structured targets that allow the electrons to achieve relativistic velocities (Relativistic Transparency[6]). This technique provides another mechanism for generating high energy density plasmas.

The contribution of **Dimitri Khaghani** dealt with X-ray imaging that finds a wide range of application for the plasma physics beamline at FAIR. From a machine stand-point, spatially resolved Kα and Lyα emission measurement from rest gas in the target chamber will give a precise measurement of the high-energy ion beam used for the HEDatFAIR collaboration. Bent crystals will image the target chamber center outside the target chamber through a thin window onto a CCD and significant signals are expected for ion intensities above 4×10^{10} ions/pulse with a spatial resolution of 100 μm. A second application of x-ray spectrometers is XANES that can be employed at FAIR and also at HHT in the phase-0 for thin low-Z targets heated by the ion beam. Equally important will be the use of such detector in the keV energy range for opacity measurements of warm dense matter. In these last cases, the detector relies on a broadband source of photons that could be provided by a 100 J sub-nanosecond laser, as it is planned for the modular start version of FAIR.

In plasmas generated at the NIF, many by-products of nuclear reactions can be collected after the compression and burn phase of the NIF capsules is over. This post-mortem analysis of the debris, particle and gaseous nuclear by-products provide indirect measurement on processes happening in HED plasmas, as described by **Dieter Schneider** in his contribution. For instance, neutron time of flight measurement after the implosion of a NIF target enables linking the neutron energy to the energy loss of alpha particles in the highly compressed plasma [7]. More advanced concepts exist that employ boron as a dopant in the capsule and detect the products of the ^{10}B(p,a) ^{7}Be reaction where the Be yield directly depends on the plasma temperature. In addition to ignition study relevant measurements, the NIF can be used for more basic nuclear physics process relevant to astrophysics [8]. These studies are relatively new and still in the conceptual and early realization phase, for which detectors are being developed and commissioned. The first results are very encouraging.

3.4 Nanosecond Plasma

Many HED physics experiments are dominated by shock waves driven by transient pressure pulses. The shock pressure ps(t) roughly follows the driving pressure during the growth phase but it reduces slowly when the pressure drops suddenly on the piston. In ideal media the process is known as “hydrodynamic SW attenuation”. Many models

[6] Relativistic Transparency reference

[7] D. Sayre et al., APS Division of Plasma Physics Meeting 2015

[8] D. L. Bleuel et al., Plasma and Fusion Research **11** 3401075, 2016

do not provide the piston acceleration, which is of interest to study the early stage of the Rayleigh-Taylor instability, when a shock driven by a transient pressure is still running inside the slab and the interface acceleration is determined by the shock propagation. The group around **Roberto Piriz** has developed a relatively simple description of the hydrodynamic attenuation (growth and decay) of shock waves which can be obtained from the approximate integration of the conservation equations, and by introducing the "retarded" driving pressure as the boundary condition on the piston. The model serves to several purposes:

- It allows for studying the Rayleigh-Taylor instability (RTI) at the early phase of evolution when the shock is still running into the medium. This phase takes place immediately after the Ritchmyer-Meshkov instability stage, and before the accelerated plate can move as a whole.
- It can also be used for studying the entropy shaping generated by a decaying shock in the ablator layer of an ICF target. This is at present a current method for mitigating the RTI in the ablation front.
- It can be easily extended to convergent spherical and cylindrical geometries for applications to shock waves generated in capsule and liner implosions.

Yongtao Zhao from the Xi'an Jiaontong University in China presented some results covering the energy deposition and wakefield excitation in case an ion beam passes through a plasma target. Effect of the projectile's initial kinetic energy, initial charge state, and nuclear charge Z for low energy ions were investigated. An enhanced energy loss has been observed in case of low energy (100 keV/u) ion beams interacting with hydrogen plasma generated in a discharging pinch. For proton projectiles, the experimental results fit well with the theoretical predictions. For Helium however, the theoretical calculations obviously overestimate the energy loss. Further on wakefield self-modulation for proton beam passing a plasma was observed in experiments. Likewise strong focusing was observed while the energy of the focused beams is uniform. The PIC simulation therefore suggests that the wake-field could form a self-modulated, periodic (pulsed), focusing, collision-less tunnel.

4 Proton microscopy, PRIOR, and the round table discussion

Proton microscopy, the use of temporally-tailored proton beams and magneto-optics to image the properties and behaviour of materials under shocked or extreme conditions, is an important capability for FAIR experimental research. The PRIOR proton microscope is one of the main tools that will be available at FAIR for HED research. In the last years, a prototype of PRIOR, PRIOR I, based on permanent magnets, has been fielded at the high-energy cave of GSI HHT. There, it demonstrated a spatial resolution of 30 μm, in line with predictions, but an unexpected ageing of the permanent magnets under the harsh environment of the accelerator makes the use of permanent magnets unpractical. The technical design of PRIOR II, built around electromagnets, has been approved by FAIR and is planned to be operational for both FAIR Phase 0 and FAIR First experiments, as shown in

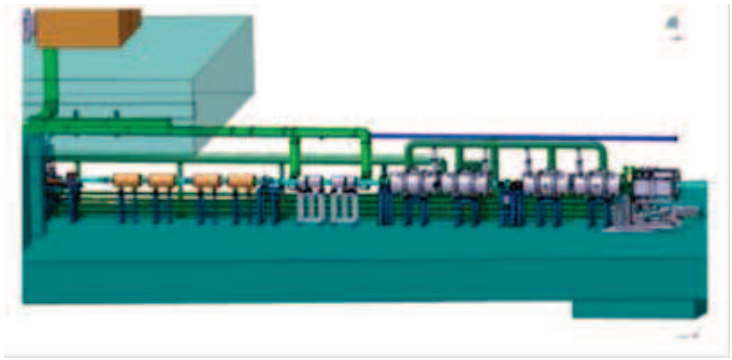

Figure 5: A view of the PRIOR setup at the APPA cave. The PRIOR magnets have a grey support.

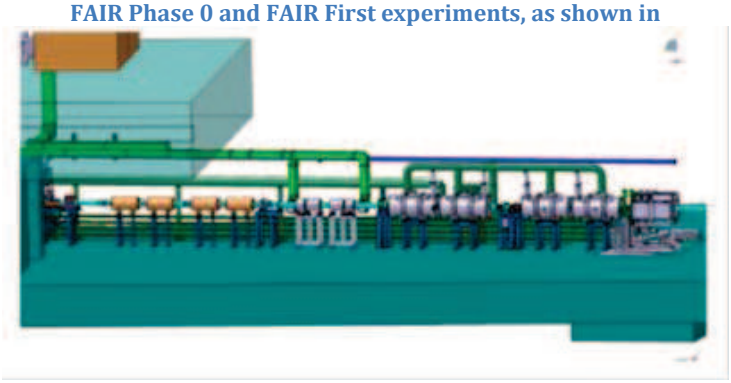

Figure 5. During the workshop, a round-table discussion was facilitated to discuss both the status of PRIOR construction and research applications.

V. Mintsev presented report on the possibilities of the proton radiography for equation of state measurements of shock compressed WDM. The key tasks of special interest for nonideal plasma physics are discussed: Plasma Phase Transition (H2, D2, N2, Noble Gases, etc.), Metal – Insulator Transition, Equation of State – Coulomb interaction, Two Phase Region (Liquid – Gas, including Critical Point), Transport Properties, Optical Properties. Methods of generation of such parameters by powerful shock waves with the aid of high explosives are considered. Compact and full sized explosively driven generators are described from the point of view of their using in the experiments in small "red" GSI chamber (on 150 g of TNT) and in large chamber on 4 kg of TNT, which is now under construction in Chernogolovka. The most attractive looks experiments with strongly coupled plasma of noble gases and plasma phase transitions in H2 and N2. Investigation of Shock Wave Compressibility of Carbon Fiber and Fiberglass for experiments at PRIOR with the help of light gas gun was discussed in the report of **V. Mochalova**.

Frank Merrill's presentation summarized the significant advances in 800 MeV Proton Radiography at Los Alamos over the past several years. Also included was recent research into the potential for Transmission High Energy Electron Radiography. Significant effort at Los Alamos has been dedicated to the development of two models for optimizing 800 MeV Radiography. One model is based on GEANT 4 and allows for the study of impact particles that have scattered substantially or that are generated in

the process of interacting with the object and imaging elements. A second model has been developed to study the radiographic performance of lens systems as well as provide a platform for removing the aberrations introduced by the radiography system. Various permanent magnet lens systems have been investigated to improve the radiation resistance of the imaging system including electromagnets.

5 Round table discussion: PHELIX at HHT

During the 2017 EMMI workshop on Plasma Physics at FAIR an open round-table discussion session was held to discuss the scientific opportunities from bringing the PHELIX laser to the existing HHT-cave at GSI. While the session was open to all workshop attendants and GSI scientists, several experts in the field were invited to give their opinion on this proposal and to present ideas and suggestions what scientific areas could be addressed. The attendants were: Prof. Siegfried Glenzer (SLAC), Dr. Thomas Schenkel (LBNL), Prof. David Riley (U. Belfast), Dr. Thomas White (U. Oxford), Dr. Marilena Tomut (GSI, materials research department), Paul Neumayer (GSI, plasma physics department). Though they were not able to attend the discussion in person, further contributions were provided by I. Krasyik, Dr. O. Rosmej (GSI) and Prof. Dominik Kraus (HZDR).

The discussion started with a short presentation by Udo Eisenbarth about the possible optical layout used to transport the beam over to the HHT cave, as shown in Figure 6. The layout is based on the previous project drawings that were made in 2006 with the significant change in requirements that the pulse should be only using the long-pulse (nanosecond) front end and can probably work with a reduced diameter in the APPA cave to save on space and cost. An interesting option that balances costs and performance is to limit the beam size to 150 mm in diameter while enabling an energy of 200 J at 2ω in sub-nanosecond pulses.

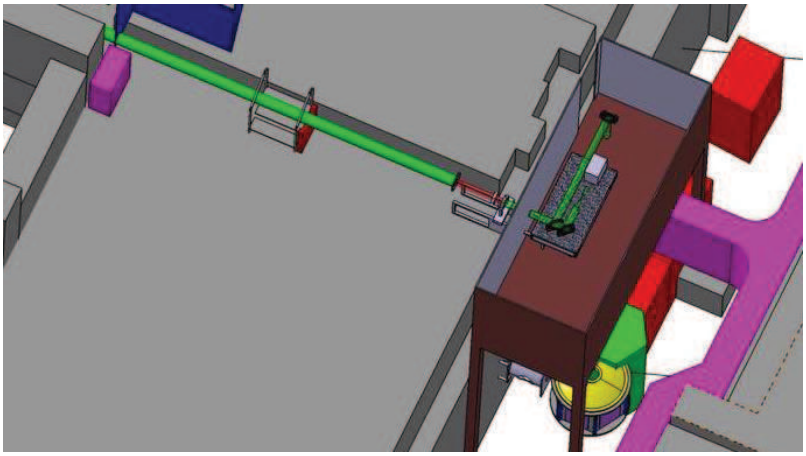

Figure 6: a view of the planned laser beamline (in green) on top of the FRS section of the ESR hall and the laser laboratory container located on top of the HHT cave.

Following this, a round table with short presentations showed the interest of the various participants. This gives a glimpse that these capabilities would raise interest in the community, attract external groups, strengthen and enlarge the FAIR collaboration. These contributions are summarized below:

M. Tomut reported on the need for novel materials and compounds to withstand high strain rates and thermal loads in high-radiation environments, to be used for components such as production targets, collimators or beam dumps at future high-power accelerators (such as the FCC) or as first wall materials in fusion reactors. Modeling of material strength is usually based on known material properties near room

temperature, low strain rates and without the simultaneous presence of high radiation fluxes. Therefore, reliably predicting a material's performance requires testing under similar conditions. Such experiments can be conducted at the HighRadMat facilities at CERN, however, the attainable energy deposition and strain rates are quite limited as only proton beams are available. Using uranium ions at HHT will allow significantly higher temperatures and strain rates, even in low-Z targets such as carbon with its many exotic novel forms (e.g. highly-oriented pyrolytic graphite, glassy carbon etc.). In contrast to a post-shot analysis, imaging with laser driven x-rays would enable an in-situ observation of the various hydrodynamic phenomena, such as cylindrical or reflected shock waves, explosion and spallation events, hydrodynamic tunneling, evaporation and plasma generation. Furthermore, x-ray diffraction would give access to microscopic properties such as changes in lattice constant, structural changes and melting.

The contribution provided by **D. Kraus** presented an example experimental setup of a carbon sample being heated by the heavy-ion beam, and using a high-energy laser produced x-ray source as a probe. X-ray diffraction and scattering will provide information on the ionic structure. Such experiments had already been conducted very successfully using laser-shocked samples at the Z6 target area by Kraus et al., revealing the complex structure of dense liquid carbon. Near-isochoric heavy-ion heating of graphite samples with different initial densities will allow reaching new and unexplored parameter regimes. Another idea proposed is to used carbon samples doped with high-Z elements. These will feature absorption edges and laser-driven x-ray sources will enable x-ray absorption spectroscopy for dense matter diagnostic techniques such as XANES and EXAFS.

Similar experiments had been proposed **D. Gericke** (not present) and **P. Neumayer**, studying rapidly heated graphite and diamond samples using x-ray diffraction. Graphite is expected to expand and melt first along the sp2-planes, which would be readily seen in the lattice parameter and diffraction strength across the planes. Diamond on the other hand will undergo graphitization. It is long known that at temperatures of several thousand degrees diamond will turn into graphite within several hours, while recent ultra-fast experiments using x-ray laser pulses showed non-thermal phase transition on the 100 fs time-scale. The experiments at GSI would access the wide parameter space in between and show transformation of diamond to highly compressed graphite on ns-timescales. Another experiment proposed addresses the topic of ionization potential depression (IPD) in strongly-coupled plasmas. This topic has recently gained increased attention due to several experiments at new facilities (LCLS, Orion, AWE), indicating that the widely used standard models for IPD fail, and new theoretical approaches are required in the strongly-coupled regime. At GSI large homogenous samples of strongly-coupled partly degenerate plasmas can be produced in a well-controlled manner and at LTE conditions – ideal for benchmarking of dense matter models – by heavy-ion heating and expansion. An intense broadband x-ray source, produced from a laser-generated high-Z plasma, would be used to perform absorption spectroscopy, probing the electronic excitation spectrum, and thus the continuum edge and the available bound states of such samples.

T. White showed results from recent experiments at the Titan (LLNL) and PHELIX laser facilities. In these experiments, carbon samples were rapidly (ps-timescale) heated by laser-generated protons or supra-thermal electrons. A second laser pulse was used to generate an intense short x-ray pulse used to probe the target, and heating of the ion lattice could be inferred from the intensity reduction of the x-ray diffraction rings. The experiments demonstrate the suitability of high-energy lasers to generate narrow-band x-ray sources sufficiently intense to yield high-quality x-ray diffraction data from short-lived samples like those produced by heavy-ion heating at HHT. This provides valuable diagnostic information such as the lattice temperature below melting, the inter-ionic

potential and lattice strength in high-temperature solids through the Debye-Waller factor, and a direct diagnostic signature for melting.

Another experiment proposed by **T. White** addresses the role of radiation damage and dislocation kinetics on elastic precursor decay in materials under shock-loading, of importance for the development of physically-based strength models. In such an experiment, the heavy-ion beam would be used to induce strong radiation damage in a sample, while it is being subjected to a strong laser-driven shock. Performing rear-side velocity measurements with a VISAR system will then yield the elastic-plastic response and material strength parameters of the sample.

S. Glenzer reported on the efforts at SLAC to study transformation of materials under extreme conditions. Employing laser-accelerated proton pulses to damage materials and the ultra-fast x-ray free electron laser LCLS to visualize the transformation on atomic scales via x-ray diffraction and scattering techniques. While ultra-short proton pulses can access the primary defect production as well as highly transient phenomena, they are strongly limited in the attainable projectile energy and charge. Here the high-energy heavy-ions from the GSI accelerator complement and significantly widen the range of possible radiation damage studies, which is also the reason why radiation biology groups and space agencies are strongly interested in experiments at FAIR. Although ultrafast time-scales cannot be accessed due to the 100 ns duration of the heavy-ion pulse, it was pointed out that a large spectrum of secondary processes (e.g. H/He-generation, diffusion and trapping, defect clustering, cascade ageing,…) in the damage cascade happen on time-scales of sub-microseconds to milliseconds. Studying these processes in-situ will require the intense x-ray sources generated by a high-energy laser.

D. Riley emphasized that x-ray scattering is the key diagnostic technique to probe static and dynamic structure of warm-dense matter. He recalled that nanosecond laser driven plasmas can reach of order 10^{-3} conversion of laser energy to x-ray line radiation, and his group is in fact the first to demonstrate elastic x-ray scattering on shock-compressed samples using such laser-driven x-ray sources. Currently his group is involved in establishing this technique on the latest generation x-ray free-electron laser LCLS.

The value for dense matter theory of direct structure factor measurements was also stressed by **C. Meister** (audience). As was also pointed out by **D. Riley** and **S. Glenzer**, who had pioneered ion structure factor measurements on laser-generated warm-dense plasmas using x-ray scattering, these measurements directly probe the ion structure which allows for direct comparison with state-of-the-art dense matter modeling.

O. Rosmej and **I. Krasyik** reported on experiments performed at the Z6 target area utilizing the PHELIX long pulse beam at energies up to 150 J to drive laser-driven shocks into mm-thick aluminum plates in order to induce spallation on the rear side. An electro-acoustical probe was used to measure the time-of-flight of the spallation fragments, and thereby infer their velocity. In addition, the samples were analyzed “post-mortem” by microscopy to measure e.g. crater size and depth. This yields information on the mechanism of destruction of condensed matter at high tensile loads and receive information about of the matter microstructure and density distribution in dynamical stress caused by the laser shock. Performing such spallation experiments using the PHELIX laser beam at HHT would allow conducting in-situ imaging of the spallation event using the proton microscope PRIOR. The expected parameters of PRIOR in terms of temporal and spatial resolution should be ideally suited to the time and spatial scales involved in these scenarios.

T. Schenkel reiterated the high interest in radiation damage studies as presented by T. White and S. Glenzer. More general, he stated the strong added potential and synergetic possibilities of complementing the heavy-ion heated warm-dense matter samples with a powerful x-ray backlighter (for radiography, diffraction, absorption, scattering

techniques), or providing an interesting driver for dynamic studies with the proton microscope PRIOR. Given the scientific potential and uniqueness of the combination of intense heavy-ion pulses with a high-energy laser, and in the context of other emerging facilities (XFEL, LCLS-II, Bella), T. Schenkel stressed that there is a clear window of opportunity if such a project were realized within the next three years. It would give first access to discovery science experiments. At the same time it would allow many of the diagnostic concepts and techniques to be developed and tested which will be required for the day-1 experiments when the FAIR facility will go into operation. And finally it could play a crucial role in the community development towards first experiments at FAIR.

There was overall consensus among the participants that having combined laser-ion capability at HHT would provide a unique experimental setup which would significantly enhance the width of the plasma physics program at GSI by attracting new users and community fostering.

6 APPENDIX 1 - List of Posters

Poster session: Monday, July 11th, 2016, 15:30 – 16:50

Id	Title	Presenter
5	Effects of the finite thickness on the Rayleigh-Taylor instability in elastic solid slabs	Ms. PIRIZ, Sofia A.
6	Evidence of Strong Damping in Raman Amplification: Comparison between Simulations and Experiment	FARMER, John
13	Spectroscopic studies of the parameters of plasma jets during their propagation in the background plasma on the PF-3 facility	Dr. ANANYEV, Sergey
14	Harmonic Generation In Magnetized Quantum Plasma with Separate Spin-up and Spin-down Evolution of Degenerated Electrons	Dr. KUMAR, Punit
19	Radiation-hydrodynamic simulations of backlighter options for FAIR	Dr. FAIK, Steffen
20	Model of swift heavy ion tracks excitation	VOLKOV, Alexander
21	A light-gas driver for studies on material properties with PRIOR	ENDRES, Michael
24	Line-imaging VISAR System for Laser-Driven Experiments	Dr. GUBSKIY, Konstantin
25	Ultra-high energy density physics in aligned nanowire arrays	Mr. KAYMAK, Vural
26	Stability of nano and microdiamonds to the action of heavy ions. Thermophysical properties of micro and nanodiamonds at the heating	Ms. ZAKATILOVA, Ekaterina
27	Volume laser destruction in the silica	Dr. EFREMOV, Vladimir
34	High-energy proton microscopy at INR proton linac (proposal)	Dr. KANTSYREV, Alexey
36	Laser-induced ablation plasma: time and space-resolved spectroscopy. Applications	Prof. GURLUI, Silviu
38	Raman amplification in the coherent-wavebreaking regime	FARMER, John
39	Ion acceleration using a flattop laser beam	AFSHARI, Masoud
41	Numerical simulation of proton-radiographic facilities at Geant4	Mr. SKOBLIAKOV, Aleksei
42	Investigation of Shock Wave Properties of Porous Materials for Experiments at PRIOR	Mrs. ZUBAREVA, Alla
43	Electron acceleration in the interaction of intense laser pulses with sharp plasma density profile	Dr. PUGACHEV, Leonid
44	Development of a diagnostic for ultra-intense laser plasma experiments based on frequency resolved optical gating	HORNUNG, Johannes
48	Remagnetization of PMQ lenses for PRIOR and PUMA proton microscopes	Mr. PANYUSHKIN, Vsevolod
50	Improved description of ion stopping in moderately coupled and partially degenerate plasma	Dr. RACZKA, Piotr
51	Diagnostical methods for high energy resolution spectroscopy of the target and projectile X-ray- fluorescence	Mr. ZAEHTER, Sero
54	Synchrotron radiation of polarized electron beams in laser wake field acceleration	Ms. PUGACHEVA, Daria
55	Development of metal plate launcher setup for VISAR Doppler velocimeter test and calibration.	Mr. GAVRILIN, Roman
57	Kelvin-Helmholtz instability in viscous warm dense matter	Dr. MEISTER, Claudia-Veronika Meister
71	Collision processes in partially ionized plasmas	Prof. ROEPKE, Gerd
72	Ionization potential depression in plasmas via structure factors	Prof. ROEPKE, Gerd

7 APPENDIX 2 - List of Participants

Dr. AFSHARI, Masoud
Ms. AMENEH, Kargarian
Dr. ANANYEV, Sergey
Prof. ANDREEV, Nikolay
Mrs. AUMÜLLER, Simone
Dr. AZADNIA, Fateme
Dr. BAGNOUD, Vincent
Dr. BATANI, Dimitri
Dr. BLAZEVIC, Abel
BOCK, Rudolf M.
Mr. BOGDANOV, Anton
Dr. BRAEUNING-DEMIAN, Angela
Dr. BRAMBRINK, Erik
Dr. CHENG, Rui
Mr. CISTAKOV, Konstantin
Prof. CSERNAI, Laszlo
Mr. DING, Johannes
Dr. DOEPPNER, Tilo
Dr. EFREMOV, Vladimir
Dr. EISENBARTH, Udo
ENDRES, Michael
Dr. FAIK, Steffen
Dr. FARMER, John
Mr. GAVRILIN, Roman
Dr. GERICKE, Dirk
Prof. GLENZER, Siegfried
Dr. GOLUBEV, Alexander
Dr. GORBUNOV, Sergey
Dr. GUBSKIY, Konstantin
Prof. GURLUI, Silviu
Dr. GÖTTE, Stefan
Dr. GÜNTHER, Marc
Mrs. HAJIZADEH, Kobra
HANTEN, Jan
Prof. HOFFMANN, Dieter HH
Mr. HORNUNG, Johannes
Prof. IOSILEVSKIY, Igor
Prof. JACOBY, Joachim
JAHN, Diana
Dr. JUHA, Libor
Prof. KANG, Wei
Dr. KANTSYREV, Alexey
Mr. KAYMAK, Vural
Dr. KHAGHANI, Dimitri
Ms. KLEINSCHMIDT, Annika
KLUGE, H.-Jürgen
Dr. KORZHIMANOV, Artem
Dr. KRAUS, Dominik
Dr. KUMAR, Punit
Prof. KÜHL, Thomas
Dr. LI, Lu
Prof. LOMONOSOV, Igor
Dr. MAHDAVIGHARAVI, Marjan
Dr. MAJOR, Zsuzsanna
Dr. MEHLHORN, Thomas
Dr. MEISTER, Claudia-Veronika
Dr. MERRILL, Frank
Prof. MINTSEV, Victor
Dr. MOCHALOVA, Valentina
Mr. MOFAKHAMI, Darius
Prof. MULSER, Peter
Dr. NEFF, Stephan
Dr. NEUMAYER, Paul
Mr. OHLAND, Jonas
Dr. ONKELS, Eckehard
Mr. PANYUSHKIN, Vsevolod
Mr. PATRIZIO, Marco
Dr. PETER, Spiller
Prof. PIRIZ, Antonio Roberto
Mrs. PIRIZ, Sofía A.
Mrs. POURALI, Mahdi
Ms. PUGACHEVA, Daria
Dr. PUGACHEV, Leonid
Prof. PUKHOV, Alexander
Dr. RACZKA, Piotr
Prof. REDMER, Ronald
Prof. RILEY, David
Dr. RODRIGUES, Gerard
ROEPKE, Gerd
Dr. ROSMEJ, Olga N.
Prof. ROTH, Markus
Prof. RUHL, Hartmut
Mr. RUIJTER, Marcel
SANDER, Steffen
Prof. SAVEL'EV, Andrey
Mr. SAVIN, Sergey
Mr. SCHANZ, Martin
Mr. SCHANZ, Victor
Dr. SCHENKEL, Thomas
Mr. SCHILLACI, Francesco
Dr. SCHNEIDER, Dieter
Dr. SCHOENBERG, Kurt
Dr. SCHOENLEIN, Andreas
Dr. SCHUMACHER, Dennis
Ms. SCHUSTER, Anja Katharina
SEIBERT, Marco
Ms. SEPTRIANI, Brigitta
Prof. SHARKOV, Boris
Mr. SKOBLIAKOV, Aleksei
Prof. SON, Eduard
Prof. SPIELMANN, Christian
Dr. TAHIR, Naeem
Dr. TAJIK NEZHAD, samira
Dr. TAUSCHWITZ, Anna
TEBARTZ, Alexandra
Prof. THOMA, Markus
Dr. TOMUT, Marilena
TRAUTMANN, Christina
Dr. VARENTSOV, Dmitry
Dr. WEYRICH, Karin
Dr. WHITE, Thomas
Mr. WINKLER, Bjoern
Mrs. ZAHN, Nadiya
Ms. ZAKATILOVA, Ekaterina
Prof. ZEPF, Matt
Prof. ZHAO, Yongtao
Mr. ZIMMER, Marc
Mr. ZOBUS, Yannik
Mrs. ZUBAREVA, Alla
ZÄHTER, Sero

List of Contributing Institutes

Al-Farabi Kazakh University
Almaty, Kazakhstan

ARTEP Inc.
Ellicott City, MD 21042, USA

Beijing National Laboratory for Condensed Matter Physics, Institute of Physics, CAS
Beijing 100190, China

Chinese Academy of Engineering Physics
CAEP - Laser Fusion Research Center
Mianyang 621900, China

CFEL, DESY - Hamburg,
Notkestr. 85, 22607 Hamburg, Germany

Colorado State University
Dep. Electrical Computer Engineering,
Dep. of Physics,
Fort Collins, Colorado 80523, USA

Dalian University of Technology
Dalian, Ganjingzi, Liaoning, China

Excitech GmbH
Branterei 33, 26419 Schortens
Germany

Facility for Ion and Antiproton Research (FAIR)
64291 Darmstadt, Germany

Friedrich-Schiller-Universität Jena
Inst. für Optik und Quantenelektronik
07743 Jena, Germany

GSI Helmholtzzentrum für Schwerionenforschung GmbH,
64291 Darmstadt, Germany

Heinrich-Heine-Universität Düsseldorf
Institut für Theoretische Physik I
Düsseldorf, Germany

Helmholtz-Zentrum Dresden- Rossendorf
Bautzener Landstr. 4, 01328 Dresden,
Germany

Helmholtz-Institut Jena
Fröbelstieg 3, 07743
Jena, Germany

Hochschule Emden/Leer - University of Applied Sciences
Institute for Laser and Optics
26723 Emden, Germany

Holon Institute of Technology
P.O. Box 305, Holon 58102, Israel

IHEP – Institute for High Energy Physics
Protvino142281, Moscow Region, Russia

Institute of Applied Physics and Computational Mathematics, CAS
Beijing 100088, China

IMP - Institute of Modern Physics
Lanzhou 730000, China

Institute of Problems of Chemical Physics (IPCP)
Chernogolovka, Russia

Institute of Theoretical and Experimental Physics of NRC Kurchatov Institute
Moscow 117259, Russia

Joint Institute for High Temperatures, RAS
Moscow 125412, Russia

Joint Institute for Nuclear Research,
Joliot-Curie 6, 141980 Dubna,
Moscow Region, Russia

Johann-Wolfang-Goethe-Universität
Institut für Angewandte Physik,
Institute für theoretische Physik
Frankfurt, Germany

Kansai Photon Science Institute
Kizugawa, Kyoto, Japan

Keldysh Institute of Applied
Mathematics - RAS
Moscow 125047, Russia

Korea Advanced Institute of Science
and Technology (KAIST)
Daejeon 34141, Republic of Korea

Lawrence Berkeley National Laboratory
Berkeley, CA 94720, USA

Lawrence Livermore National
Laboratory
Livermore, CA 94550, USA

Lebedev Physical Institute, RAS
Leninskij Prospekt, 53,119991
Moscow, Russia

Moscow Engineering Physics Institute
(MEPhI), Nat. Research Nucl. Univ.
Moscow 115409, Russia

Max Planck Institut für Struktur und
Dynamik der Materie
Notkestr. 85, 22607 Hamburg, Germany

Moscow State University
Faculty of Physics
International Laser Center
Moscow 119991, Russia

National Research Center 'Kurchatov
Institute',Kurchatov Sq. 1,
123182 Moscow, Russia

Naval Research Laboratory
Plasma Physics Division
Washington, DC 20375, USA

Osaka University
Open and Transdisciplinary Research
Initiatives Institute
Suita, Osaka 565-0871, Japan

Osaka University
Institute of Laser Engineering (ILE)
Suita, Osaka, 565-0871, Japan

Polish Academy of Sciences
Institute of Nuclear Physics,
31-342 Krakow, Poland

Russian Federal Nuclear Center - VNIIEF
607200 Sarov, Russia

Sandia National Laboratories
Albuquerque, NM 87185,
USA

Shanghai Jiao Tong University
Laboratory for Laser Plasmas,
Depart. of Physics and Astronomy
Shanghai 200240, China

Technische Universität Darmstadt
Inst. für Kernphysik (IKP),
Techn. Quant. Electronics (IAP)
64289 Darmstadt, Germany

Technische Universität Dresden
Institut für Kern- und
Teilchenphysik
01069 Dresden, Germany

Technische Universität Kaiserslautern,
Fachbereich Physik und Landes-
forschungszentrum OPTIMAS
67663 Kaiserslautern, Germany

Technische Universität München,
Physik Department E12
85748 Garching, Germany

Ulsan National Institute of Science and
Technology, Ulsan 44919, Korea

Universidad de Buenos Aires
Departemento de Fisica
1428 Buenos Aires, Argentina

Universitat Politécnica de Valencia
Dpto. de Matemática Aplicada
Valencia, Spain

University of California Berkeley
Department of Physics
Berkeley, CA 94720, USA

Université Bordeaux, CELIA
Centre Lasers Intenses et Applications
33405 Talence, France

University of California Berkeley
Berkeley, CA, USA

University of Chinese Academy of Sciences, School of Physical Sciences, Beijing 100190, China

Université Paris Sud
L.P.G.P., CNRS
91405 Orsay, France

University of Prague
Institute of Plasma Physics
Za Slovankou 3, 182 00 Prague, Czech Republic

University of Rochester
Laboratory for Laser Energetics
Rochester, NY 14623-1299, USA

University of Strathclyde
SUPA -Department of Physics
Glasgow G11XQ, United Kingdom

University of Warwick
Centre for Fusion, Space- and Astrophysics, Physics Depart.
Coventry CV4 7A1, UK

University of Washington
Dep. Aeronautica and Astronautics
Seattle, WA 98195, USA

Weizmann Institute of Science
Rehovot 7610001, Israel

Xi'an Jiaotong University
School of Science
Xi'an, 710049, Shaanxi, China

Zelinsky Institute of Organic Chemistry
Leninsky Pros. 47, Moscow 119991, Russia

Author Index